JAERI 1061

JAERI 1061

Dynamic Analysis of
Natural Circulation Boiling Water Reactor

1964年6月

日本原子力研究所

Japan Atomic Energy Research Institute

日本原子力研究所は，研究成果，調査結果の報告のため，つぎの3種の刊行物を，それぞれの通しナンバーを付して，不定期に発行しております.

1.	研究報告	まとまった研究の成果あるいはその一部における重要な結果の報告	JAERI 1001-3999
2.	調査報告	総説，展望，紹介などを含め，研究の成果，調査の結果をまとめたもの	JAERI 4001-5999
3.	資料	研究成果の普及，開発状況の紹介，施設共同利用の手引など	JAERI 6001-6999

このうち既刊分については「JAERI レポート一覧」にタイトル・要旨をまとめて掲載し，また新刊レポートは雑誌『原研』でその都度紹介しています．これらの刊行物に関する版権，複写のお問合せは，日本原子力研究所技術情報部あてお申し越しください.

なお，上記3種の報告は，日本原子力研究所生活協同組合（茨城県那珂郡東海村）で実費頒布をいたしております.

Japan Atomic Energy Research Institute publishes the nonperiodical reports with the following classification numbers.

1. **JAERI** 1001-3999 Research Reports.
2. **JAERI** 4001-5999 Survey Reports and Reviews.
3. **JAERI** 6001-6999 Information and Guiding Booklets.

編集兼発行　日本原子力研究所　東京都港区芝田村町1の1 (電)591-5481

JAERI 1061 Dynamic Analysis of Natural Circulation Boiling Water Reactor

ERRATA

Page	Line	
5	ordinate of Fig.3.1	$(\times 10^3\ cm^3/\frac{kcal}{sec \cdot cm})$ should read $K_1/Q^*(\times 10^3\ cm^3/\frac{kcal}{sec \cdot cm})$
5	4	varing should read varying
11	1	reponse should read response
16	7 from bottom	G_{18} and G_{19} should read G_{18}' and G_{19}'
21	top of Fig. 18	0° should be deleted
27	6 and 10	$\frac{\delta \bar{V}}{\delta V_0}$ should read $\frac{\delta \bar{V}}{\delta V_0 / V_0^*}$
29	2	tranfer should read transfer
33	2 from bottom	shuld should read should
35	bottom	close should read closed
40	Eq. (88)	αT should read α_T
41	5	considerablely should read considerably
47	18 from bottom	considerablely should read considerably
47	bottom	assistence should read assistance
58	2	C should read c
58	13	$T_1 = \frac{G_1(0)}{\lim_{s \to 0} sG_1(s)}$ should read $T_1 = \frac{G_1(0)}{\lim_{s \to \infty} sG_1(s)}$
59	Captions of Figs. A.2.1 and A.2.2 should be interchanged	
60	14	$d\bar{V}$ should read $\delta\bar{V}$
62	Fig. A.6.1	Vessel pressuer should read Vessel pressure
25	6 and 10	$\frac{\delta \bar{V}}{\delta V_0}$ should read $\frac{\delta \bar{V}}{\delta V_0 / V_0^*}$
32	Fig.24	$(z_2 - z_1)\,Q^*$ should read $(z_2 - z_0)\,Q^*$
57	Eq. (A9)	C's should read c's

JAERI 1061 UDC 621.039.524: 621.039.516

Dynamic Analysis of Natural Circulation Boiling Water Reactor

Summary

This report is a second report in a series of studies on the dynamic behavior of the natural circulation boiling water reactors.

The simplified versions of the transfer functions derived in the preceding report, JAERI-1044, are obtained. Simplified models are then constructed based on the simplified transfer functions thus derived, in order to readily investigate the dynamic characteristics from the design parameters. Some of the dynamic characteristics based on the simplified models are given. The dynamic characteristics of the feedback transfer functions and the system stability are also investigated. Comparisons with other studies are briefly given in order to make clear the significance of this study.

Studies are with special reference to the JPDR, a 12.5 MWe boiling water reactor. However, models derived here are quite general.

December, 1963

Junichi Miida, Nobuhide Suda
Division of Nuclear Engineering
Tokai Research Establishment
Japan Atomic Energy Research Institute

自然循環式沸騰水型原子炉の動特性解析

要　旨

この報告は，自然循環式沸騰水型原子炉の動特性についての研究の第2部である．

前の報告 JAERI-1044 で導いた伝達関数の簡単化した形を求めた．この簡単化した伝達関数をもとにして，設計データから容易に動特性が検討できるような簡単なモデルを作成した．このモデルによって求めた動特性の例を示した．フィードバック伝達関数の特性および安定性の解析もおこなった．この研究の意味をはっきりさせるために他の諸研究との簡単な比較をおこなった．

諸計算は JPDR(12.5 MWe 沸騰水型原子炉プラント)についておこなった．

1963 年 12 月

東海研究所原子力工学部計測制御研究室
三井田純一，須田信英

Contents

目　　次

1. INTRODUCTION

The mathematical model of the dynamic characteristics of boiling water reactors is necessary for four purposes; first to evaluate the stability of the reactor, second for the physical interpretation of the measured transfer functions, third to provide information for more efficient core design, and finally to provide information for control system design.

This report is second report in a series of studies along the above line on the dynamic behavior of boiling water reactor power plants.

The purpose of the present study is first to obtain simplified versions of the transfer functions derived in the preceding report[1], second to construct simplified models based on the derived simplified transfer functions which enable one to readily investigate the dynamic characteristics from design parameters. Some of the dynamic characteristics based on the simplified models are given. The dynamic characteristics of the feedback transfer functions and the system stability are also investigated. Comparisons with other studies are briefly given in order to make clear the significance of this study.

Studies are with special reference to the JPDR, a 12.5 MWe boiling water reactor. However, models derived here are quite general.

The rest of this series of studies will appear in subsequent reports, where analog computer studies and control system studies will be given.

2. SIMPLIFIED TRANSFER FUNCTIONS

The transfer functions derived in the preceding report, JAERI-1044, are so complicated that it is not easy to simulate them on an analog computer and also to obtain their numerical values for different frequencies for the purpose of stability study.

In view of the situation they are simplified and approximate forms are obtained. Most of them are in the form of combinations of single time constant terms.

Frequency characteristics are given to compare the digital computer calculation of exact transfer functions derived in the preceding report and the numerical calculations of simplified transfer functions obtained in this report.

Most of the numerical calculations of the transfer functions in this chapter are for the full power condition of JPDR, although the power dependences of the transfer functions are investigated and are summarized in TABLE 3.

The order of descriptions is different from that of the preceding report; inlet velocity transfer functions and recirculation flow transfer functions are in the last part of this Chapter since they may be ignored for the simplification of the model.

Simplified transfer functions are summarized in Chapter 2.9 and in TABLE 1.

The symbol * is attached to the equation number of the equations which appeared in JAERI-1044 and which also repeat in this text, in order to distinguish these equations from those which have newly appeared in this report.

2.1 Zero Power Transfer Function

The zero power transfer function, $G_R(s)$, which relates the nuclear power generated in the fuel to the excess reactivity, is given by

$$G_R(s)=\frac{\delta n/n^*}{\delta k/\beta}=\frac{s+\lambda}{\frac{l}{\beta}s\left(s+\frac{\beta}{l}+\lambda\right)} \qquad (1)^*$$

where one group of delayed neutrons is considered.

In the model described here the excess reactivity consists of several contributions.

$$\delta k=\delta k_{ex}+\delta k_{void}+\delta k_T \qquad (1)$$

where δk_{ex}, δk_{void} and δk_T are reactivity changes caused by external disturbances such as control rod movement, by change in void volume, and by change in fuel temperature, respectively.

The zero power transfer function for JPDR is obtained by use of the following parameters; $l=5\times10^{-5}$ sec, $\lambda=0.077$ sec^{-1}, $\beta=0.0064$.

$$G_R(s)=0.077\cdot\frac{1+13s}{s(1+0.0078s)} \qquad (2)$$

2.2 Fuel Heat Transfer Function

The fuel heat transfer functions, $G_{f1}(s)$ and $G_{f2}(s)$, which relate the nuclear power generated in the fuel to the heat flux in the fuel surface and to the average fuel temperature, respectively, are given in JAERI-1044 by means of a very simple model with lumped parameters.

$$G_{f1}(s)=\frac{\delta Q/Q^*}{\delta n/n^*}=\frac{1}{1+T_f s} \qquad (2)^*$$

$$G_{f2}(s)=\frac{\delta\theta_f}{\delta n/n^*}=\frac{\theta_f^*-\theta_w^*}{1+T_f s} \quad (3)^*$$

The $G_{f2}(s)$ constitutes a feedback loop through temperature coefficient of reactivity, α_T, as shown in **Fig. 21**.

The transfer functions for JPDR are obtained below. The time constant of fuel heat transfer T_f is very large compared with that of metallic fuel elements, since fuel elements used in JPDR are uranium oxide. T_f is estimated to be 12 sec. The difference between the the average fuel temperature and the moderator temperature, $\theta_f^*-\theta_w^*$, may be estimated to be 400°C.

Thus, the transfer functions are

$$G_{f1}(s)=\frac{\delta Q/Q^*}{\delta n/n^*}=\frac{1}{1+12s} \quad (3)$$

$$G_{f2}(s)=\frac{\delta\theta_f}{\delta n/n^*}=\frac{400}{1+12s} \quad (4)$$

2.3 Core Void Transfer Functions

The void transfer functions, $G_1(s)$, $G_2(s)$, $G_3(s)$ and $G_4(s)$, which relate void to the power, to the inlet velocity, to the boiling boundary shift and to the system pressure, respectively, have been given in JAERI-1044. Some of their characteristics and simplifications are given below.

2.3.1 Power to void transfer function, $G_1(s)$

The power to void transfer function given in Eq. (27)* is

$$G_1(s)=\frac{\delta\bar{V}}{\delta Q/Q^*}=\frac{v_s}{\Delta v}\tau_{12}V_0{}^*A_{co}\frac{1}{\tau_e s-1}\left(\frac{1-\frac{1}{y_2}}{\ln y_2}-\frac{1-e^{-\tau_{12}s}}{\tau_{12}s}\right) \quad (27)^*$$

The frequency response of $G_1(s)/Q^*$ at full power is calculated and shown in **Fig. 1**, since the frequency response of $\frac{\delta\bar{V}}{\delta Q^*}(s)$ is of interest. The responses are also calculated for

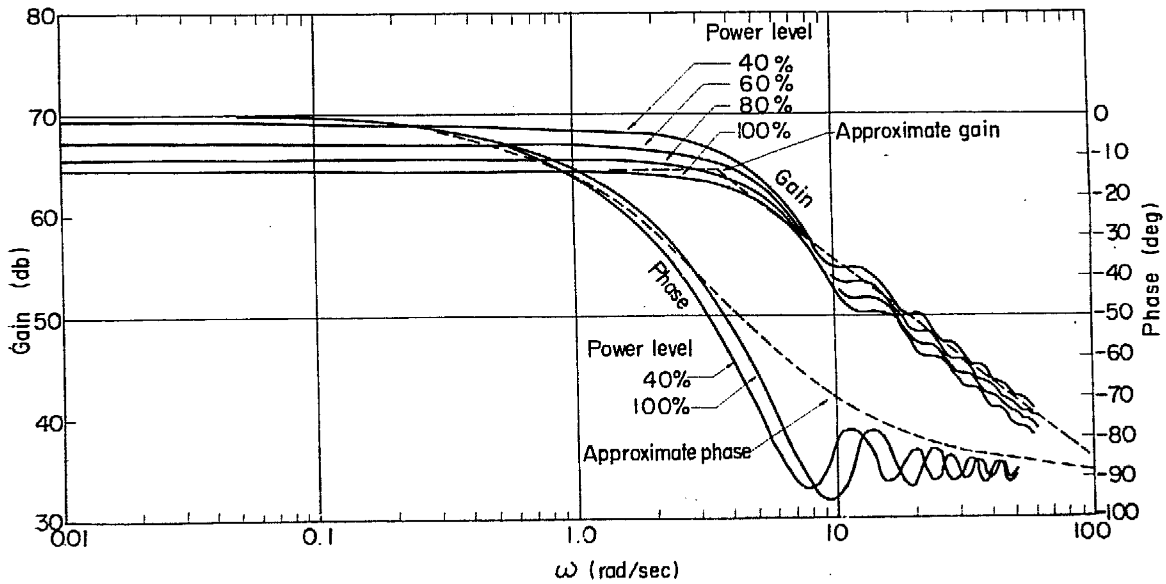

Fig. 1 Frequency characteristics of $G_1(s)/Q^*$

other power levels, i.e. 80%, 60% and 40% of the full power, where inlet velocity V_0^* is assumed to be independent of power level.

The response of $\delta\bar{V}$ to the step change in $\delta Q/Q^*$ is readily calculated from $G_1(s)$ resulting in

$$\delta\bar{V}(t)=\frac{v_s}{\Delta v}V_0^*A_{co}\tau_{12}\left\{\frac{t}{\tau_{12}}-\frac{e^{t/\tau_e}-1}{y_2\ln y_2}\right\} \quad \text{for} \quad 0<t\leq\tau_{12}$$

and

$$\delta\bar{V}(t)=\text{const}=\frac{v_s}{\Delta v}V_0^*A_{co}\tau_{12}\left\{1-\frac{y_2-1}{y_2\ln y_2}\right\} \quad \text{for} \quad t\geq\tau_{12} \tag{5}$$

The step response is plotted in **Fig. 2**.

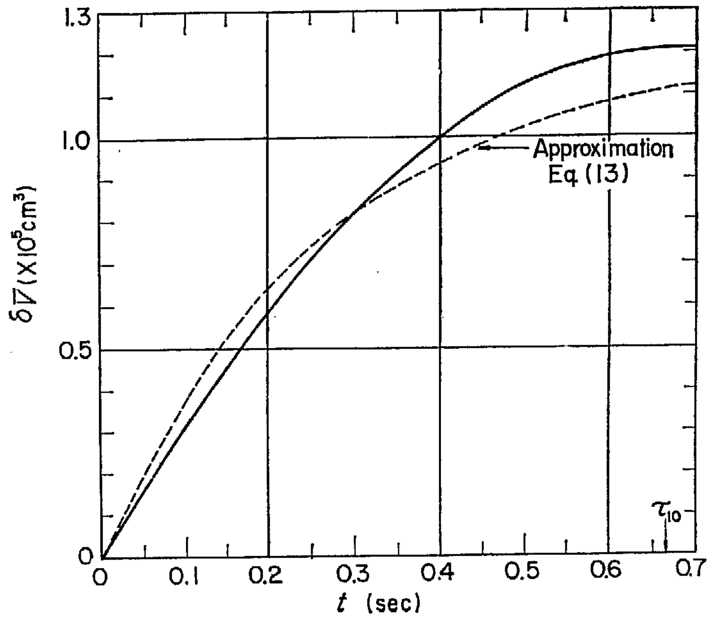

Fig. 2 Response of void to step change in $\delta Q/Q^*$ (calculated from $G_1(s)$ of Eq. (27)*)

From **Fig. 1** and **Fig. 2** it can be seen that the response of $G_1(s)$ may be approximated by a single time constant delay in the form of

$$G_1(s)\simeq\frac{K_1}{1+T_1 s} \tag{6}$$

K_1 is easily obtained as below.

$$K_1=\lim_{s\to 0}G_1(s)=\left(\frac{v_s}{\Delta v}V_0^*A_{co}\right)\tau_{12}\left[1-\frac{y_2-1}{y_2\ln y_2}\right] \tag{7}$$

The dependence of K_1/Q^* upon the power level is of interest, since this is a static gain of $\delta\bar{V}/\delta Q^*$. K_1/Q^* is plotted is plotted in **Fig. 3.1** as a function of the power level. It can be seen that this static gain increases with decreasing power level. This is qualitatively consistent with experimental results on EBWR[2].

Several methods for obtaining the approximate formula of the single time constant, T_1 are considered, as given in **Appendix 1**. Here the 45°-phase-lag method is adopted, which gives the best result. In this method T_1 is given by $T_1=\omega_1^{-1}$, where ω_1 is a solution of the equation;

$$\text{Arg } G_1(j\omega_1)=-\frac{\pi}{4} \tag{8}$$

Solving the above equation (see **Appendix 1**), one obtains

$$T_1=\frac{1}{\omega_1}=\frac{\tau_{12}}{2x_1(y_2)} \tag{9}$$

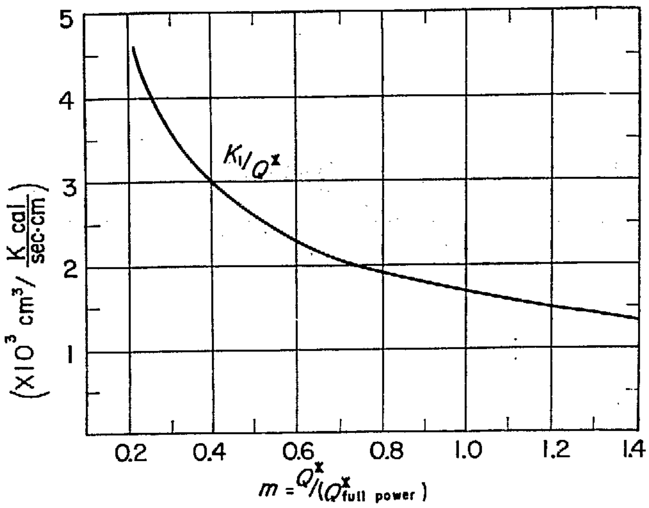

Fig. 3. 1 Power dependence of K_1/Q^*

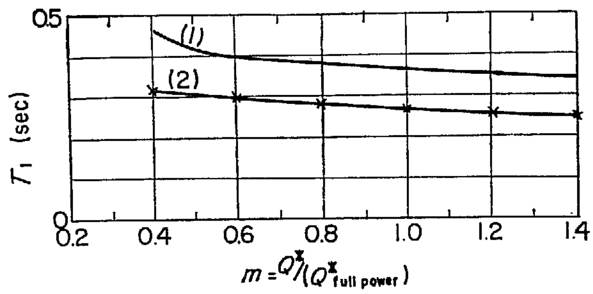

(1) Approximation by gain characteristics
(2) Approximation by 45°-phase-lag
× Approximation by step response

Fig. 3. 2 Power dependence of T_1

where

$$x_1(y_2)=\frac{c+\sqrt{c^2+8\left(\frac{\pi}{2}-1\right)(a+1)\ln y_2}}{4(a+1)},$$

$$a=\frac{y_2-1}{y_2\ln y_2}, \quad \text{and} \quad c=\pi+2-\ln y_2-\frac{y_2-1}{y_2}.$$

It can be seen that $x_1(y_2)$ is a slowly varing function of y_2 in the range of $y_2=1\sim3$. Thus one obtains a closely approximate formula of T_1 by expanding $x_1(y_2)$ at $y_2=2$ into a series,

$$T_1=\tau_{12}(0.3816+0.0109y_2) \qquad (10)$$

Using the parameter values of K_1 and T_1 obtained from Eqs. (7) and (10), the response of a single time constant delay given in Eq. (6) to the step change in $\delta Q/Q^*$ is also shown by the dotted line in **Fig. 2.** The approximate step response crosses the theoretical step response closely at 63.2% of the final value, and this result indicates that the 45°-phase-lag method is satisfactory.

In order to facilitate the calculation of K_1, the function of y_2 in Eq. (7) is given in **Fig. 4.** From Eqs. (7) and (10), several important conclusions can be derived.

(1) The time constant of the whole void volume in the boiling region for power change is roughly 40% of the void transit time, τ_{12}, from the boiling boundary to the top of the core.

(2) The time constant T_1 is almost independent of the power level. This is also con-

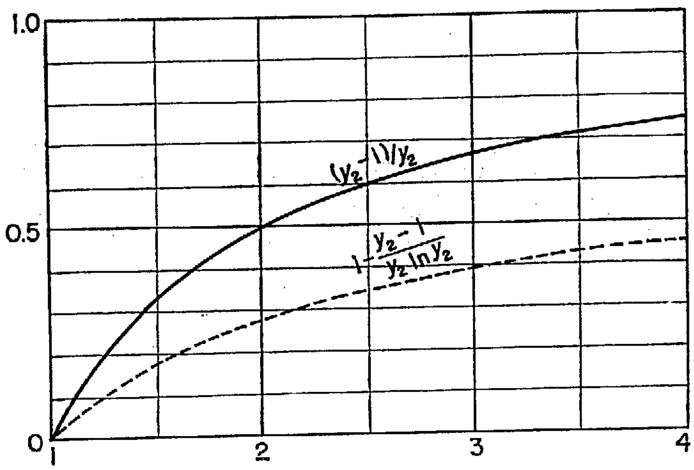

Fig. 4 Functions of y_2

sistent with experimental results on EBWR[2]. T_1 is plotted in **Fig. 3. 2** as a function of the power level based on the JPDR data (absolute pressure=62. 5 kg/cm^2), where the inlet velocity and the boiling boundary are assumed to be independent of the power level. The above assumptions may be justified by experimental data on EBWR[2].

(3) The dynamic behavior of core void does not change when power level and pressure are proportionally changed. Suppose that a reactor is operated at a power level Q_1 and pressure p_1, and the dynamic behavior of the reactor at $2Q_1$ and p_1 is desired, then the similar behavior is obtained by operating the reactor at Q_1 and $p_1/2$.

This conclusion is quite important and useful, and also consistent with the measured transfer functions of EBWR[2].

The above conclusion can be derived as shown below.

The important parameters in Eqs. (7) and (10) are τ_{12} and y_2. The defininitions of these parameters are repeated here for convenience,

$$\tau_{12}=\tau_e \cdot \ln y_2 \tag{11}$$

$$y_2=1+\frac{z_2-z_1}{V_0^* \cdot \tau_e} , \tag{12}$$

where $$\tau_e=\frac{1}{Q^*}\left(\frac{\Delta i}{\Delta v}\right) .$$

Thus, τ_{12} and y_2 are functions of a single parameter, τ_e, assuming that the inlet velocity V_0^* and the boiling length (z_2-z_1) are constant. If τ_e is held constant, τ_{12} and y_2, thus K_1 and T_1, are held constant, assuming that $v_s/\Delta v$ in Eq. (7) is almost independent of pressure.

Thus the dynamic behavior of core void will be unchanged, so far as the single parameter τ_e is held constant.

$(\Delta i/\Delta v)$ is a parameter of saturated steam and saturated water properties, and is a function of pressure. This is plotted in **Fig. 5**, which shows that $(\Delta i/\Delta v)$ is almost proportional to pressure.

Thus, τ_e is held constant, when power, Q^*, and pressure, p, are proportionally changed.

(4) In order to investigate the dependence of the dynamic behavior upon the power level under a constant pressure, y_2 may be conveniently used instead of Q^*, since co-factors of K_1 and T_1 are functions of a single parameter y_2 and all the parameters concerning thermo-hydraulics and core dimensions are included in y_2.

The power dependence of y_2, $\ln y_2$, τ_e and τ_{12} is given in **Appendix 2** as a function of power level.

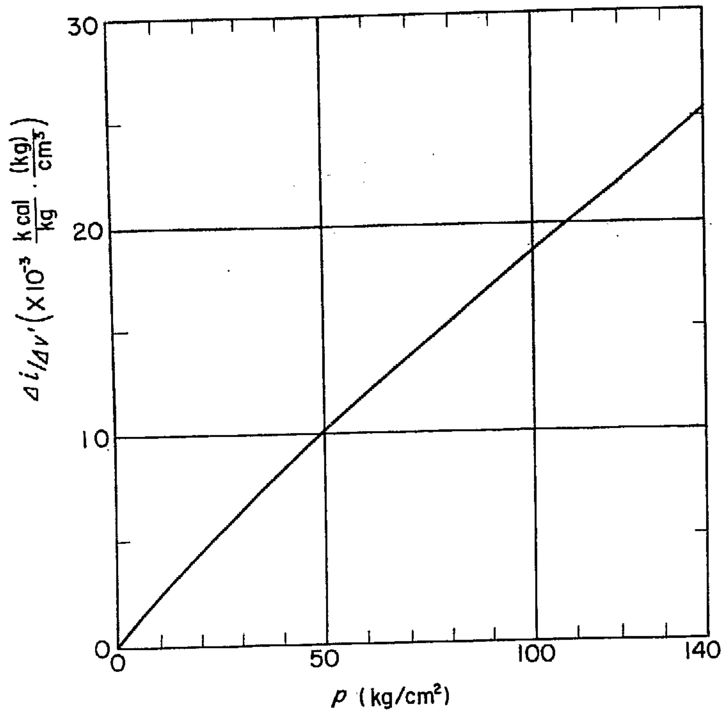

Fig. 5 Pressure dependence of $\Delta i/\Delta v'$

The approximate form of $G_1(s)$ for JPDR is thus obtained. From Eqs. (7) and (10), one obtains $K_1 = 1.21 \times 10^5$ cm³ and $T_1 = 0.2667$ sec, and

$$G_1(s) \simeq \frac{\delta \bar{V}}{\delta Q^*/Q^*} = \frac{1.21 \times 10^5}{1+0.27s} \quad \text{cm}^3 \tag{13}$$

The approximate frequency response of $G_1(s)$ by Eq. (13) is plotted in **Fig. 1** by the dotted line.

2.3.2 Inlet velocity to void transfer function, $G_2(s)$

The inlet velocity to void transfer function given in Eq. (28)* is

$$G_2(s) = \frac{\delta \bar{V}}{\delta V_0/V_0^*} = -G_1(s) \tag{28)*$$

Thus, $G_2(s)$ is equal to $G_1(s)$ with a reverse sign.

A single time constant approximation of $G_2(s)$ is also the same form as that of $G_1(s)$. It should be noted that the time constant of the whole void volume in the boiling region, when the inlet velocity changes, is also roughly 40% of the void transit time τ_{12}.

Thus, the approximate form of $G_2(s)$ for JPDR is

$$G_2(s) \simeq -\frac{K_1}{1+T_1 s} = -\frac{1.21 \times 10^5}{1+0.27s} \quad \text{cm}^3 \tag{14}$$

2.3.3 Boiling boundary shift to void transfer function, $G_3(s)$

The boiling boundary shift to void transfer function given in Eq. (29)* is

$$G_3(s) = \frac{\delta \bar{V}}{\delta z_1} = \left[\frac{v_s}{\Delta v} \frac{A_{co}}{y_2}\right] \frac{-1+y_2 e^{-\tau_{12}s}}{\tau_e s - 1} \tag{29)*$$

The frequency response of $G_3(s)$ at full power is calculated and shown in **Fig. 6**.

The response of $\delta \bar{V}$ to the step change to δz_1 is readily calculated from $G_3(s)$, resulting in

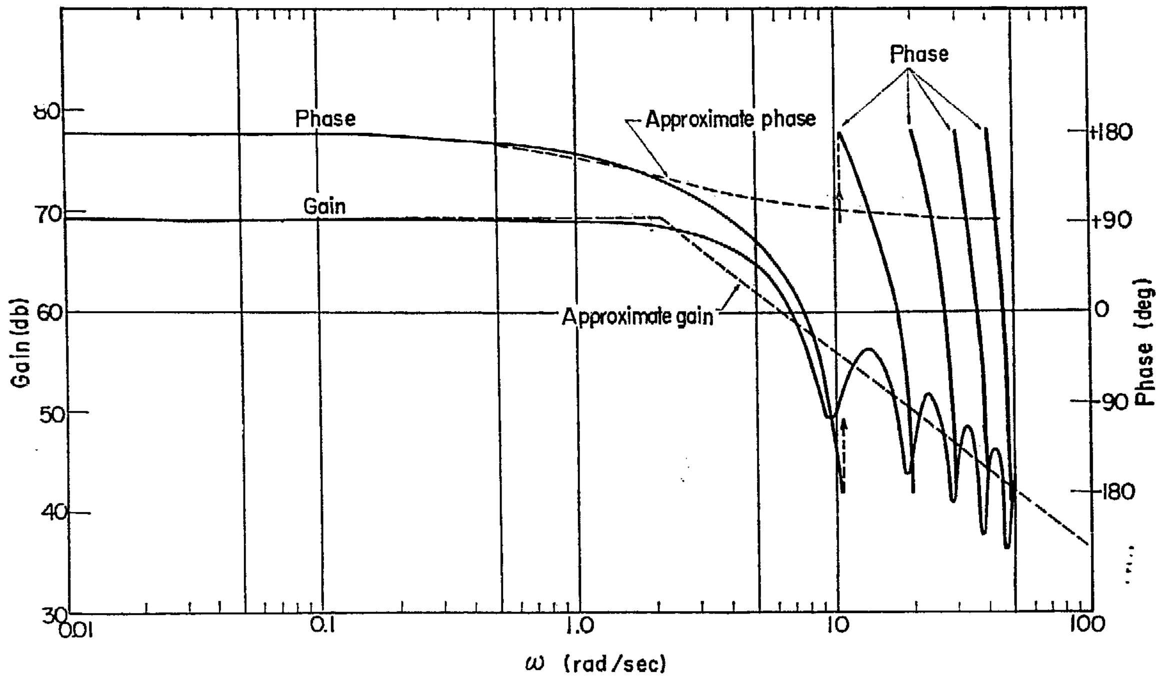

Fig. 6 Frequency characteristics of $G_3(s)$

$$\left.\begin{aligned}\delta\bar{V}(t) &= -\left(\frac{v_s}{\Delta v}\cdot A_{co}\right)\frac{1}{y_2}(e^{t/\tau_e}-1) && \text{for } 0<t\leq\tau_{12}\\ \delta\bar{V}(t) &= -\left(\frac{v_s}{\Delta v}\cdot A_{co}\right)\cdot\frac{y_2-1}{y_2} && \text{for } t\geq\tau_{12}\end{aligned}\right\} \qquad (15)$$

The step response is plotted in **Fig. 7**.

From **Fig. 6** and **Fig. 7**, it can be seen that the response of $G_3(s)$ may also be roughly approximated by a single time constant delay in the form of

$$G_3(s) = \frac{K_3}{1+T_3 s} \qquad (16)$$

K_3 is easily obtained as below.

$$K_3 = \lim_{s\to 0} G_3(s) = -\left(\frac{v_s}{\Delta v}A_{co}\right)\frac{y_2-1}{y_2} \qquad (17)$$

It should be noted that the static gain K_3 slowly increases with increasing power level, since $(y_2-1)/y_2$ increases with increasing y_2.

In order to facilitate the calculation of K_3, $(y_2-1)/y_2$ is also plotted in **Fig. 4**.

For obtaining the approximate formula of the single time constant T_3, the 45°-phase-lag method is also adopted in the same way as in the case of T_1. In this method one obtains

$$T_3 = \frac{1}{\omega_3} = \frac{\tau_{12}}{x_3(y_2)} \qquad (18)$$

where

$$x_3(y_2) = \frac{1}{2}\left\{\left(\frac{\pi}{2}-b\right)+\sqrt{\left(\frac{\pi}{2}-b\right)^2+c}\right\},$$

$$b = \ln y_2 - \frac{y_2-1}{y_2}$$

and $$c = 4\left(\frac{\pi}{2}-1-\frac{1}{y_2}\right)\ln y_2$$

It can be seen that $x_3(y_2)$ is a slowly varying function of y_2 in the range of $y_2=1\sim3$. Thus, one obtains an approximate formula of T_3 by expanding $x_3(y_2)$ at $y_2=2$ into a series,

$$T_3=\tau_{12}(0.6080+0.050y_2) \tag{19}$$

Using the parameter values of K_3 and T_3 obtained from Eqs. (17) and (19), the response of a single time constant delay given in Eq. (16) to the step change in δz_1 is also shown in **Fig. 7** by the dotted line. The approximate step response crosses the theoretical step response closely at 63.2% of the final value.

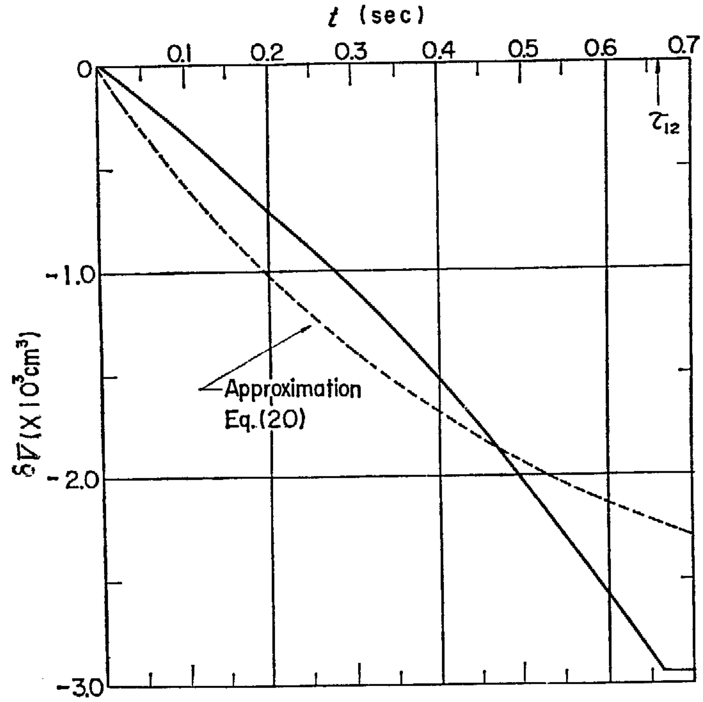

Fig. 7 Response of void to step change in δz_1 (calculated from $G_3(s)$ of Eq. (29)*)

From Eqs. (17) and (19) important conclusions can be derived.

(1) The time constant of the whole void volume in the boiling region, when the boiling boundary shifts, is roughly 70% of the void transit time τ_{12}. It should be noted that T_3 is roughly 1.7 times larger than T_1, since the boiling boundary shift to void effect acts on the bottom of the boiling region, while the power to void effect acts on the whole boiling region.

(2) The time constant T_3 is almost independent upon the power level. T_3 is plotted in **Fig. 8** as a function of the power level.

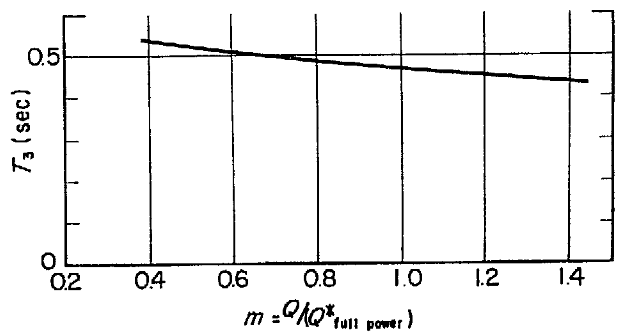

Fig. 8 Power dependence of T_3

(3) From Eqs. (16) and (19) is obtained the same conclusion as the (3) of conclusion in Section **2.3.1**, i.e., the similar dynamic behavior of boiling boundary shift to void is obtained

when power level and pressure are proportionally changed.

The approximate from of $G_3(s)$ for JPDR is obtained from Eqs. (17) and (19).

$$K_3=-2.94\times 10^3 \quad \mathrm{cm^3/cm},$$
$$T_3=0.4664 \quad \mathrm{sec},$$
$$G_3(s)\simeq -\frac{2.94\times 10^3}{1+0.466s}\ \mathrm{cm^3/cm} \tag{20}$$

The approximate frequency and step responses of $G_3(s)$ by Eq. (20) are plotted in **Fig. 6** and **Fig. 7**, respectively, by the dotted lines.

The comparison with the exact calculations shows this approximation is satisfactory.

2.3.4 Pressure to void transfer function, $G_4(s)$

The pressure to void transfer function given in Eq. (30)* is

$$G_4(s)=\frac{\delta\bar{V}}{\delta p}=-\frac{v_s}{\Delta v}\tau_e V_0{}^*A_{co}\Big[\frac{v_w}{v_s}(C'-D')(y_2-1-\ln y_2)+D'\ln y_2$$
$$+(A'-C')\left(1-\frac{1}{y_2}\right)-E\frac{\ln y_2}{y_2}+(A'-C'-D')\frac{\tau_{12}}{\tau_e}\frac{1-e^{-\tau_{12}s}}{\tau_{12}s}$$
$$+\frac{1}{\tau_e s-1}\left\{F\left(\frac{1}{y_2}-e^{-\tau_{12}s}\right)-E\frac{\ln y_2}{y_2}\right\}+\frac{E}{(\tau_e s-1)^2}\left(\frac{1}{y_2}-e^{-\tau_{12}s}\right)\Big] \tag{30*}$$

The frequency response of $G_4(s)$ at full power is calculated and shown in **Fig. 9**.

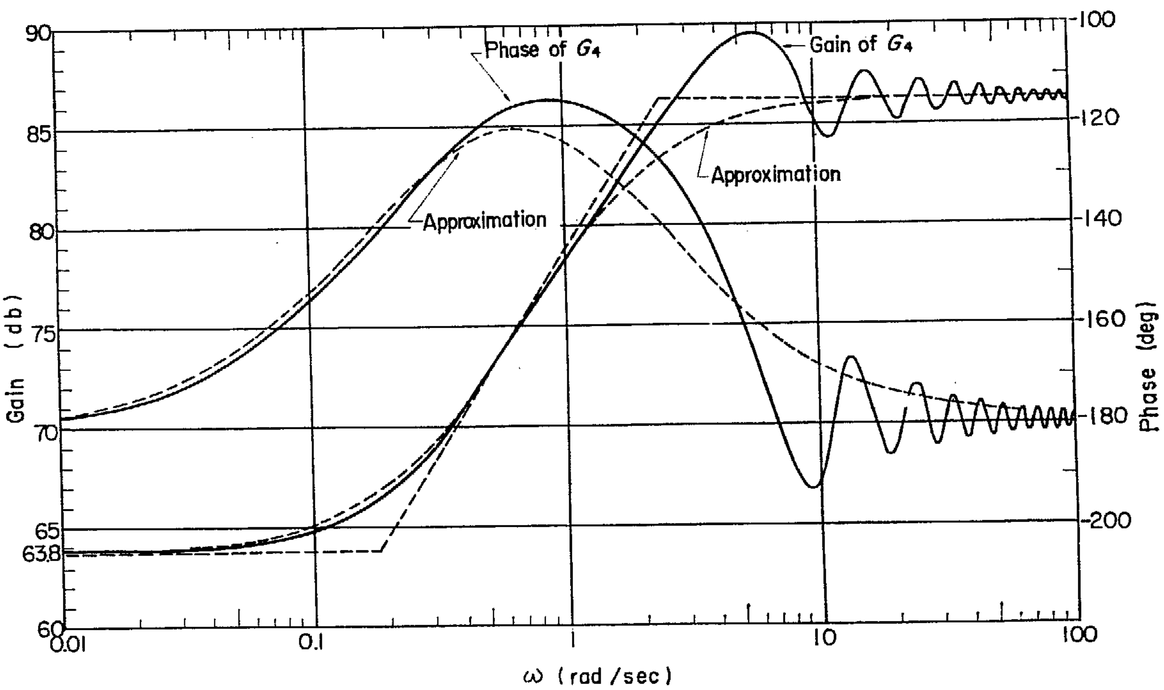

Fig. 9 Frequency characteristics of $G_4(s)$

The first term in brackets in Eq. (30)* may be ignored, since it is 0.8% of the sum of the other constant terms at full power and 3% at 150% full power. Thus, omitting this term, one obtains

$$G_4(s)=-\frac{v_s}{\Delta v}V_0{}^*A_{co}\cdot\tau_{12}\Big[D'+(A'-C')\frac{y_2-1}{y_2\ln y_2}-\frac{E}{y_2}+(A'-C'-D')\frac{1-e^{-\tau_{12}s}}{\tau_{12}s}$$
$$+\frac{1}{\tau_e s-1}\left(F\frac{1-y_2e^{-\tau_{12}s}}{y_2\ln y_2}-\frac{E}{y_2}\right)+\frac{E}{(\tau_e s-1)^2}\,\frac{1-y_2e^{-\tau_{12}s}}{y_2\ln y_2}\Big] \tag{21}$$

The reponse of $\delta\bar{V}$ to the step change in δp is readily calculated from $G_4(s)$, resulting in

$$\delta\bar{V}(t)=-\frac{v_s}{\Delta v}V_0{}^*A_{co}\cdot\tau_{12}\Big[a'+(A'-C'-D')\frac{t}{\tau_{12}}+\Big(\frac{F}{y_2\ln y_2}-\frac{E}{y_2}\Big)(e^{t/\tau_e}-1)$$

$$+\frac{E}{y_2\ln y_2}\Big\{\Big(\frac{t}{\tau_e}-1\Big)e^{t/\tau_e}+1\Big\}\Big] \quad \text{for} \quad 0<t\leq\tau_{12} \qquad (22)$$

and

$$\delta\bar{V}(t)=-\frac{v_s}{\Delta v}V_0{}^*A_{co}\cdot\tau_{12}(A'-C')\Big(1-\frac{y_2-1}{y_2\ln y_2}\Big) \quad \text{for} \quad t\geq\tau_{12}$$

where $a'=D'+(A'-C')\dfrac{y_2-1}{y_2\ln y_2}-\dfrac{E}{y_2}$.

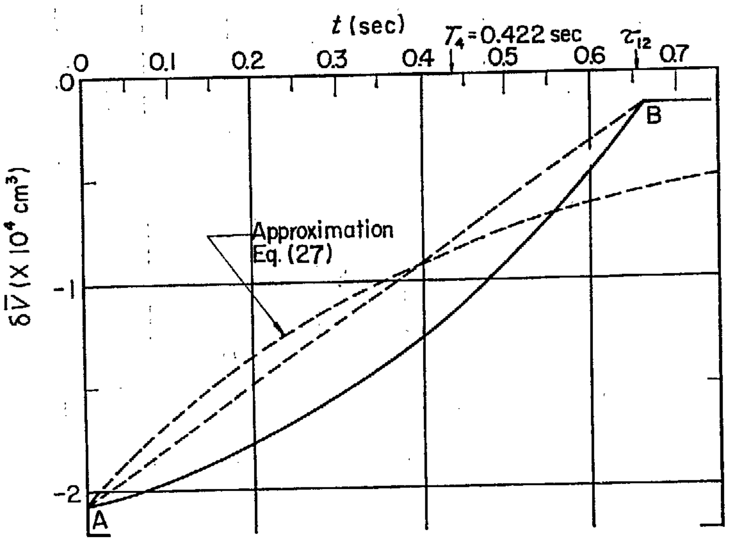

Fig. 10 Response of void to step change in δp (calculated from $G_4(s)$ of Eq. (30)*)

The step response is plotted in **Fig. 10**. From **Fig. 9** and **Fig. 10**, it can be seen that the response of $G_4(s)$ may be roughly approximated by a single time constant delay in the form of

$$G_4(s)\simeq a+\frac{c}{1+T_4s}=b\frac{1+\frac{a}{b}T_4s}{1+T_4s} \qquad (23)$$

where $b=a+c$

a is the step change in $\delta\bar{V}$ at $t=0$, i.e. the initial value, and b is the final value of $\delta\bar{V}$ in **Fig. 10**. Thus, a, b and c are obtained from $G_4(s)$ as

$$a=-\frac{v_s}{\Delta v}V_0{}^*A_{co}\cdot\tau_{12}\Big[D'+(A'-C')\frac{y_2-1}{y_2\ln y_2}-\frac{E}{y_2}\Big]$$

$$b=-\frac{v_s}{\Delta v}V_0{}^*A_{co}\cdot\tau_{12}(A'-C')\Big(1-\frac{y_2-1}{y_2\ln y_2}\Big) \qquad (24)$$

$$c=-\frac{v_s}{\Delta v}V_0{}^*A_{co}\cdot\tau_{12}\Big[(A'-C'-D')-2(A'-C')\frac{y_2-1}{y_2\ln y_2}+\frac{E}{y_2}\Big]$$

The values of a and b are plotted as a function of power level in **Fig. 11**. The value of a decreases appreciably with increasing power level; the transient overshoot of the step response becomes smaller, i.e. the void becomes harder as the power level increases.

In order to obtain the approximate formula of T_4, $G_4(s)$ is first approximated by a transfer function with a step response of straight line between point A and B in **Fig. 10**.

The first approximation is

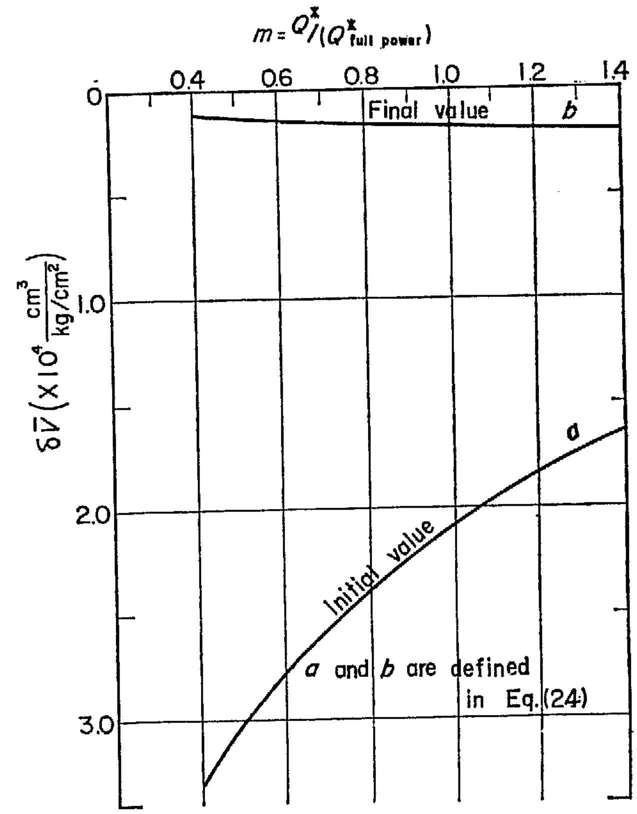

Fig. 11 Power dependence of a and b

$$G_4(s) \simeq a + c\frac{1-e^{-\tau_{12}s}}{\tau_{12}s} \tag{25}$$

The above equation is further approximated in the form of Eq. (23), where the time constant T_4 is determined by the 45°-phase-lag method applied to $(1-e^{-\tau_{12}s})/\tau_{12}s$.

The result is

$$T_4 = \frac{2}{\pi}\tau_{12} = 0.637\tau_{12} \tag{26}$$

Several important conclusions are derived.

(1) The time constant of the whole void volume in the boiling region for pressure change is roughly 60% of the void transit time τ_{12}.

(2) The time constant T_4 is almost independent of power level and is plotted in **Fig. 12** as a function of power level.

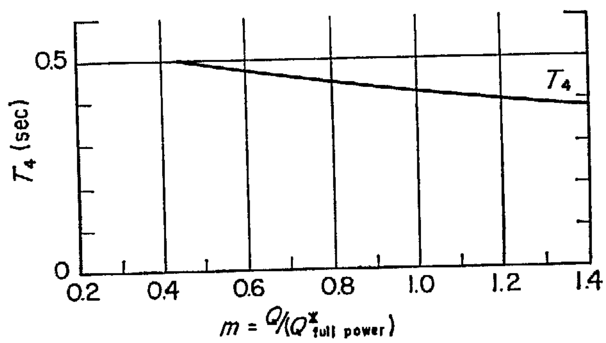

Fig. 12 Power dependence of T_4

The approximate form of $G_4(s)$ for JPDR is obtained from Eqs. (23), (24) and (26), giving

$$a = -0.2076\times10^5 \quad \mathrm{cm^3/kg/cm^2}$$
$$b = -0.0171\times10^5 \quad \text{〃}$$
$$c = 0.1905\times10^5 \quad \text{〃}$$
$$T_4 = 0.4215 \quad \mathrm{sec}$$

and

$$G_4(s) \simeq \left(-0.2076 + \frac{0.1905}{1+0.4215s}\right)\times10^5$$

$$= -0.0171\times10^5 \frac{1+5.117s}{1+0.422s}\ \frac{\mathrm{cm^3}}{\mathrm{kg/cm^2}} \tag{27}$$

The approximate frequency and step responses of $G_4(s)$ by Eq. (27) are plotted in **Fig. 9** and **Fig. 10**, respectively, by the dotted line.

The comparison with the exact calculations shows this approximation is satisfactory.

2.4 Core Boiling Boundary Transfer Functions

The core boiling boundary transfer functions, $G_5(s)$, $G_6(s)$, $G_7(s)$ and $G_8(s)$, which relate boiling boundary to the power, to the inlet velocity, to the inlet enthalpy and to the system pressure, respectively, have been given in JAERI-1044. Some of their characteristics and simplifications are given below.

2.4.1 Power to boiling boundary transfer function, $G_5(s)$

The power to boiling boundary transfer function given in Eq. (39a)* is

$$G_5(s) = \frac{\delta z_1}{\delta Q/Q^*} = -(z_1 - z_0)\frac{1-e^{-\tau_{01}s}}{\tau_{01}s} \qquad \text{(39a)*}$$

The frequency response of $G_5(s)$ is calculated and shown in **Fig. 13.** $G_5(s)$ is almost independent of the power level, since the non-boiling length $(z_1 - z_0)$ and the inlet velocity V_0^*, thus τ_{01}, are considered independent of power level.

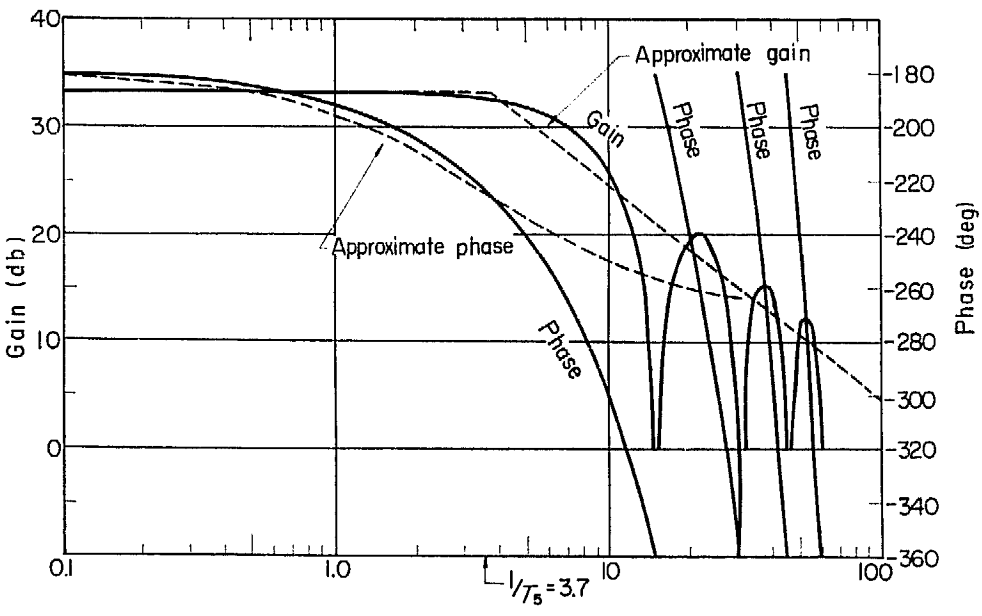

Fig. 13 Frequency characteristics of $G_5(j\omega)$

The response of δz_1 to the step change in $\delta Q/Q^*$ is readily calculated.

$$\left.\begin{aligned} &\delta z_1(t) = -(z_1-z_0)\,t/\tau_{01} && \text{for } 0<t\leq\tau_{01} \\ \text{and}\quad &\delta z_1(t) = \text{const} = -(z_1-z_0) && \text{for } t\geq\tau_{01} \end{aligned}\right\} \tag{28}$$

The step response is plotted in **Fig. 14**. Thus, 1% change in $\delta Q/Q^*$ results in -0.465 cm change in δz_1.

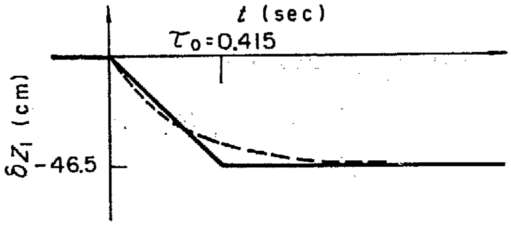

Fig. 14 Response of δz_1 to step change in $\delta Q/Q^*$ (calculated from Eq. (28))

$G_5(s)$ may be approximated by a single time constant delay in the form of

$$G_5(s) \simeq \frac{K_5}{1+T_5 s} \tag{29}$$

K_5 is readily obtained as

$$K_5 = -(z_1 - z_0) \tag{30}$$

T_5 is also obtained by the 45°-phase-lag method applied to $1/(1+T_5 s)$.

$$T_5 = \frac{2}{\pi}\tau_{01} = 0.6366\tau_{01} \tag{31}$$

It can be seen that the timeconstant T_5 is almost 64% of the flow transit time τ_{01} in non-boiling region.

The approximate form of $G_5(s)$ for JPDR is thus obtained,

$$K_5 = -46.5 \quad \text{cm},$$

$$T_5 = 0.6366 \times 0.415 = 0.27 \quad \text{sec},$$

$$G_5(s) = -\frac{46.5}{1+0.27s} \quad \text{cm} \tag{32}$$

The approximate frequency response is plotted in **Fig. 13** by the dotted line, and the approximate step response in **Fig. 14**.

2.4.2 Inlet velocity to boiling boundary transfer function, $G_6(s)$

The inlet velocity to boiling boundary transfer function given in Eq. (39b)* is

$$G_6(s) = \frac{\delta z_1}{\delta V_0/V_0^*} = -G_5(s) \tag{39b)*}$$

Thus, $G_6(s)$ is equal to $G_5(s)$ with a reverse sign.

A single time constant approximation of $G_6(s)$ is also the same form as that of $G_5(s)$. Thus, the approximate form of $G_6(s)$ for JPDR is

$$G_6(s) \simeq -\frac{K_5}{1+T_5 s} = \frac{46.5}{1+0.27s} \quad \text{cm} \tag{33}$$

2.4.3 Inlet enthalpy to boiling boundary transfer function, $G_7(s)$

The inlet enthalpy to boiling boundary transfer function given in Eq. (39c)* is

$$G_7(s) = \frac{\delta z_1}{\delta i_0} = -(z_1 - z_0)\frac{\rho_w}{\tau_{01} Q^*} e^{-\tau_{01}s} = K_7 e^{-\tau_{01}s} \tag{39c)*}$$

where K_7 is equal to $-(z_1 - z_0)\frac{\rho_w}{\tau_{01} Q^*}$.

This function is very simple and represents a pure delay. However, it should be noted that it is not easy to simply simulate a pure delay on an analog computer.

It should be also noted that the gain of $G_7(s)$ is inversely proportional to the power Q^*, since τ_{01} is almost independent of power level.

The numerical form of $G_7(s)$ for JPDR is

$$G_7(s) = -7.07e^{-0.415s} \quad \mathrm{cm} \Big/ \frac{\mathrm{kcal}}{(\mathrm{kg})} \tag{34}$$

This transfer function shows that the temperature change 1°C in the inlet subcooled water results in -8.5 cm change in the boiling boundary, since the enthalpy gradient to temperature at the operating condition is nearly 1.2 kcal/°C.

2.4.4 Pressure to boiling boundary transfer function, $G_8(s)$

The pressure to boiling boundary transfer function given in Eq. (39d)* is

$$G_8(s) = \frac{\delta z_1}{\delta p} = (z_1 - z_0)\frac{\tau_e}{\tau_{01}}B' = K_8 \tag{39d)*}$$

This transfer function is constant. However, it is almost proportional to τ_e, thus, depends upon power level appreciably, since τ_{01} and $(z_1 - z_0)$ are almost independent of power level.

In Eq. (39d)* the second term is neglected, which is given in Eq. (39)* by

$$-(z_1 - z_0)\frac{D}{v_w}\cdot\frac{1 - e^{-\tau_{01}s}}{\tau_{01}s} \tag{35}$$

This term is about 1% of the first term. The physical interpretation of these terms is as follows. The first term, Eq. (39d)*, represents the effect of change in saturation temperature, and the second term the effect of change in mass flow at boiling boundary, caused by water density change directly due to pressure change.

The response of δz_1 to the step change in δp is shown in **Fig. 15**, where the first term response is plotted by the dotted line and the combined response of the first and second terms by the solid line.

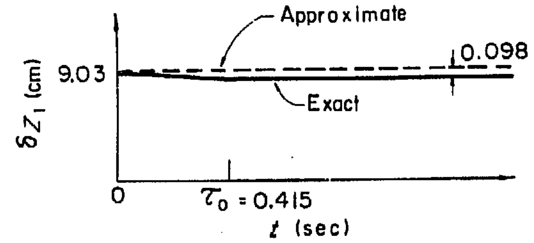

Fig. 15 Response of δz_1 to step change in δp (calculated from Eq. (39d)* and Eq. (35))

The numerical value of $G_8(s)$ for JPDR is calculated from Eq. (39 d)*.

$$G_8(s) = 9.03 \quad \mathrm{cm} \Big/ \frac{\mathrm{kg}}{\mathrm{cm}^2} \tag{36}$$

2.5 Vessel Pressure Transfer Function

Vessel pressure transfer functions, $G_{16}(s)$, $G_{17}(s)$, $G_{18}(s)$ and $G_{19}(s)$, which relate the vessel pressure to the steam flow to load, to the feedwater flow, to the power and to the feedwater enthalpy, respectively, have been derived in JAERI-1044 by a distributed parameter model.

In order to obtain the physical interpretation and the simplification of these transfer functions, some modifications are made.

The energy flow balance is obtained, by multiplying Eq. (62)* by $\Delta i/\Delta v$.

$$H_{pr}\cdot s\cdot\delta p = (z_2 - z_1)\delta Q - \Delta i\cdot\delta W_L + \frac{v_w}{\Delta v}\cdot\Delta i\cdot\delta W_f - Q^*\delta z_1 \tag{37}$$

Here, H_{pr} is defined as

$$H_{pr}=\frac{\Delta i}{\Delta v}\cdot A_{pr}=(H_{pr})_{ves}+(H_{pr})_{co}, \tag{38}$$

where
$$(H_{pr})_{ves}=\{M_s^*(A+B)+M_w^*B\}-\frac{\Delta i}{\Delta v}\{M_s^*(C+D)+M_w^*D\}-\frac{\bar{V}_{sat}}{J},$$

$$(H_{pr})_{co}=\frac{\Delta i}{\Delta v}V_0^*E(\tau_{23}-\tau_{12})-\frac{\Delta i}{\Delta v}V_0^*(C'-A')\{\tau_c(y_2-1)+\tau_{23}y_2\}$$

B_{pr} is ignored in deriving Eq. (37) as it is small compared with A_{pr} and almost 0.6% of the A_{pr}.

The physical interpretation of Eq. (37) is of interest. Each term on the right-hand side represents the energy flow into the vessel through the external disturbances; δz_1 is considered as an external disturbance although it is affected by δQ, δV_0, δi_0 and δp.

The first term is the power change in the boiling region, the second is the energy flow carried by the steam flow to load, the third is the energy flow carried by the feedwater flow and the fourth is the power change caused by the boiling boundary shift. The mismatch of these energy flows is balanced by the change rate in the energy content inside the constant volume of the vessel, resulting in pressure change. Thus, H_{pr} represents a derivative of the energy content inside the vessel with respect to pressure.

$(H_{pr})_{ves}$ is associated with saturated steam and water in the vessel excluding the core and riser, and is determined only by the masses and properties of steam and water. The first term is associated with the heat content of steam and water, and the second term with the energy change due to steam flashing and condensation.

$(H_{pr})_{co}$ is associated with the core and riser, determined by the thermo-hydraulic parameters and core dimensions.

It should be noted that $(H_{pr})_{co}$ may be ignored as it is small compared with $(H_{pr})_{ves}$ and of the order of 1% of $(H_{pr})_{ves}$ as shown below in the numerical calculation for JPDR.

It is evident that G_{pr} in terms of H_{pr} is

$$G_{pr}=\frac{\Delta i}{\Delta v}\cdot\frac{1}{H_{pr}}\cdot\frac{1}{s} \tag{39}$$

Thus, the simplified vessel pressure transfer functions are obtained as

$$G_{16}=\frac{\delta p}{\delta W_L}=-\Delta i\cdot\frac{1}{H_{pr}s}=G_{16}'\cdot\frac{1}{H_{pr}s} \tag{40}$$

$$G_{17}=\frac{\delta p}{\delta W_f}=\frac{v_w}{\Delta v}\cdot\Delta i\cdot\frac{1}{H_{pr}s}=G_{17}'\cdot\frac{1}{H_{pr}s} \tag{41}$$

$$G_{18}=\frac{\delta p}{\delta Q/Q^*}=(z_2-z_1)Q^*\frac{1}{H_{pr}s}=G_{18}'\cdot\frac{1}{H_{pr}s} \tag{42}$$

$$G_{19}=\frac{\delta p}{\delta z_1}=-Q^*\cdot\frac{1}{H_{pr}s}=G_{19}'\cdot\frac{1}{H_{pr}s} \tag{43}$$

The modified block diagram is obtained by the above functions, as shown in **Fig. 16.** G_{16}', G_{17}', G_{18}' and G_{19}' are the newly defined functions indicated in the diagram.

It should be noted that G_{16}' and G_{17}' are independent of power level, and G_{18} and G_{19} are proportional to power level.

It should be also noted that G_{17} may be ignored as it is small, since the major part of the effect of δW_f is the path through δi_0 and δz_1 to δp, i.e. $G_{19}\cdot G_7\cdot G_{22}$ as shown in **Fig. 21.** G_{17} is of the order of 5% of the $G_{19}\cdot G_7\cdot G_{22}$.

The numerical values of those transfer functions for JPDR are;

$G_{16}'=-\Delta i=-373.4$ kcal/(kg)

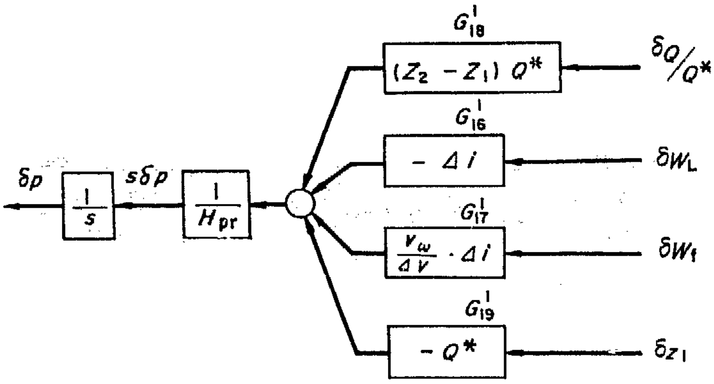

H_{pr} is defined in Eq.(38)

Fig. 16 Block diagram of modified vessel pressure transfer function

$$G_{17}' = \frac{v_w}{\Delta v}\cdot \Delta i = 16.19 \qquad \text{kcal/(kg)}$$

$$G_{18}' = (z_2 - z_1)Q^* = 7.4\times 10^3 \qquad \text{kcal/sec}$$

$$G_{19}' = -Q^* = -70.80 \qquad \text{kcal/sec}\cdot\text{cm}$$

$$H_{pr} = (H_{pr})_{ves} + (H_{pr})_{co} = (4.814\times 10^3) + (4.4\times 10)$$

$$= 4.86\times 10^3 \qquad \text{kcal}\Big/\frac{\text{kg}}{\text{cm}^2}$$

2.6 Inlet Water Enthalpy Transfer Function

Inlet water enthalpy transfer functions, $G_{21}(s)$, $G_{22}(s)$, $G_{23}(s)$ and $G_{24}(s)$, which relate the inlet water enthalphy at the core inlet to the recirculation flow, to the feed water flow, to the pressure and to the feed water enthalpy, respectively, have been derived in JAERI-1044 by a distributed parameter model.

These transfer functions are

$$G_{21} = \frac{\delta i_0}{\delta W_R} = \frac{W_f^*}{W_0^*}\,\frac{i_w - i_f}{W_R^* + W_f^*}e^{-\tau_d s} = K_{21}e^{-\tau_d s} \tag{69a)*}$$

$$G_{22} = \frac{\delta i_0}{\delta W_f} = -\frac{W_R^*}{W_0^*}\,\frac{i_w - i_f}{W_R^* + W_f^*}e^{-\tau_d s} = K_{22}e^{-\tau_d s} \tag{69b)*}$$

$$G_{23} = \frac{\delta i_0}{\delta p} = \frac{W_R^*}{W_0^*}Be^{-\tau_d s} + \frac{1}{W_0^*}\,\frac{\bar{V}_{sub}}{J}\,s = K_{23}e^{-\tau_d s} + K_{23}'s \tag{69c)*}$$

$$G_{24} = \frac{\delta i_0}{\delta i_f} = \frac{W_f^*}{W_0^*}e^{-\tau_d s} = K_{24}e^{-\tau_d s} \tag{69d)*}$$

where K_{21} through K_{24} are newly-defined parameters and their definitions are evident.

It should be noted that they are very simple and include pure delay terms, which, however, are not simply simulated on an analog computer.

$G_{21}(s)$ and $G_{24}(s)$ are proportional to power level, assuming that W_0^* is independent of power level and W_f^* is almost equal to W_L^* which is proportional to power level.

On the other hand, $G_{22}(s)$ and $G_{23}(s)$ little depend on power level, since the following relations hold:

$$W_R^* = W_0^* - W_f^* = W_0^* - W_L^*$$

and W_f^* is almost 4% of W_0^* at full power. Thus, these transfer functions may be assumed to be independent of power level. However, this is not the case when a reactor is operated with a greater exit quality at full power.

The numerical forms of inlet water enthalphy transfer functions for JPDR are readily calculated.

$$G_{21}(s)=\frac{\delta i_0}{\delta W_R}=0.01385e^{-12s} \qquad \frac{\text{kcal/(kg)}}{\text{(kg)/sec}}$$

$$G_{22}(s)=\frac{\delta i_0}{\delta W_f}=-0.315e^{-12s} \qquad \frac{\text{kcal/(kg)}}{\text{(kg)/sec}}$$

$$G_{23}(s)=\frac{\delta i_0}{\delta p}=1.23e^{-12s}+0.489s \qquad \frac{\text{kcal/(kg)}}{\text{kg/cm}^2}$$

$$G_{24}(s)=\frac{\delta i_0}{\delta i_f}=0.042e^{-12s} \qquad \text{——}$$

2.7 Inlet Velocity Transfer Function (Hydrodynamics)

The inlet velocity transfer functions, $G_V/G_v(s)$, $G_q(s)/G_v(s)$, $G_{s1}(s)/G_v(s)$ and $G_p(s)/G_v(s)$, which relate the inlet velocity to the void volume in the core, to the power, to the boiling boundary shift and to the system pressure, respectively, have been given in JAERI-1044.

It is concluded that

(1) A resonance tendency appears around $\omega=2$ in the gain characteristics of the inlet velocity transfer functions.

The resonance frequency of $\omega=2$ is roughly explained below. The transit time of variation around the natural circulation loop may be estimated roughly 3 sec, which is obtained by assuming that the transit time is equal to T_v' defind in Eq. (48). Thus, the resonance frequency is $2\pi/3\simeq2$ rad/sec.

(2) The effects of the inlet velocity transfer functions are considered to be very small.

However, some of their characteristics and simplifications are of interest and are given below. The pressure dependence of these transfer functions is not considered.

2.7.1 The characteristics and approximation of $1/G_v(s)$

$G_v(s)$ given in Eq. (54b)* is

$$G_v(s)=G_v^{01}+G_v^{12}+G_v^{23}+G_v^{34}+G_v^{45}+G_v^{50}+[FPD]' \qquad (54b)^*$$

Each term on the right-hand side is defined in Eqs. (41a)*, (42a)*, (43a)*, (45a)*, (46a)*, (47a)* and (54c)*, respectively.

The approximate transfer function of $G_v(s)$ may be obtained in the form of a single time constant.

$$G_v(s)\simeq K_v(1+T_v\cdot s) \qquad (44)$$

K_v and T_v are defined as

$$K_v=\left(\frac{\rho_w}{A_{co}}V_0^*\right)K_v', \qquad (45)$$

$$T_v=\frac{T_v'}{K_v'} \qquad (46)$$

where

$$K_v'=(y_2-1)\left(1+\mu\frac{\tau_{23}g}{y_2V_0^*}\right)+\frac{[FPD]'}{\frac{\rho_w}{A_{co}}V_0^*} \qquad (47)$$

$$T_v'=\tau_{01}+\tau_{12}+\mu^2(\tau_{23}+\tau_{34})+\mu^2_d\tau_{45}+\tau_{50} \qquad (48)$$

The above equations are obtained by finding the asymptotes to the gain characteristics of $G_v(s)$ for $s\rightarrow j0$ and $s\rightarrow j\infty$. In Eq. (47) the following term has been neglected as it is small compared to the remaining terms, i.e., $-\mu\left\{\mu(y_2+1)-\frac{g\tau_r}{y_2V_0^*}\right\}+2\mu^2_d$. Thus, K_v and T_v are simply expressed in terms of the design parameters.

The numerical values of K_v and T_v for JPDR are readily obtained, $K_v=0.902$(kg)/cm²·sec, and $T_v=0.24$ sec.

Thus, $$1/G_v(s)\simeq\frac{1.11}{1+0.24s}\ \text{cm}^2\cdot\text{sec/(kg)} \tag{49}$$

The gain and phase characteristics of $1/G_v(s)$ are shown in **Fig. 17**, where the approximate form of Eq. (49) is shown by the dotted line and the exact calculation of Eq. (54b)* by the solid line.

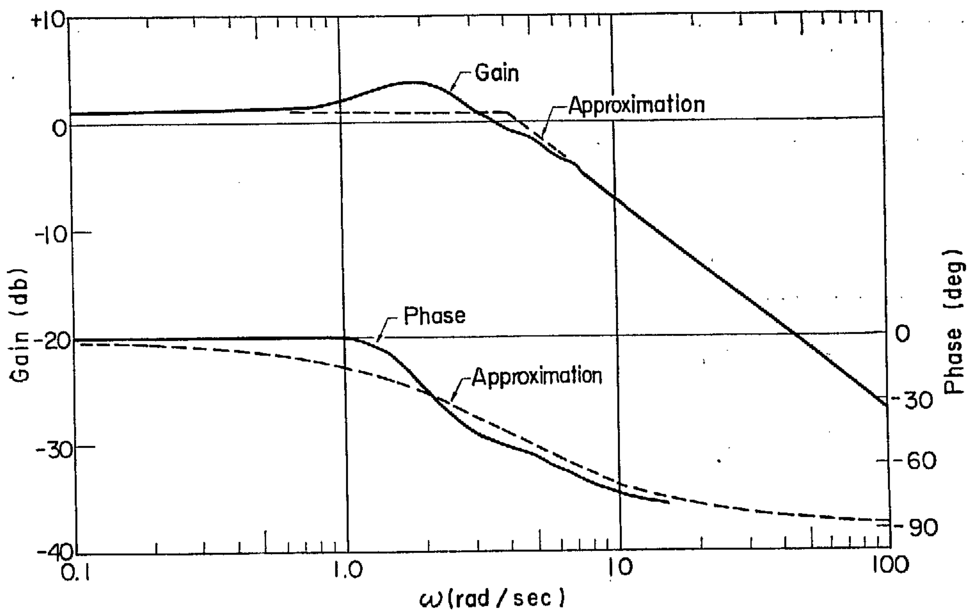

Fig. 17 Frequency characteristics of $1/G_v(s)$

It should be noted that a slight resonance peak in the gain characteristics is observed around $\omega=2$. It can be shown that this resonance peak becomes larger as the frictional pressure drop, i. e., $[FPD]'$ decreases.

2.7.2 Void to inlet velocity transfer function

The void in the core to inlet velocity transfer function is expressed as $G_V/G_v(s)$, where G_V is constant and equal to $g(\rho_w-\rho_s)\frac{1}{A_{co}^2}$.

Thus, the frequency characteristics of the void to inlet velocity transfer function are the same as $1/G_v(s)$.

It should be noted that the resonance peak appears in the exact gain characteristics of this transfer function as stated in the previous section.

This transfer function represents the process, in which the change in the inlet velocity is caused by driving head change of natural circulation due to the void volume change only in the core.

On the other hand, the change in void volume in the riser also results in the change in the driving head of natural circulation. These effects are included in the transfer functions which relate the inlet velocity to the power, to the boiling boundary shift, and to the system pressure.

The approximate form of the void to inlet velocity transfer function is

$$\frac{G_V(s)}{G_v(s)}=\frac{\delta V_0}{\delta \bar{V}}\simeq\frac{g(\rho_w-\rho_s)}{A_{co}{}^2K_v}\cdot\frac{1}{1+T_vs} \tag{50}$$

The numerical form of Eq. (50) for JPDR is readily obtained.

$$\frac{G_V(s)}{G_v(s)}=\frac{\delta V_0}{\delta \bar{V}}\simeq\frac{1.34\times10^{-4}}{1+0.24s}\quad \frac{\text{cm}}{\text{sec}}\Big/\text{cm}^3 \tag{51}$$

It can be seen from the physical understanding that the effect of this transfer function is very small since the inlet velocity change at steady state due to $10^3\,\text{cm}^3$ change in void volume in the core is calculated to be 0.134 cm/sec.

2.7.3 Power to inlet velocity transfer function

The power to inlet velocity transfer function is expressed as $G_q(s)/G_v(s)$, where $G_q(s)$ is given in Eq. (54d)*

$$G_q(s)=G_q{}^{12}+G_q{}^{23}+G_q{}^{34} \tag{54d*}$$

Each term on the right-hand side is defined in Eqs. (42c)*, (43b)* and (45b)*, respectively.

The approximate transfer function of $G_q(s)$ may be obtained also in the form of a single time constant.

$$G_q(s)\simeq K_q(1+T_qs) \tag{52}$$

K_q and T_q are defined as

$$K_q=\left(\frac{\rho_w}{A_{co}}V_0{}^{*2}\right)K_q' \tag{53}$$

$$T_q=\frac{T_q'}{K_q'} \tag{54}$$

where
$$K_q'=(y_2-1)\left\{\frac{\mu g}{y_2V_0{}^*}(\tau_{23}-\tau_r)-(1-\mu^2)\right\} \tag{55}$$

$$T_q'=-\left\{\tau_{12}\left(\frac{y_2-1}{\ln y_2}-1\right)+\mu^2(y_2-1)(\tau_{23}+\tau_{34})\right\} \tag{56}$$

It is evident that T_q is always negative.

The above equations are obtained in the same way as in the case of $G_v(s)$. Thus, K_q and T_q are simply expressed in terms of the design parameters.

By the use of Eq. (44), the approximate form of the power to inlet velocity transfer function is

$$\frac{G_q(s)}{G_v(s)}=\frac{\delta V_0}{\delta Q/Q^*}\simeq\frac{K_q}{K_v}\cdot\frac{1+T_qs}{1+T_vs}=V_0{}^*\frac{K_q'}{K_v'}\cdot\frac{1+T_qs}{1+T_vs} \tag{57}$$

The numerical values of K_q and T_q for JPDR are readily obtained, giving $K_q=14.5\,(\text{kg})/\text{cm}\cdot\text{sec}^2$ and $T_q=-0.45$ sec.

$$G_q(s)\simeq14.5(1-0.45s)\quad\frac{(\text{kg})}{\text{cm}\cdot\text{sec}^2} \tag{58}$$

$$\frac{G_q(s)}{G_v(s)}=\frac{\delta V_0}{\delta Q/Q^*}\simeq16.1\frac{1-0.45s}{1+0.24s}\quad\text{cm/sec} \tag{59}$$

The frequency characteristics of $G_q(s)/G_v(s)$ are shown in **Fig. 18**, where the approximate form of Eq. (59) is shown by the dotted line and the exact calculation of $G_q(s)/G_v(s)$ by the solid line.

It should be noted that an appreciable resonance peak in the exact gain characteristics of $G_q(s)/G_v(s)$ is observed around $\omega=2$.

It can be seen that the effect of this transfer function is very small, since 1% change in $\delta Q/Q^*$ at steady state results in 0.16 cm/sec change in δV_0.

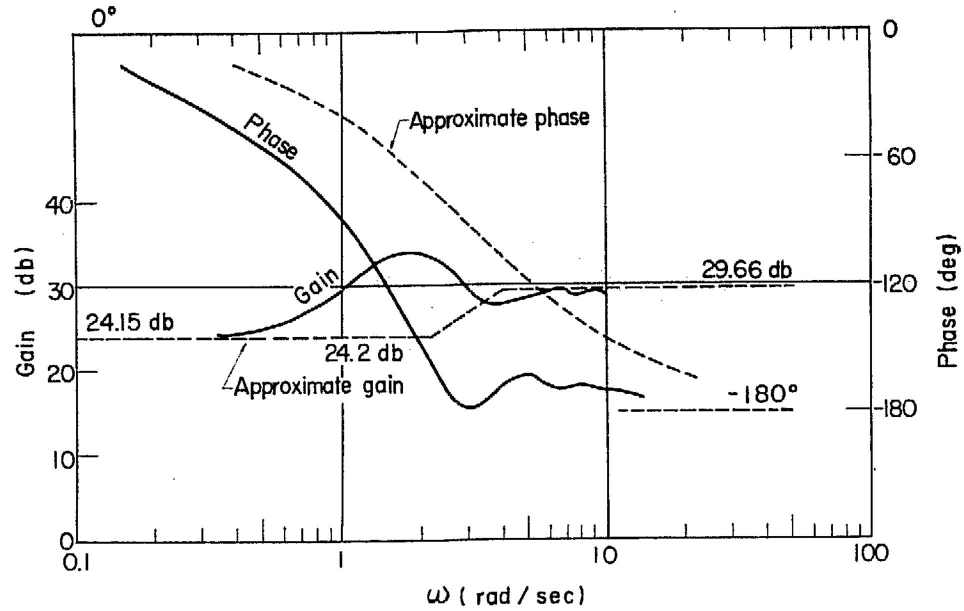

Fig. 18 The frequency characteristics of $\frac{\delta V_o}{\delta Q/Q^*}=G_q(s)/G_v(s)$

2.7.4 Boiling boundary shift to inlet velocity transfer function

The boiling boundary shift to inlet velocity transfer function is expressed as $G_{z1}(s)/G_v(s)$, where $G_{z1}(s)$ is given in Eq. (54e)*

$$G_{z1}(s)=G_{z1}^{01}+G_{z1}^{12}+G_{z1}^{23}+G_{z1}^{34} \tag{54e)*}$$

Each term on the right-hand side is defined in Eqs. (41b)*, (42d)*, (43c)* and (45c)*, respectively.

The approximate transfer function of $G_{z1}(s)$ may be obtained also in the form of a single time constant.

$$G_{z1}(s)\simeq K_{z1}(1+T_{z1}s) \tag{60}$$

K_{z1} and T_{z1} are defined as

$$K_{z1}=\left(\frac{\rho_w}{A_{co}}V_0^*\frac{1}{\tau_e}\right)K_{z1}' \tag{61}$$

$$T_{z1}=\frac{T_{z1}'}{K_{z1}'} \tag{62}$$

where $$K_{z1}'=-\frac{\mu g}{y_2V_0^*}(\tau_{23}-\tau_r)+(1-\mu^2) \tag{63}$$

$$T_{z1}'=\tau_{12}+\mu^2(\tau_{23}+\tau_{34})-\tau_e \tag{64}$$

It should be noted that T_{z1} is always negative.

The above equations are obtained in the same way as in the case of $G_v(s)$. Thus, K_{z1} and T_{z1} are simply expressed in terms of the design parameters.

By the use of Eq. (44), the approximate form of the boiling boundary shift to inlet velocity transfer function is

$$\frac{G_{z1}(s)}{G_v(s)}=\frac{\delta V_0}{\delta z_1}\simeq\frac{K_{z1}}{K_v}\frac{1+T_{z1}s}{1+T_vs}=\frac{K_{z1}'}{K_v'}\frac{1}{\tau_e}\frac{1+T_{z1}s}{1+T_vs} \tag{65}$$

The numerical values of K_{z1} and T_{z1} for JPDR are readily obtained, giving $K_{z1}=-0.140$ (kg)/cm^2·sec^2 and $T_{z1}=0.049$ sec.

$$G_{z1}(s)\simeq-0.14(1-0.049s)\quad\frac{\text{(kg)}}{\text{cm}^2\cdot\text{sec}^2} \tag{66}$$

$$\frac{G_{z1}(s)}{G_v(s)}=\frac{\delta V_0}{\delta z_1}\simeq -0.156\frac{1-0.049s}{1+0.24s}\quad\frac{1}{\text{sec}} \tag{67}$$

The frequency characteristics of $G_{z1}(s)/G_v(s)$ are shown in Fig. 19, where the approximate form of Eq. (67) is shown by the dotted line and the exact calculation of $G_{z1}(s)/G_v(s)$ by the solid line.

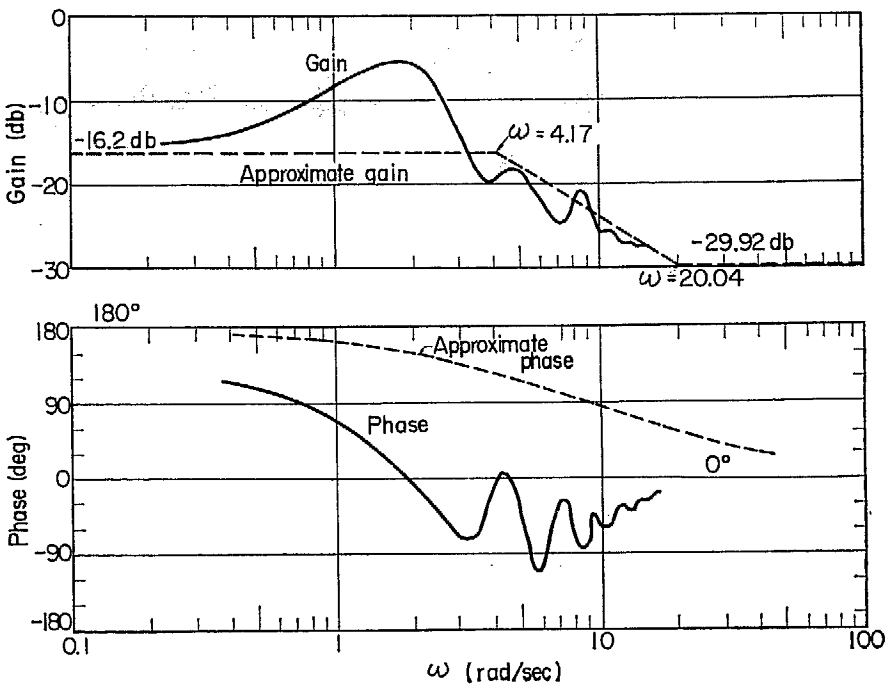

Fig. 19 The frequency characteristics of $\frac{\delta V_0}{\delta z_1}=G_{z1}(s)/G_v(s)$

It should be noted that an appreciable resonance peak in the exact gain characteristics of $G_{z1}(s)/G_v(s)$ is observed around $\omega=2$ as in the case of $G_q(s)/G_v(s)$.

It can be seen that the effect of this transfer function is very small, since 1 cm change in δz_1 at steady state results in 0.156 cm/sec change in δV_0.

2.7.5 Pressure to inlet velocity transfer function

The pressure to inlet velocity transfer function is expressed as $G_p(s)/G_v(s)$, where $G_p(s)$ is given in Eq. (54f)*

$$G_p(s)=G_p^{01}+G_p^{12}+G_p^{23}+G_p^{34}+G_p^{45} \tag{54f)*$$

Each term on the right-hand side is defined in Eqs. (41c)*, (42e)*, (43d)*, (45d)* and (46b)*, respectively.

The approximate transfer function of $G_p(s)$ may be obtained in a quadratic form of s.

$$G_p(s)\simeq K_p(1+\xi s^2) \tag{68}$$

K_p and ξ defined as

$$K_p=\left(\frac{\rho_w}{A_{co}}V_0^{*2}\right)K_p' \tag{69}$$

$$\xi=\frac{\xi'}{K_p'} \tag{70}$$

where

$$\left.\begin{aligned}K_p'&=a_{01}+a_{12}+a_{23}+a_{34}+a_{45}\\ \xi'&=\xi_{12}'+\xi_{23}'+\xi_{34}'\end{aligned}\right\} \tag{71}$$

The parameters of a_{01} through a_{45} and ξ_{12}' through ξ_{34}' are defined in **Appendix 3**.

The above equations are obtained by finding the asymptotes to the gain characteristics of $G_p(s)$ for $s \to j0$ and $s \to j\infty$. Eq. (71) shows that K_p and ξ are not so simply expressed in terms of the design parameters.

By the use of Eq. (44), the approximate form of the pressure to inlet velocity transfer function is

$$\frac{\delta V_0}{\delta p} = G_p(s)/G_v(s) \simeq \frac{K_p}{K_v}\left(1+\frac{\xi}{T_v}s\right) = \frac{V_0{}^* K_p'}{K_v'}\left(1+\frac{\xi}{T_v}s\right) \tag{72}$$

The numerical values of K_p and ξ for JPDR are obtained from Eqs. (70) and (71), giving $K_p = -0.515\frac{(\text{kg})\cdot\text{cm}}{\text{cm}^2\cdot\text{sec}^2}\Big/\frac{\text{kg}}{\text{cm}^2}$ and $\xi = -1.45\ \text{sec}^2$.

Thus,

$$G_p(s) \simeq -0.515(1-1.45s^2)\quad \frac{(\text{kg})\cdot\text{cm}}{\text{cm}^2\cdot\text{sec}^2}\Big/\frac{\text{kg}}{\text{cm}^2} \tag{73}$$

and

$$G_p(s)/G_v(s) = \frac{\delta V_0}{\delta p} \simeq -0.572(1-6.04s)\quad \frac{\text{cm}}{\text{sec}}\Big/\frac{\text{kg}}{\text{cm}^2} \tag{74}$$

The frequency characteristics of $G_p(s)/G_v(s)$ are shown in **Fig. 20**, where the approximate form of Eq. (74) is shown by the dotted line and the exact calculation of $G_p(s)/G_v(s)$ by the solid line.

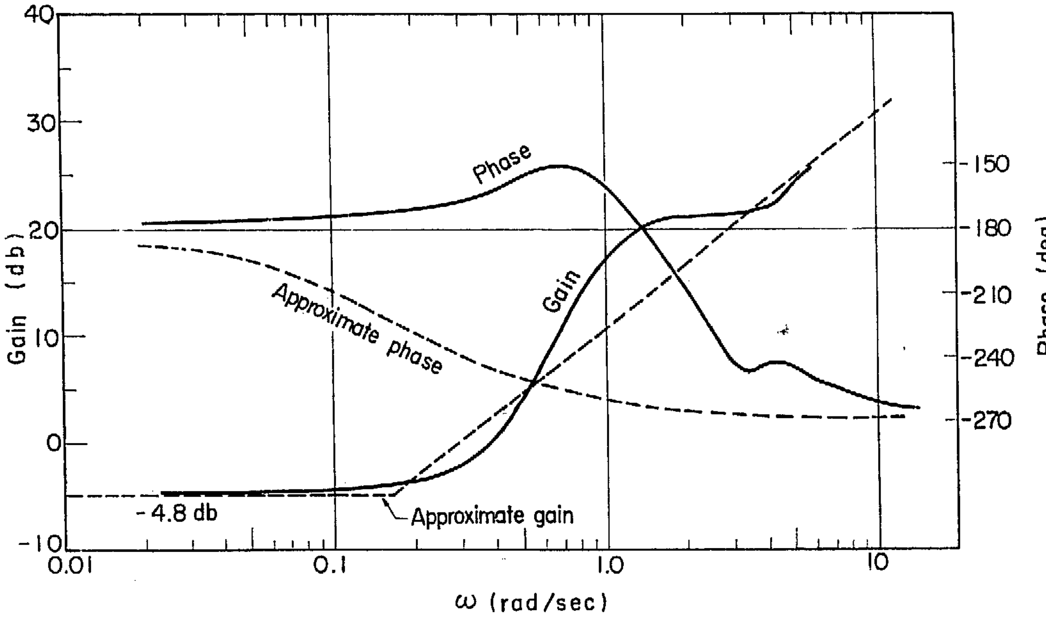

Fig. 20 The frequency characteristics of $\frac{\delta V_0}{\delta p} = \frac{G_p(s)}{G_v(s)}$

It should be noted that a resonance peak in the exact gain characteristics of $G_p(s)/G_v(s)$ is also observed around $\omega \doteqdot 2$.

2.8 Recirculation Flow Transfer Function

The recirculation flow transfer functions, $G_{25}(s)$, $G_{26}(s)$ and $G_{27}(s)$, which relate the recirculation flow to the feedwater flow, to the inlet velocity and the pressure, respectively have been given in JAERI-1044.

These transfer functions are

$$G_{25}=\frac{\delta W_R}{\delta W_f}=-1 \tag{63a}^*$$

$$G_{26}=\frac{\delta W_R}{\delta V_0/V_0^*}=\frac{V_0^*}{v_w} \tag{63b}^*$$

$$G_{27}=\frac{\delta W_R}{\delta p}=-V_0^*\frac{D}{v_w^2}-\frac{M_{sub}^*}{v_{sub}}\cdot\frac{\partial v_{sub}}{\partial p}\cdot s \tag{63c}^*$$

They are very simple and all independent of power level, since V_0^* may be considered to be independent of power level.

It should be noted that the effect of the recirculation flow on the whole system dynamics may be ignored, as shown in the later section.

The numerical forms of those transfer functions for JPDR are readily calculated.

$$G_{25}(s)=\frac{\delta W_R}{\delta W_f}=-1 \qquad \text{——}$$

$$G_{26}(s)=\frac{\delta W_R}{\delta V_0/V_0^*}=500 \qquad \text{(kg)/sec}$$

$$G_{27}(s)=\frac{\delta W_R}{\delta p}=-1.205-20.8s \qquad \frac{\text{(kg)/sec}}{\text{kg/cm}^2}$$

2.9 Summary of Simplified Transfer Functions

The simplified transfer functions derived so far for a natural circulation boiling water reactor, are summarized and given in TABLE 1. The interrelations between these transfer

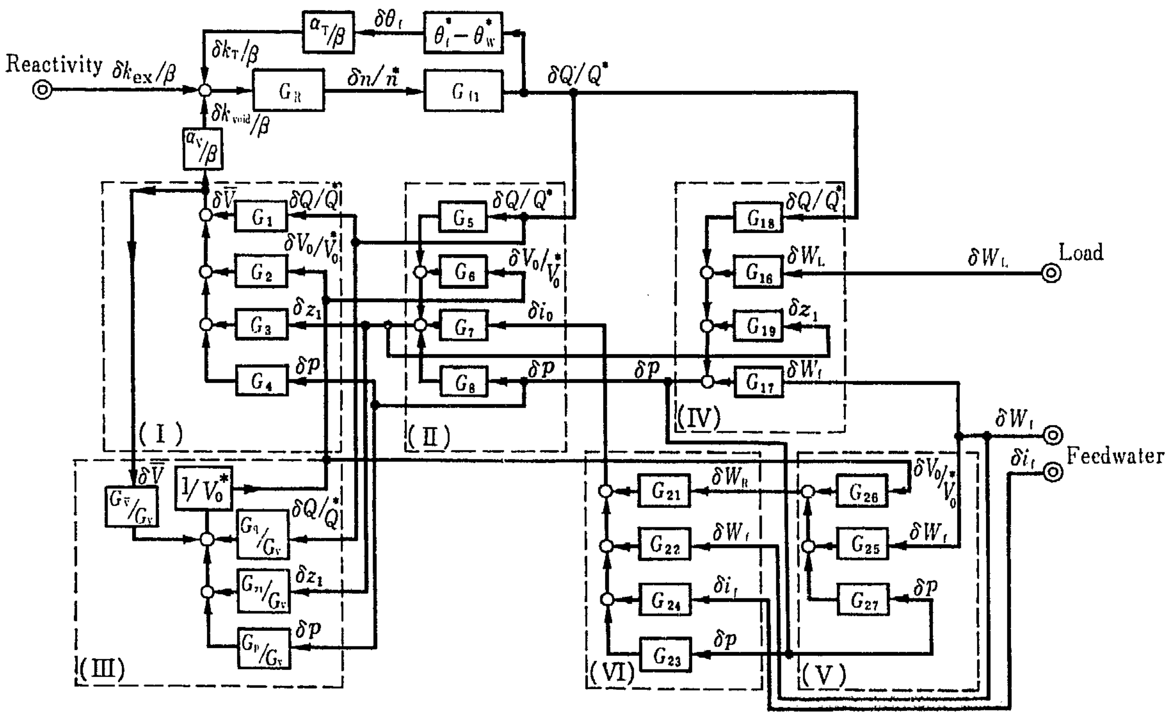

(I) Core Void Transfer Function
(II) Boiling Boundary Transfer Function
(III) Inlet Velocity Transfer Function (Hydrodynamics)
(IV) Vessel Pressure Transfer Function
(V) Recirculation Flow Transfer Function
(VI) Inlet Water Enthalpy Transfer Function

Fig. 21 Transfer functions of natural circulation boiling water reactor

TABLE 1 Simplified transfer functions

Symbol	Output/Input	Transfer function
G_R	$\frac{\delta n/n^*}{\delta k/\beta}$	$\frac{s+\lambda}{\frac{l}{\beta}s\left(s+\frac{\beta}{l}+\lambda\right)}$
G_{f1}	$\frac{\delta Q/Q^*}{\delta n/n^*}$	$\frac{1}{1+T_f s}$
G_{f2}	$\frac{\delta\theta_f}{\delta n/n^*}$	$\frac{\theta_f^*-\theta_w^*}{1+T_f s}$
G_1	$\frac{\delta\bar{V}}{\delta Q/Q^*}$	$\frac{K_1}{1+T_1 s}$
(G_2)	$\frac{\delta\bar{V}}{\delta V_0}$	$-\frac{K_1}{1+T_1 s}$
G_3	$\frac{\delta\bar{V}}{\delta z_1}$	$\frac{K_3}{1+T_3 s}$
G_4	$\frac{\delta\bar{V}}{\delta p}$	$b\frac{1+\frac{a}{b}T_4 s}{1+T_4 s}$
G_5	$\frac{\delta z_1}{\delta Q/Q^*}$	$\frac{K_5}{1+T_5 s}$
(G_6)	$\frac{\delta z_1}{\delta V_0}$	$-\frac{K_5}{1+T_5 s}$
G_7	$\frac{\delta z_1}{\delta i_0}$	$K_7 e^{-\tau_{01}s}$
G_8	$\frac{\delta z_1}{\delta p}$	K_8
G_{16}	$\frac{\delta p}{\delta W_L}$	$-\Delta i\cdot\frac{1}{H_{pr}}\cdot\frac{1}{s}$
G_{17}	$\frac{\delta p}{\delta W_f}$	$\frac{v_w}{\Delta v}\Delta i\cdot\frac{1}{H_{pr}}\cdot\frac{1}{s}$

Symbol	Output/Input	Transfer Function
G_{18}	$\frac{\delta p}{\delta Q/Q^*}$	$(z_2-z_1)Q^*\cdot\frac{1}{H_{pr}}\cdot\frac{1}{s}$
G_{19}	$\frac{\delta p}{\delta z_1}$	$-Q^*\cdot\frac{1}{H_{pr}}\cdot\frac{1}{s}$
(G_{21})	$\frac{\delta i_0}{\delta W_R}$	$K_{21}e^{-\tau_d s}$
G_{22}	$\frac{\delta i_0}{\delta W_f}$	$K_{22}e^{-\tau_d s}$
G_{23}	$\frac{\delta i_0}{\delta p}$	$K_{23}e^{-\tau_d s}+K_{23}'\cdot s$
G_{24}	$\frac{\delta i_0}{\delta i_f}$	$K_{24}e^{-\tau_d s}$
$(G_{\bar{v}}/G_v)$	$\frac{\delta V_0}{\delta\bar{V}}$	$\frac{g(\rho_w-\rho_s)}{A_{co}^2K_v}\cdot\frac{1}{1+T_v s}$
(G_q/G_v)	$\frac{\delta V_0}{\delta Q/Q^*}$	$V_0^*\frac{K_q'}{K_v'}\cdot\frac{1+T_q s}{1+T_v s}$
(G_{z1}/G_v)	$\frac{\delta V_0}{\delta z_1}$	$\frac{1}{\tau_e}\frac{K_{z1}'}{K_v'}\cdot\frac{1+T_{z1}s}{1+T_v s}$
(G_p/G_v)	$\frac{\delta V_0}{\delta p}$	$V_0^*\frac{K_p'}{K_v'}\left(1+\frac{\xi}{T_v}s\right)$
(G_{25})	$\frac{\delta W_R}{\delta W_f}$	-1
(G_{26})	$\frac{\delta W_R}{\delta V_0/V_0^*}$	$\frac{V_0^*}{v_w}$
(G_{27})	$\frac{\partial W_R}{\delta p}$	$-V_0^*\frac{D}{v_w^2}-\frac{M_{sub}^*}{v_{sub}}\frac{\partial v_{sub}}{\partial p}\cdot s$

Brackets in the columns of symbol indicate transfer functions, which need not be used when δV_0 and δW_R are ignored.

functions are shown in **Fig. 21**.

The parameters appearing in **TABLE 1** are summarized below in terms of design parameters.

$$K_1=\left(\frac{v_s}{\Delta v}V_0^*A_{co}\right)\tau_{12}\left(1-\frac{y_2-1}{y_2\ln y_2}\right) \tag{7}$$

$$T_1=\tau_{12}(0.3816+0.0109\,y_2) \tag{10}$$

$$K_3=-\left(\frac{v_s}{\Delta v}A_{co}\right)\frac{y_2-1}{y_2} \tag{17}$$

$$T_3=\tau_{12}(0.6080+0.050\,y_2) \tag{19}$$

$$\left.\begin{aligned} a&=-\left(\frac{v_s}{\Delta v}V_0^*A_{co}\right)\tau_{12}\left\{D'+(A'-C')\frac{y_2-1}{y_2\ln y_2}-\frac{E}{y_2}\right\}\\ b&=-\left(\frac{v_s}{\Delta v}V_0^*A_{co}\right)\tau_{12}(A'-C')\left(1-\frac{y_2-1}{y_2\ln y_2}\right)\end{aligned}\right\} \tag{24}$$

$$T_4=0.637\tau_{12} \tag{26}$$

$$K_5=-(z_1-z_0) \tag{30}$$

$$T_5=0.637\tau_{01} \tag{31}$$

$$K_7=-(z_1-z_0)\frac{\rho_w}{\tau_{01}Q^*} \tag{39c)*}$$

$$K_8=(z_1-z_0)\frac{\tau_e}{\tau_{01}}\cdot B' \qquad (39d)^*$$

$$H_{pr}\simeq(H_{pr})_{ves}=\{M_s^*(A+B)+M_w^*B\}-\frac{\Delta i}{\Delta v}\{M_s^*(C+D)+M_w^*D\}-\frac{\bar{V}_{sat}}{J} \qquad (38)$$

$$K_{21}=\frac{W_f^*}{W_0^*}\cdot\frac{i_w-i_f}{W_R^*+W_f^*} \qquad (69a)^*$$

$$K_{22}=-\frac{W_R^*}{W_0^*}\cdot\frac{i_w-i_f}{W_R^*+W_f^*} \qquad (69b)^*$$

$$K_{23}=\frac{W_R^*}{W_0^*}\cdot B \qquad (69c)^*$$

$$K_{23}'=\frac{\bar{V}_{sub}}{W_0^*J} \qquad (69c)^*$$

$$K_{24}=\frac{W_f^*}{W_0^*} \qquad (69d)^*$$

$$K_v=\left(\frac{\rho_w}{A_{co}}V_0^*\right)K_v' \qquad (45)$$

$$K_v'=(y_2-1)\left(1+\mu\frac{\tau_{23}g}{y_2V_0^*}\right)+\frac{[FPD]'}{\frac{\rho_w}{A_{co}}V_0^*} \qquad (47)$$

$$T_v=\frac{T_v'}{K_v'} \qquad (46)$$

$$T_v'=\tau_{01}+\tau_{12}+\mu^2(\tau_{23}+\tau_{34})+\mu^2{}_d\tau_{45}+\tau_{50} \qquad (48)$$

$$K_q'=(y_2-1)\left\{\frac{\mu g}{y_2V_0^*}(\tau_{23}-\tau_r)-(1-\mu^2)\right\} \qquad (55)$$

$$T_q=\frac{T_q'}{K_q'} \qquad (54)$$

$$T_q'=-\left\{\tau_{12}\left(\frac{y_2-1}{\ln y_2}-1\right)+\mu^2(y_2-1)(\tau_{23}+\tau_{34})\right\} \qquad (56)$$

$$K_{z1}'=-\frac{\mu g}{y_2V_0^*}(\tau_{23}-\tau_r)+(1-\mu^2) \qquad (63)$$

$$T_{z1}=\frac{T_{z1}'}{K_{z1}'} \qquad (62)$$

$$T_{z1}'=\tau_{12}+\mu^2(\tau_{23}+\tau_{34})-\tau_e \qquad (64)$$

$K_p'=a_{01}+a_{12}+a_{23}+a_{34}+a_{45}$ (see **Appendix 3**) (71)

$$\xi=\frac{\xi'}{K_p'} \qquad (70)$$

$\xi'=\xi_{12}'+\xi_{23}'+\xi_{34}'$ (see **Appendix 3**) (71)

The simplified transfer functions given in **TABLE 1** in which the numerical values of the above parameters are substituted, are shown in **TABLE 2**, where the forms used in analog simulation are also given for comparison.

TABLE 2 Transfer functions obtained by analytical approximation and those for analog simulation

Symbol	Output / Input	Obtained by formula of TABLE 1		Analog Simulation
G_R	$\frac{\delta n/n^*}{\delta k/\beta}$	$0.077\frac{1+13s}{s(1+0.0078s)}$	—	$1+\frac{0.077}{s}$
G_{f1}	$\frac{\delta Q/Q^*}{\delta n/n^*}$	$\frac{1}{1+12s}$	—	Same as the left.
G_{f2}	$\frac{\delta\theta_f}{\delta n/n^*}$	$\frac{400}{1+12s}$	—	Same as the left.
G_1	$\frac{\delta\bar{V}}{\delta Q/Q^*}$	$\frac{1.21\times10^5}{1+0.27s}$	cm^3	Same as the left.
(G_2)	$\frac{\delta\bar{V}}{\delta V_0}$	$-\frac{1.21\times10^5}{1+0.27s}$	〃	Same as the left.
G_3	$\frac{\delta\bar{V}}{\delta z_1}$	$-\frac{2.94\times10^3}{1+0.466s}$	cm^3/cm	$-2.93\times10^3\left(\frac{1.5}{1+0.3s}-\frac{0.5}{1+0.13s}\right)$
G_4	$\frac{\delta\bar{V}}{\delta p}$	$-0.0171\times10^5\frac{1+5.117s}{1+0.422s}$	$\frac{cm^3}{kg/cm^2}$	$1.91\times10^4\left(\frac{1.5}{1+0.35s}-\frac{0.5}{1+0.13s}\right)$ -2.06×10^4
G_5	$\frac{\delta z_1}{\delta Q/Q^*}$	$-\frac{46.5}{1+0.27s}$	cm	Same as the left.
(G_6)	$\frac{\delta z_1}{\delta V_0}$	$\frac{46.5}{1+0.27s}$	〃	Same as the left.
G_7	$\frac{\delta z_1}{\delta i_0}$	$-7.07e^{-0.415s}$	$\frac{cm}{kcal/(kg)}$	$-7.07\frac{1-0.21s}{1+0.21s}$
G_8	$\frac{\delta z_1}{\delta p}$	9.03	$\frac{cm}{kg/cm^2}$	Same as the left.
G_{16}	$\frac{\delta p}{\delta W_L}$	$-\frac{373.4}{4.86\times10^3}\cdot\frac{1}{s}$	$\frac{kg/cm^2}{(kg)/sec}$	$-\frac{0.0801}{s}$
G_{17}	$\frac{\delta p}{\delta W_f}$	$\frac{16.19}{4.86\times10^3}\cdot\frac{1}{s}$	〃	$\frac{0.00334}{s}$
G_{18}	$\frac{\delta p}{\delta Q/Q^*}$	$\frac{7.4\times10^3}{4.86\times10^3}\cdot\frac{1}{s}$	kg/cm^2	$\frac{1.525}{s}$
G_{19}	$\frac{\delta p}{\delta z_1}$	$-\frac{70.8}{4.86\times10^3}\cdot\frac{1}{s}$	kg/cm^3	$-\frac{0.0152}{s}$
(G_{21})	$\frac{\delta i_0}{\delta W_R}$	$0.01385e^{-12s}$	$\frac{kcal/(kg)}{(kg)/sec}$	0.01382[Delay]*
G_{22}	$\frac{\delta i_0}{\delta W_f}$	$-0.315e^{-12s}$	〃	−0.317[Delay]*
G_{23}	$\frac{\delta i_0}{\delta p}$	$1.23e^{-12s}+0.489s$	$\frac{kcal/(kg)}{kg/cm^2}$	1.23[Delay]*+0.5s
G_{24}	$\frac{\delta i_0}{\delta i_f}$	$0.042e^{-12s}$	—	0.042[Delay]*
$(G_{\bar{V}}/G_v)$	$\frac{\delta V_0}{\delta\bar{V}}$	$\frac{1.34\times10^{-4}}{1+0.24s}$	$\frac{cm}{sec}\Big/cm^3$	$\frac{1.32\times10^{-4}}{1+0.25s}$
(G_q/G_v)	$\frac{\delta V_0}{\delta Q/Q^*}$	$16.1\frac{1-0.45s}{1+0.24s}$	cm/sec	$16.1\frac{1-1.32s}{1+0.75s}$
(G_{z1}/G_v)	$\frac{\delta V_0}{\delta z_1}$	$-0.156\frac{1-0.049s}{1+0.24s}$	sec^{-1}	$-0.154\frac{1-0.19s}{1+s}$
(G_p/G_v)	$\frac{\delta V_0}{\delta p}$	$-0.572(1-6.04s)$	$\frac{cm}{sec}\Big/\frac{kg}{cm^2}$	$-0.542(1-5.46s)$
(G_{25})	$\frac{\delta W_R}{\delta W_f}$	-1	—	Same as the left.

Symbol	Output / Input	Obtained by formula of TABLE 1		Analog simulation
(G_{26})	$\frac{\delta W_R}{\delta V_0/V_0^*}$	500	(kg)/sec	Same as the left.
(G_{27})	$\frac{\delta W_R}{\delta p}$	$-1.205-20.8s$	$\frac{\text{(kg)/sec}}{\text{kg/cm}^2}$	Same as the left.

[Delay]* is simulated by cascade connection of a single time constant delay of 2 sec and Pade approximation of e^{-10s} by four terms.

3. SIMPLIFIED MODEL BASED ON TRANSIENT ANALYSIS

Analog computer studies on transient analyses based on the simplified tranfer functions derived in Chapter 2 have been made, which will be given in Chapter 5.

The following results have been obtained, which are of great use for simplifying the block diagram.

(1) The effects of δV_0 and δW_R on the dynamic characteristics of the whole system are small and may be ignored.

(2) The effect of $s\delta p$ on δi_0 is small and may be ignored. Thus, G_{23} may be assumed to be equal to $\frac{W_R^*}{W_0^*}B\cdot e^{-\tau_d s}$.

The simplified block diagram based on the above assumptions is shown in Fig. 22 (Simplified Block Diagram, Type-1).

The model of this diagram is good over a moderate frequency range and is appropriate for stability and transient analyses and control system design.

It is important how the parameters in the simplified transfer functions depend on power level, n^* or Q^* which is proportional to n^*. Some of them depend on Q^* and others are constant. The power-level dependences of their gains and time constants are given in TABLE 3.

Some of the computer results on which the present simplification is based, are given in Appendix 4.

TABLE 3. Power dependence of transfer functions

Symbol	Power dependence of gain	Power dependence of time constant	Analog simulation
G_1	K_1/Q^* is slightly dependent on Q^*	almost independent	possible
G_3	dependent on Q^*	almost independent	possible
G_4	dependent on Q^*	almost independent	possible
G_5	independent of Q^*	independent	possible
G_7	inversely proportional to Q^*	independent	approximation
G_8	proportional to τ_0	——	possible
G_{16}	independent	——	possible
G_{17}	independent	——	possible
G_{18}	proportional to Q^*	——	possible
G_{19}	proportional to Q^*	——	possible
G_{22}	almost independent	——	approximation
G_{23}	almost independent	——	approximation
G_{24}	proportional to Q^*	——	approximation

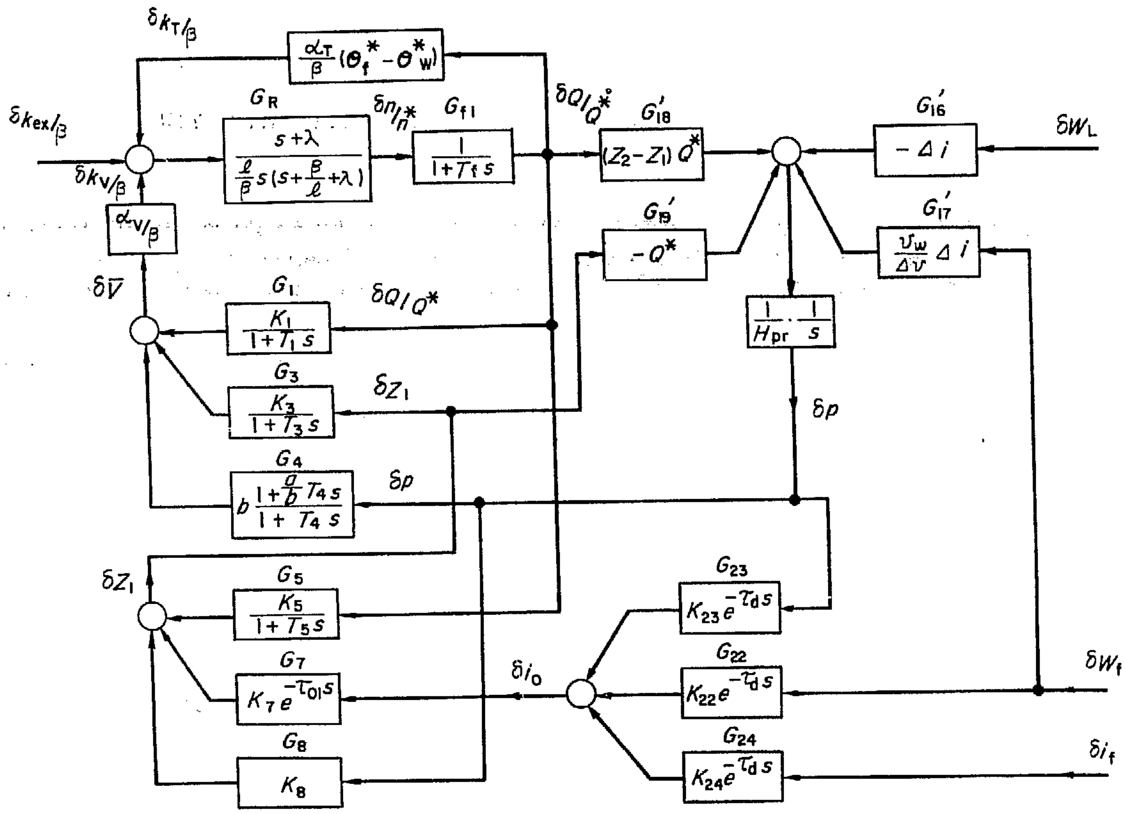

Fig. 22. 1 Simplified block diagram (Type-1) of natural circulation boiling water reactor (The effects of δV_0 and δW_R are ignored. K_{23}'s in G_{23} is also ignored.)

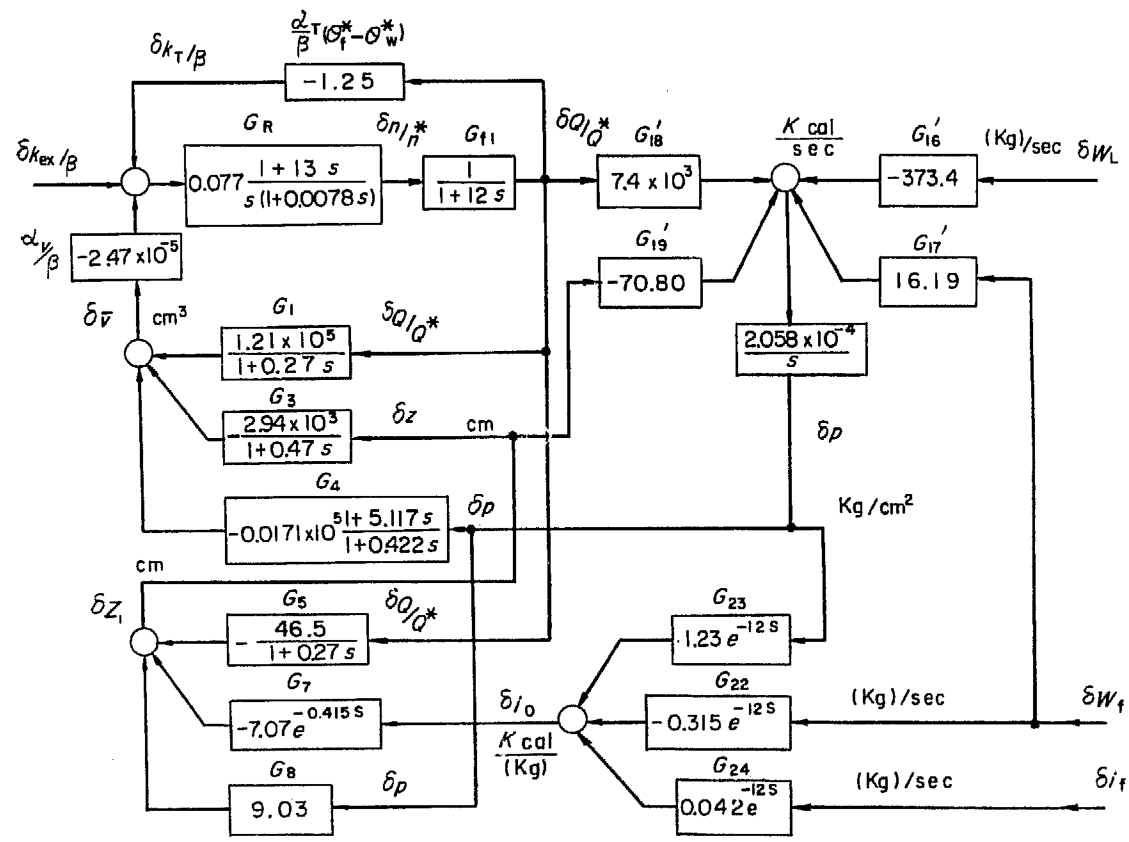

Fig. 22. 2 Simplified block diagram (Type-1) with numerical values substituted

4. SIMPLIFIED MODEL WITH SMALL TIME CONSTANTS NEGLECTED

In order to further simplify the model shown in Type 1 of Fig. 22. 1, the feedback transfer function is reduced to two feedback paths; one from power to void and the other from power through pressure to void. This modification is made by manipulating the block diagram so as to eliminate δz_1 and δi_0.

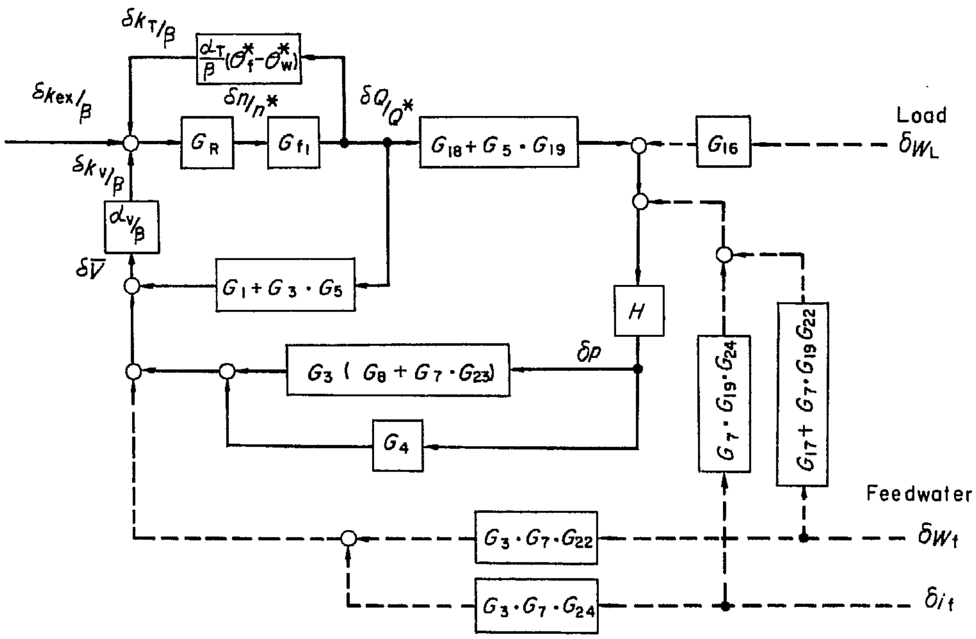

$$H = \frac{1}{1 - G_{19}(G_8 + G_7 \cdot G_{23})}$$

Fig. 23 Modification of feedback transfer function (δz_1 and δi_0 are eliminated.)

The result is shown in Fig. 23. It is summarized that the feedback transfer function consists of:

(1) The power to void transfer function, including a direct effect and an indirect effect through boiling boundary variation, i. e.,

$$G_1 + G_3 \cdot G_5,$$

and

(2) The power through pressure to void transfer function, i. e., the cascade function of $G_{18} + G_5 \cdot G_{19}$, H, and $G_4 + G_3(G_8 + G_7 \cdot G_{23})$,

where $\quad H = \{1 - G_{19}(G_8 + G_7 \cdot G_{23})\}^{-1}$. (75)

The paths from the external disturbances, i. e., δW_L, δW_f and δi_f, are also shown by the dotted lines in Fig. 23.

When the dynamic behavior for longer times is of interest, further simplification is possible by ignoring smaller time constants, for example, those less than 1 sec, in the transfer functions. These assumptions are appropriate for the study on the control of boiling water reactors.

Thus, a simplified model is obtained and shown in Fig. 24 (Simplified Block Diagram, Type-2). In deriving this block diagram, the following assumptions are made.

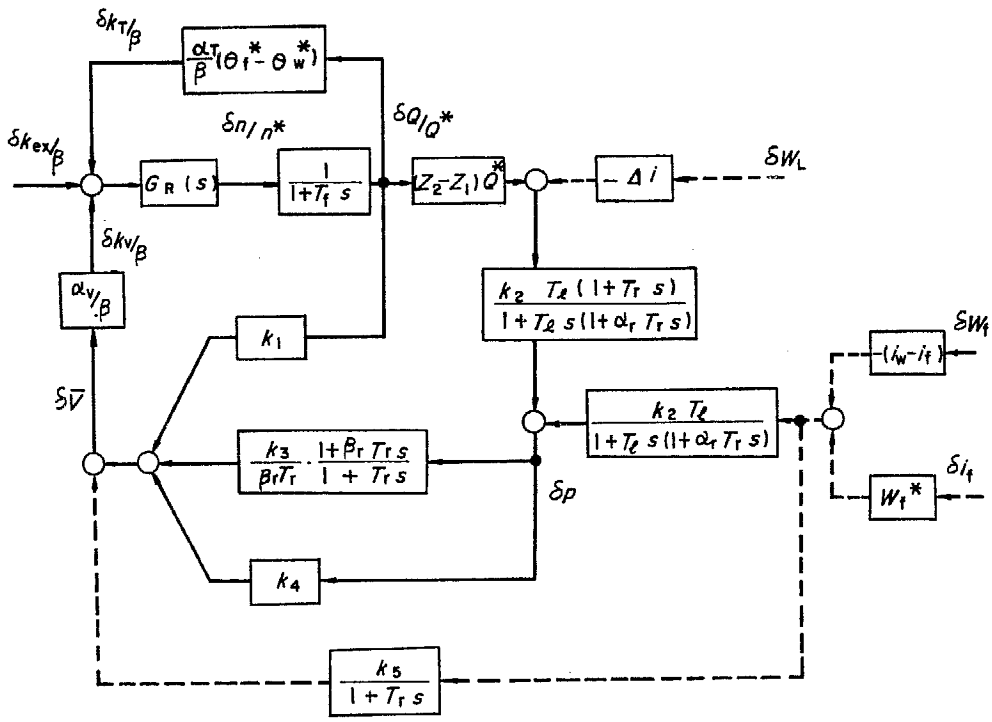

Fig. 24 Simplified block diagram (Type-2) of natural circulation boiling water reactor (Smaller time constants are neglected.)

(1) Smaller time constants are ignored, i. e., τ_e, τ_{01} and τ_{12} of the order of 1 sec or less.
(2) $e^{-(\tau_{01}+\tau_d)s}$ is approximated by $1/\{1+(\tau_{01}+\tau_d)s\}$.
(3) $v_s/\Delta v \simeq 1$.
(4) $D' = \frac{1}{v_w}\frac{\partial v_w}{\partial p} \simeq 0$.

The derivation of **Fig. 24** is given in **Appendix 5**. The parameters appearing in the diagram are summarized below.

$$k_1 = V_0{}^*A_{co}\tau_{12}\left(1-\frac{y_2-1}{y_2 \ln y_2}\right)+(z_1-z_0)A_{co}\frac{y_2-1}{y_2} \tag{76}$$

$$k_2 = \frac{1}{H_{pr}+W_0{}^*T_rB} \tag{77}$$

$$\alpha_r = H_{pr}\cdot k_2 \tag{78}$$

$$T_r = \tau_{01}+\tau_d \tag{79}$$

$$T_l = \frac{H_{pr}}{\alpha_r W_0{}^*B}\left(1-\frac{W_R{}^*}{W_0{}^*}\right)^{-1} \tag{80}$$

$$k_3 = -A_{co}\frac{y_2-1}{y_2}\cdot\frac{W_0{}^*T_rB}{Q^*} \tag{81}$$

$$\beta_r = \left(1-\frac{W_R{}^*}{W_0{}^*}\right)^{-1} \tag{82}$$

$$k_4 = -V_0{}^*A_{co}\tau_{12}(A'-C')\cdot\left(1-\frac{y_2-1}{y_2 \ln y_2}\right) \tag{83}$$

$$k_5 = \frac{A_{co}}{Q^*}\frac{y_2-1}{y_2} \tag{84}$$

The numerical values of the above parameter are readily calculated.

$k_1 = 2.47\times10^5$ cm^3

$k_2 = 8 \times 10^{-5} \quad \dfrac{\text{kg}}{\text{cm}^2 \cdot \text{kcal}}$

$k_3 = -3.05 \times 10^5 \quad \dfrac{\text{cm}^5 \cdot \text{sec}}{\text{kg}}$

$k_4 = -1.64 \times 10^3 \quad \text{cm}^5/\text{kg}$

$k_5 = 39.9 \quad \dfrac{\text{cm}^3 \cdot \text{sec}}{\text{kcal}}$

$\alpha_r = 0.389$

$\beta_r = 25$

$T_r = 12$ sec

$T_l = 490$ sec

$\alpha_r T_r = 4.67$ sec

The resulting block diagram for the JPDR parameters is shown in Fig. 25.

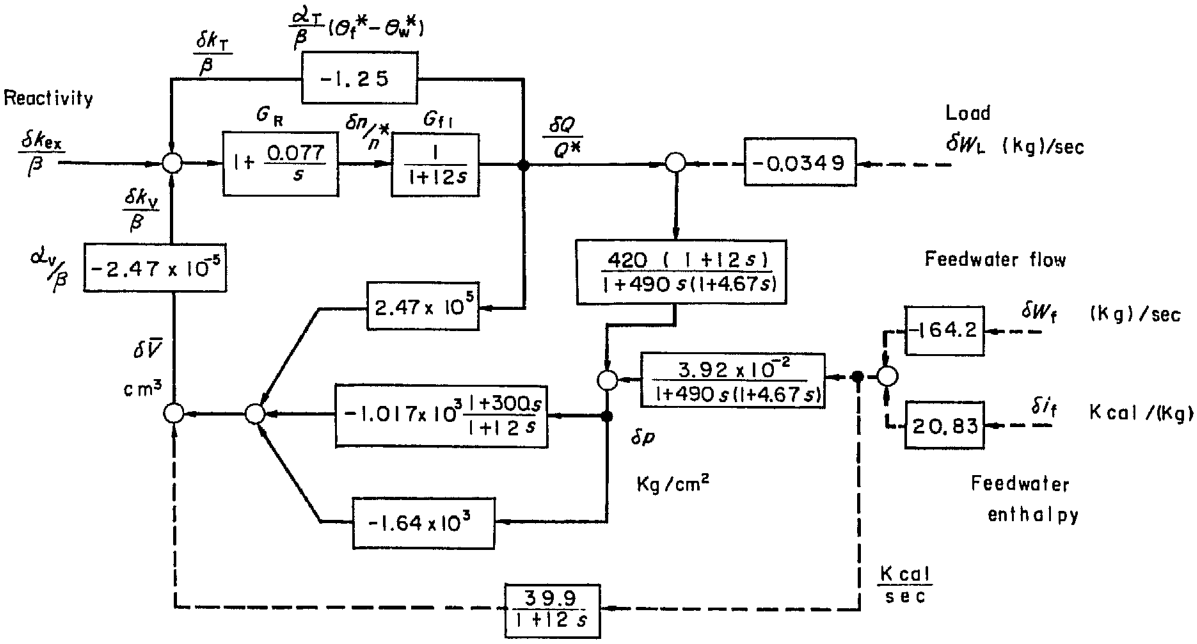

Fig. 25 Simplified block diagram (Type-2) for JPDR
(approximation valid in low frequency region, $\omega < 1$ rad/sec.)

Quite an important conclusion is derived from Fig. 25. If δW_L is increased by some amount with W_f, i_f and δk_{ex} kept constant, then the void increases, thus, the power continues decreasing very slowly. This indicates that the system is unstable and it is a slowly diverging, non-oscillatory system as shown in Chapt. 5.3. An external control system is necessary for the steady operation of this system.

In the same case as mentioned above, if $\delta k_{ex}/\beta$ is increased by some amount so as to make δp equal to zero, then the power ceases to decrease and settles at a certain power level, matching the load change. This is one scheme of the control systems for single cycle natural circulation boiling water reactors.

From the viewpoint of the control of boiling water reactors, this suggests that the control may be best achieved by manipulating either control rods or steam flow to load by the command signal of pressure so that the pressure is kept constant.

It shuld also be noted from Fig. 25 that a similar stabilizing effect may be explained to exist for the effects of δW_f and δi_f.

If δW_L is increased by some amount, then increasing δW_f and decreasing δi_f have also a stabilizing effect on the system.

This is the principle of control of dual cycle boiling water reactors.

5. SOME OF THE DYNAMIC CHARACTERISTICS BASED ON DERIVED TRANSFER FUNCTIONS

Analog computer studies on transient analyses based on the simplified transfer functions derived in Chapter 2 have been made. Some of the results obtained are given below; the dynamic characteristics in greater detail and the analyses of control system will be given in the following reports.

5.1 Some Transient Responses Obtained by Analog Computer

Most of the transfer functions simulated on an analog computer are the same as those obtained by the simplified transfer functions derived in Chapter 2 (TABLE 1). However, some of them are a little different from those in Chapter 2. For example, $G_3(s)$, $G_4(s)$, and the inlet velocity transfer functions are approximated by graphical fitting, and the transfer functions including pure delay terms are simulated either by Pade's approximation or by combinations of single time constant terms. It is expected that the differences in the results between the simplified transfer functions of Chapter 2 and the more accurate ones used here are small. The transfer functions simplified in Chapter 2 and used for simulation are listed in TABLE 2.

It should be noted that the results shown here include the whole system dynamics, i. e., δV_0 and δW_R are not ignored, so that the effect of simplification on the whole system may be obtained. The transient responses of δn, $\delta \overline{V}$, δp, δz_1 and δV_0 to step change in reactivity are shownin Fig. 26.

The diagrams indicate that the initial transients of all variables die out in 20~30 sec and thereafter the deviations of all variables continue to increase with an almost constant period. In view of these results, it can be seen that the close loop transfer functions have several

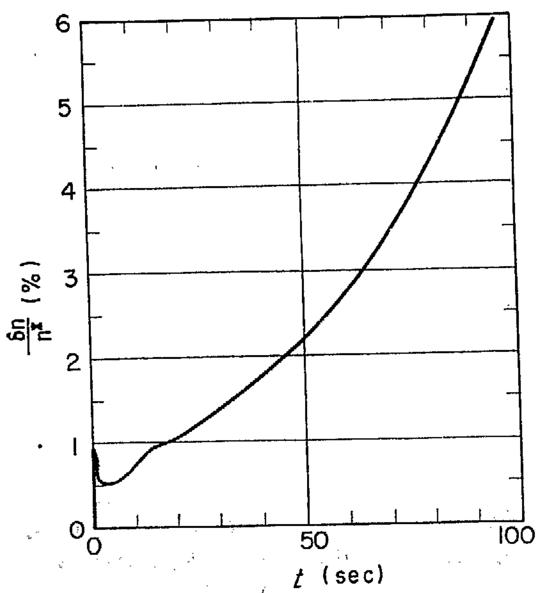

Fig. 26.1 Response of $\delta n/n^*$ to step change in δk=1 cent

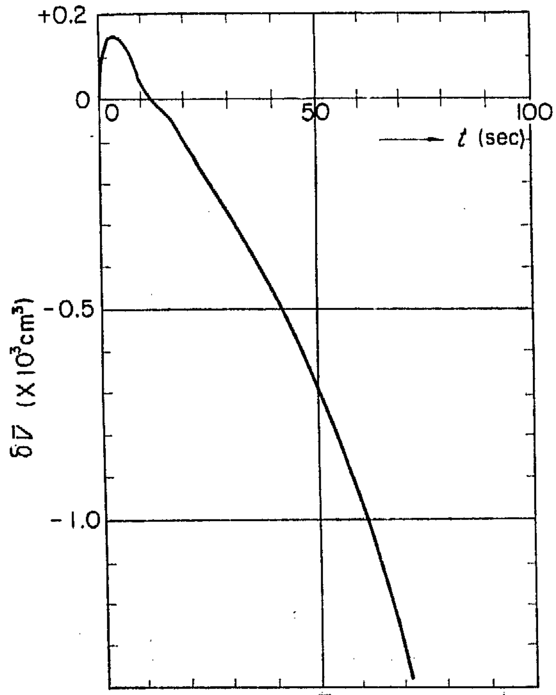

Fig. 26.2 Response of $\overline{V}$ to step change in δk=1 cent

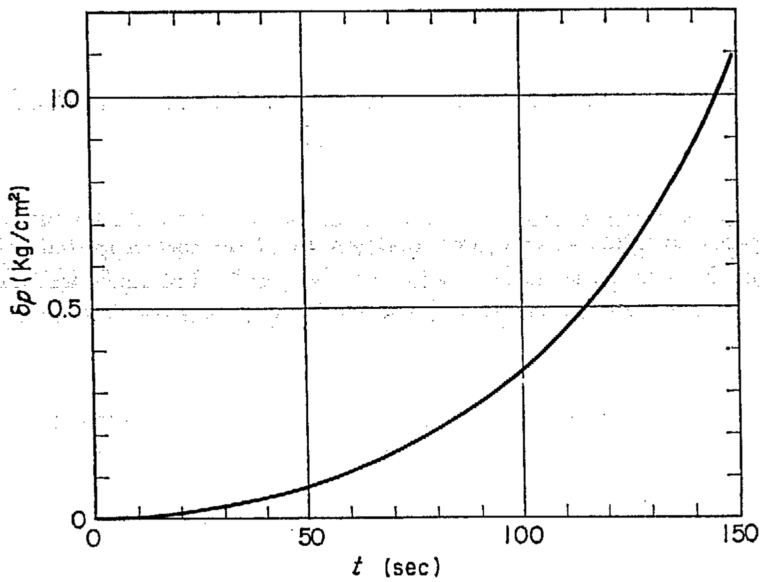

Fig. 26.3 Response of δp to step change in δk=0.2 cent

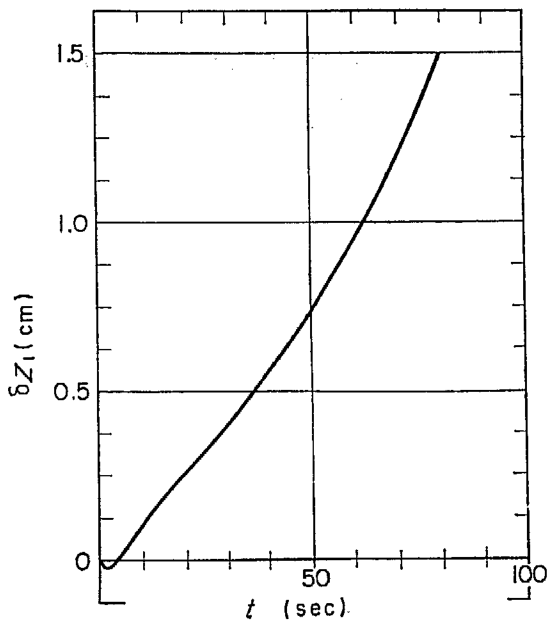

Fig. 26.4 Response of δz_1 to step change in δk=1 cent

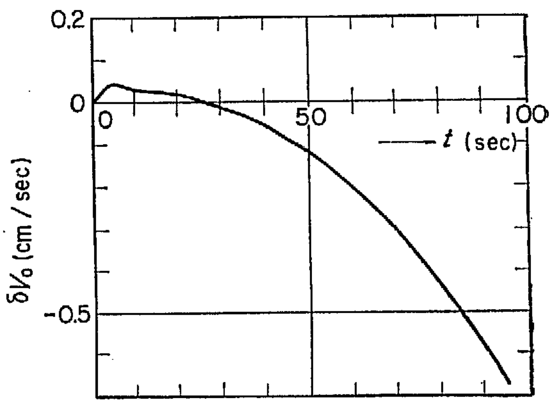

Fig. 26.5 Response of δV_0 to step change in δk=1 cent

smaller time constants, as well as a single large time constant associated with a small positive root of the characteristic equation. This small positive root is investigated in Chapter 5.3. Since the divergent tendency associated with this small positive root is very slow, being of the order of one to several per cent of change in 100 sec when reactivity disturbance is 1 cent, it is not a serious concern from the viewpoint of control and safety.

The physical interpretation is given below. In this analysis reactivity disturbance is introduced under the constant steam flow to load, i.e., $\delta W_L=0$, so that steam is accumulated in the vessel, thus pressure increases, then void volume decreases, and as a result power increases. On the other hand, in the initial transient, void volume increases, thus power decreases, since the power to void effect is dominant and the pressure to void effect is negligibly small during the initial short time.

5.2 Dynamic Characteristics of Feedback Transfer Function

Feedback transfer function is defined as a transfer function which relates void volume, $\delta\bar{V}$, to power, $\delta Q/Q^*$. It is the most important part of transfer functions, being characteristic of boiling water reactors.

The feedback transfer function is complicated, although those of nuclear kinetics and fuel heat transfer are simple in form.

Step responses and frequency characteristics are obtained in order to analyze the system stability and to obtain power transfer functions for comparison with measured power transfer functions.

Analog computer studies on feedback transfer functions have been made, where the parts of nuclear kinetics, fuel heat transfer, and temperature feedback are disconnected from the whole of simulation system.

The response of void volume to step change in power, $\delta Q/Q^* = 0.01$, is shown in **Fig. 27.1**. The void response when the pressure is kept constant, is also obtained, as shown in **Fig. 27.1**. The difference between them is remarkable, and the pressure effect on void is great after several seconds.

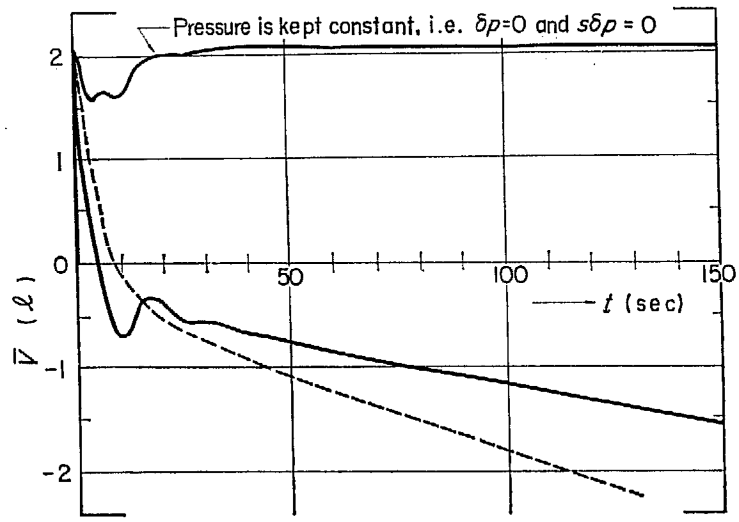

Fig. 27.1 Transient response of feedback transfer function (void response to step change in heat flux, $\delta Q/Q^* = 0.01$)

The approximate void response to step change in $\delta Q/Q^* = 0.01$ is readily calculated and may be compared with **Fig. 27.1**. From the simplified block diagram (Type-2) in **Fig. 25**, an approximate transfer function is obtained as

$$\frac{\delta\bar{V}(s)}{\delta Q(s)/Q^*} = 2.47\times10^5 - 10^3\left\{\frac{1.017(1+300s)}{1+12s} + 1.64\right\}\frac{420(1+12s)}{1+490s(1+4.67s)}$$

$$= 10^5\left\{2.47 - \frac{2.72}{1+4.7s} - \frac{8.44}{1+485.3s}\right\} \tag{85}$$

Thus, the step response of $\delta\bar{V}$ to $\delta Q/Q^* = 0.01$ is

$$\delta\bar{V}(t) = 10^3\left\{2.47 - 2.72\left(1-e^{-\frac{t}{4.7}}\right) - 8.44\left(1-e^{-\frac{t}{485.3}}\right)\right\} \quad \text{for } t \geq 0. \tag{86}$$

Equation (86) is plotted by the dotted line in **Fig. 27.1**.

The responses of δV_0, δp and δz_1 to step change in heat flux for 50 sec are shown in **Fig. 27.2**. δV_0 increases rapidly due to increase in void volume, then decreases following decrease in void volume. However, the amount of δV_0 in transient state is very small.

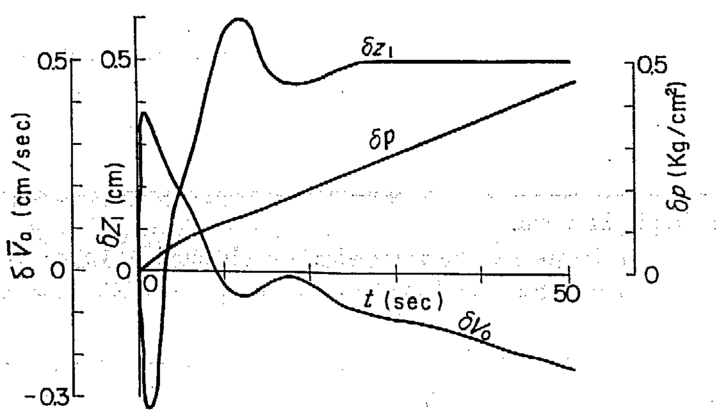

Fig. 27.2 Transient response of feedback transfer function (responses of δV_0, δp and δz_1 to step change in heat flux, $\delta Q/Q^*=0.01$)

It can also be seen that the transient response of δz_1 is almost out of phase of δV_0 . This is easily explained by physical interpretation.

The frequency characteristics of the feedback transfer function, which relates $\delta k_v/\beta$ to $\delta Q/Q^*$, are calculated by digital computation by the use of a formula of analog simulation. Throughout this calculation, pure delay terms are used instead of Pade's formula of analog simulation. The result is shown in a Bode diagram in **Fig. 28.1** and in Nyquist diagram in **Fig. 28.2.** The frequency characteristics of the aproximate transfer function shown in **Fig. 25** are also shown by the dotted line in **Fig. 28.1** and **Fig. 28.2.** The frequency characteristics of the closed loop transfer function is shown in **Fig. 28.3** which consists of the feedback transfer function obtained above, zero power and fuel transfer functions and temperature feedback transfer function.

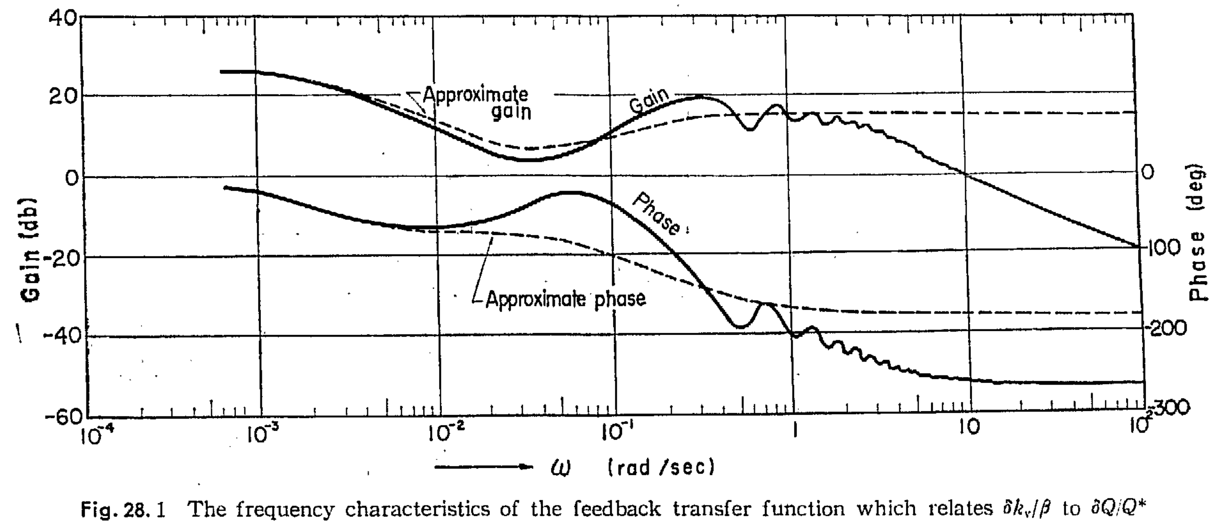

Fig. 28.1 The frequency characteristics of the feedback transfer function which relates $\delta k_v/\beta$ to $\delta Q/Q^*$

5.3 Stability Analysis

The stability of the whole system will be investigated by means of the Nyquist stability criterion and roots of the characteristic equation.

The divergent tendency as mentioned in Chapter **5.1** indicates that the system has at least a single positive real root. This is proved by the application of the Nyquist stability criterion to the open loop transfer function of the system. The open loop transfer function is obtained by multiplying together zero power transfer function, fuel heat transfer function and feedback transfer function. Here the feedback transfer function is considered to consist

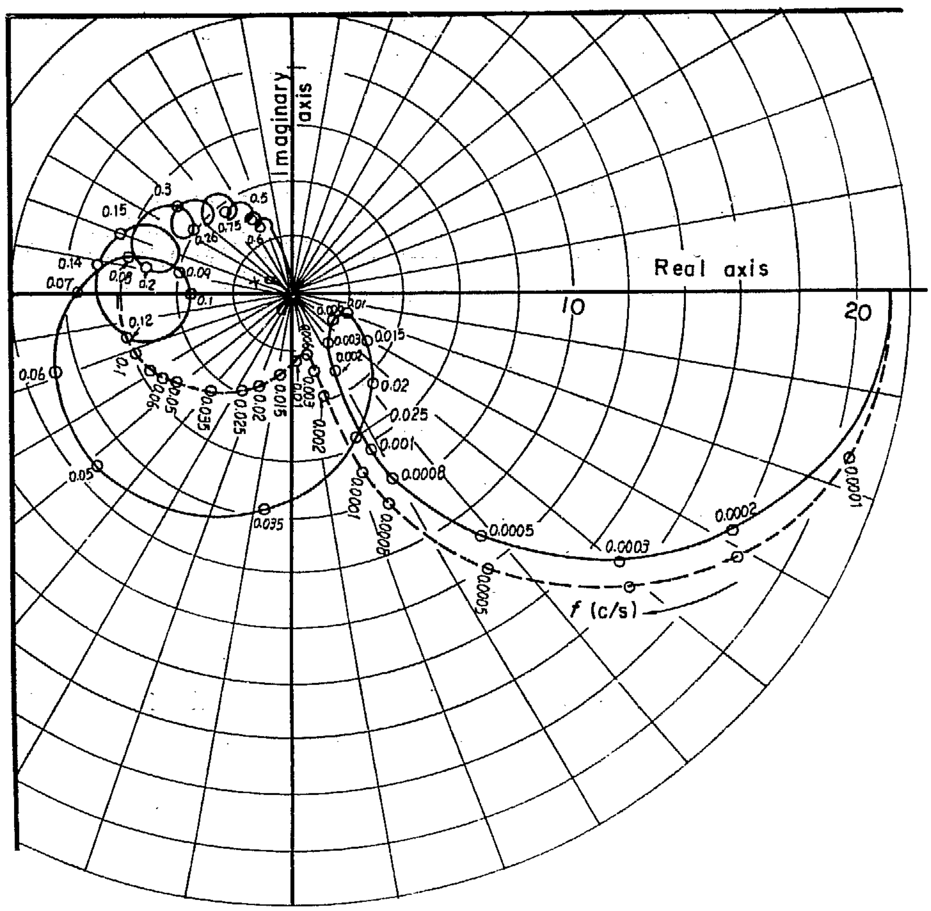

Fig. 28. 2 The Nyquist plot of the frequency characteristics of feedback transfer function which relates $\delta k_v/\beta$ to $\delta Q/Q^*$

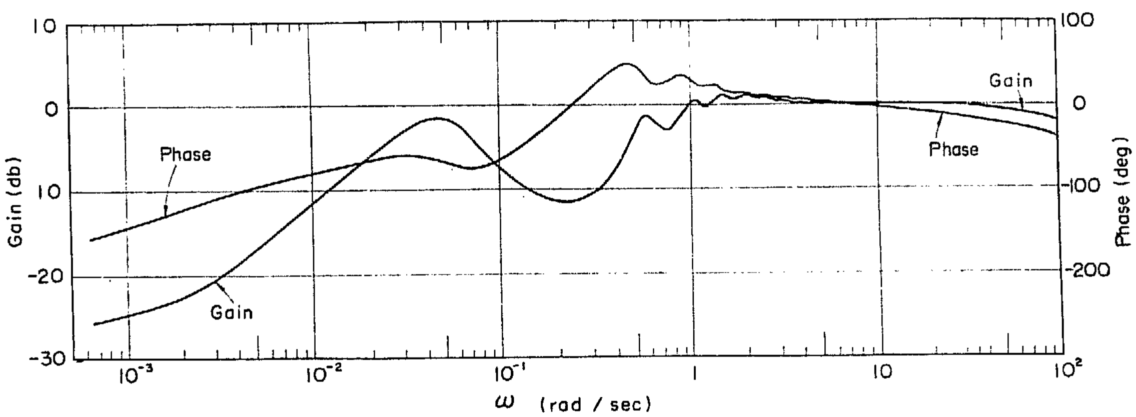

Fig. 28. 3 The frequency characteristics of the close loop transfer function, $\frac{\delta n/n^*}{\delta k_{ex}/\beta}$, with temperature feedback and void feedback of Fig. 28. 1

of temperature coefficient feedback and power to void feedback in parallel; the latter has been obtained in Chapter 5.1.

The open loop transfer function is schematically shown in Fig. 29. It is concluded from this figure that the system has a single positive real root based on Nyquist stability criterion, since the number of encirclements of the locus around the point (−1, 0) is one.

The magnitude of this positive real root is obtained by solving the characteristic equation. However, solving this equation is difficult, since it is so complicated. An approximate solution is obtained by solving a simplified equation, which is derived by ignoring small time constants in the characteristic equation. This simplification may be adequate, since the root is expected to be very small, i. e., of the order of $0.01\sim0.05\ \text{sec}^{-1}$.

The characteristic equation is

$$1-G_{RT}(s)\cdot G_{FB}(s)=0 \tag{87}$$

where $G_{FB}(s)$ is the feedback transfer function relating $\delta k_v/\beta$ to $\delta Q/Q^*$, and $G_{RT}(s)$ is defined as

$$G_{RT}(s)=\frac{G_R(s)\dfrac{1}{1+T_f s}}{1-\dfrac{\alpha T}{\beta}(\theta_f^*-\theta_w^*)\cdot G_R(s)\dfrac{1}{1+T_f s}}. \tag{88}$$

It should be noted that $G_{RT}(s)$ is almost constant and nearly equal to 0.8 for a small s of the order of $0.01\sim0.05$. $G_{FB}(s)$ is well approximated by Eq. (85) multiplied by α_v/β. Then the characteristic equation of Eq. (87) reduces to

$$1-0.8\left(-6.1+27.6\frac{1+122.4s}{(1+485.3s)(1+4.7s)}\right)=0 \tag{89}$$

A positive root of the above quadratic equation is readily obtained, giving $s=0.0285\ \text{sec}^{-1}$. The positive period is equal to $1/s=35.1$ sec, which agrees very well with the value of 35.5 sec obtained from one of the analog computer results in **Fig. 26.3**, where the steady period is read around $t=80\sim100$ sec.

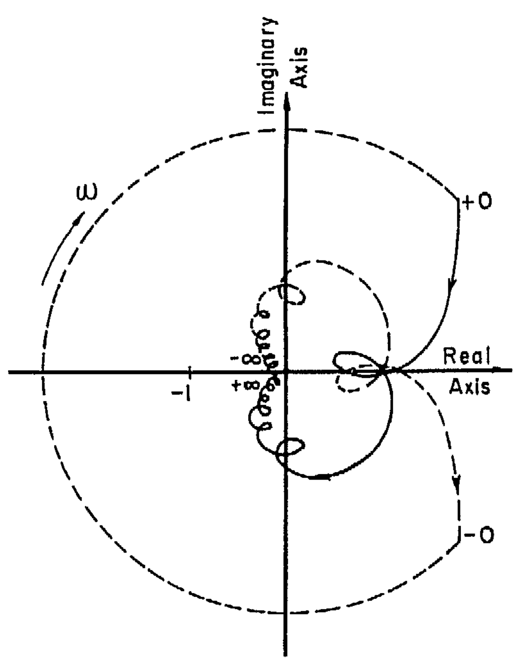

Fig. 29 The schematic Nyquist plot of open loop transfer function which relates $-\frac{1}{\beta}(\delta k_v+\delta k_T)$ to net reactivity

In the case of the plot in **Fig. 29**, it is assumed that the fuel heat transfer function is of a single time constant model; thus, the phase shift of the open loop transfer function at $\omega=\infty$ is equal to $-180°$. However, when a more accurate model which is approximated by a higher order time constant model or a distributed parameter model is adopted, the phase shift at

$\omega=\infty$ lags more than $-180°$. Thus, it is true based on the Nyquist diagram of Fig. 29 that the instability at a higher frequency appears as the loop gain increases. It should be noted that, as the fuel time constant is larger for oxide fuel element in JPDR than for metallic fuel elements, the gain margin of the open loop transfer function for the latter case is very large, thus, the instability will not appear for a considerablely higher power level encountered in usual high power density boiling water reactors with a long fuel time constant.

6. COMPARISON WITH OTHER STUDIES

The BORAX experiments showed that boiling water reactors are unstable under certain operating conditions. This observation led to many investigations of the dynamic behavior and stability of boiling water reactors. The early work by J. MacPhee[3] compared the stability of boiling waters with that of pressurized water reactors. A rather simple model of the dynamic behavior is used in this analysis. Efforts have been made at various organizations to derive more complete models. J. J. Hogle derived the power to void and the pressure to void transfer functions[4]. M. A. Head and E. R. Owen completed a model including pressure vessel dynamics and control systems[5]. This model was used with minor changes for the dynamic analysis of the Dresden[6], RWE[7] and Consumers Big Rock Reactors[8].

E. S. Beckjord[9] worked out another model which was used to compare the analytical transfer functions of the EBWR[2] with the experimental ones. J. A. Thie also derived a model[10] which is a little different from Beckjord's. The Beckjord's model was refined by A. Z. Akcasu[11]; this refined model was used for the analysis of the EBWR high power operation[12].

In the OECD Halden Project, J. A. Fleck, Jr., derived a model with particular emphasis on the hydrodynamic aspect of the dynamic behavior[13][14]. The dynamic analysis of the Halden reactor was made first applying the Beckjord's model[15] and later using the Fleck's method[16]. An effort to derive a new model is being made there[17].

A. Kirchenmayer performed a series of study and developed a model[18][19][20].

M. Iriarte[21] also derived a model.

Most of the early works handle the reactor core dynamics by a lumped parameter model, completely ignoring[5][6] or, at best, only partially taking into consideration[9][10] the effect of the void transit time. The preliminary study by the present authors also adopted a lumped parameter model. When the authors, inspired by the transient analysis by Kanai and others[22], started to derive the distributed parameter model, there was no model published which took account of the void transit in the core in a consistent manner. The models by Akcasu[11] and by Kirchenmayer[19], which were developed almost at the same time as the present authors, are also derived in a very similar way. Hence they are most suitable for comparing with the present model. It is not intended to make a complete comparison, but some comments on the differences between the Akcasu's model and the present one will be given below. The Akcasu's model needs some refinement, as discussed in the appendices of Refs. 11 and 12. Therefore the refined model, which is derived and used in Ref. 12, is compared with the present model.

The block diagram of the Akcasu's model is shown in **Fig. 30**[12], where the corresponding transfer functions of the present model are also shown. The following differences are readily noted:

(1) The hydrodynamics of the core is considered in more detail in the present model than in Akcasu's. In the latter is ignored the effect of $\delta V_0/V_0^*$ on the boiling boundary shift and so on.
(2) The effects of δW_R (G_{21} and G_{25} through G_{27}) are totally ignored in Akcasu's model.
(3) The effect of δW_f on δp (G_{17}) is ignored in Akcasu's model.
(4) The boiling and nonboiling heat transfers are not distinguished in the present model.
(5) The effect of the moderator temperature is not taken into consideration in the present model.

As for the power-void effect, the pressure-void effect, the power-boundary effect and the

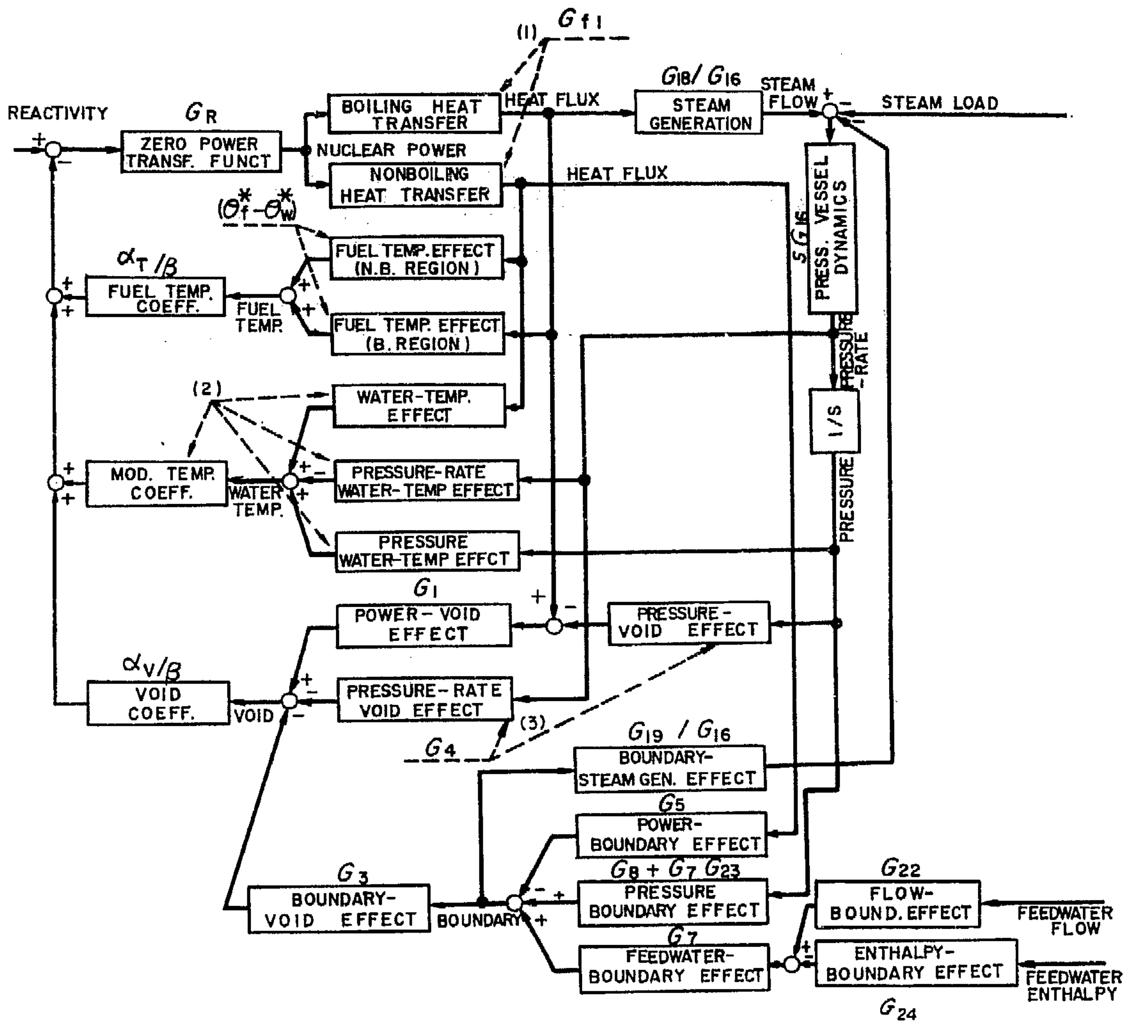

Notes:
(1) Boiling and nonboiling heat transfers are not distinguished in the present model.
(2) Moderator temperature effect is not taken into consideration in the present model.
(3) G_4 corresponds to (POWER-VOID EFFECT)×(PRESSURE-VOID EFFECT) +(PRESSURE-RATE EFFECT)

Fig. 30 Block diagram of Akcasu's model compared with the present model

boundary-void effect, the direct comparisons are not possible since they are derived under different assumptions. Instead, the major differences in assumptions are listed below.

(6) Akcasu assumes a constant steam velocity; in the present model, although the slip between the water and steam is ignored, the velocity varies along the core axis.

(7) A sinusoidal flux distribution and a flux weighting on voids are used by Akcasu. No weighting is considered here.

The pressure-boundary effect is compared with $G_8+G_7\times G_{23}$, the pressure vessel dynamics with G_{16} through G_{19}, the flow-boundary effect with $G_7\times G_{22}$, and the enthalpy-boundary effect with $G_7\times G_{24}$. It is noted that they are identical to each other, except the following minor differences:

(8) In Akcasu's model, the heat flux at the boiling boundary is obtained, assuming a sinusoidal flux distribution. In the present model, since the uniform distribution is assumed, it is equal to the average heat flux.

(9) The ratio of the recirculation flow to the total flow, W_R^*/W_0^*, is approximated to be unity in Akcasu's model.

(10) In AKCASU's model, the second term, G_{23}, is ignored, which has a small influence, as described in Chap. 3.

(11) In AKCASU's model, the term B_{pr} in G_{pr} is ignored. This term, however, is also ignored in the numerical calculations of the present model.

(12) In AKCASU's model, $v_s/\Delta v$ is approximated to be unity.

(13) In AKCASU's model, the third term in $(H_{pr})_{ves}$, i.e., $-\frac{\bar{V}_{sat}}{J}$, and the whole $(H_{pr})_{co}$ are ignored.

It is easy to substitute the numerical values of the parameters for JPDR into the AKCASU's model and to calculate the transfer functions. The result is shown in Fig. 31.

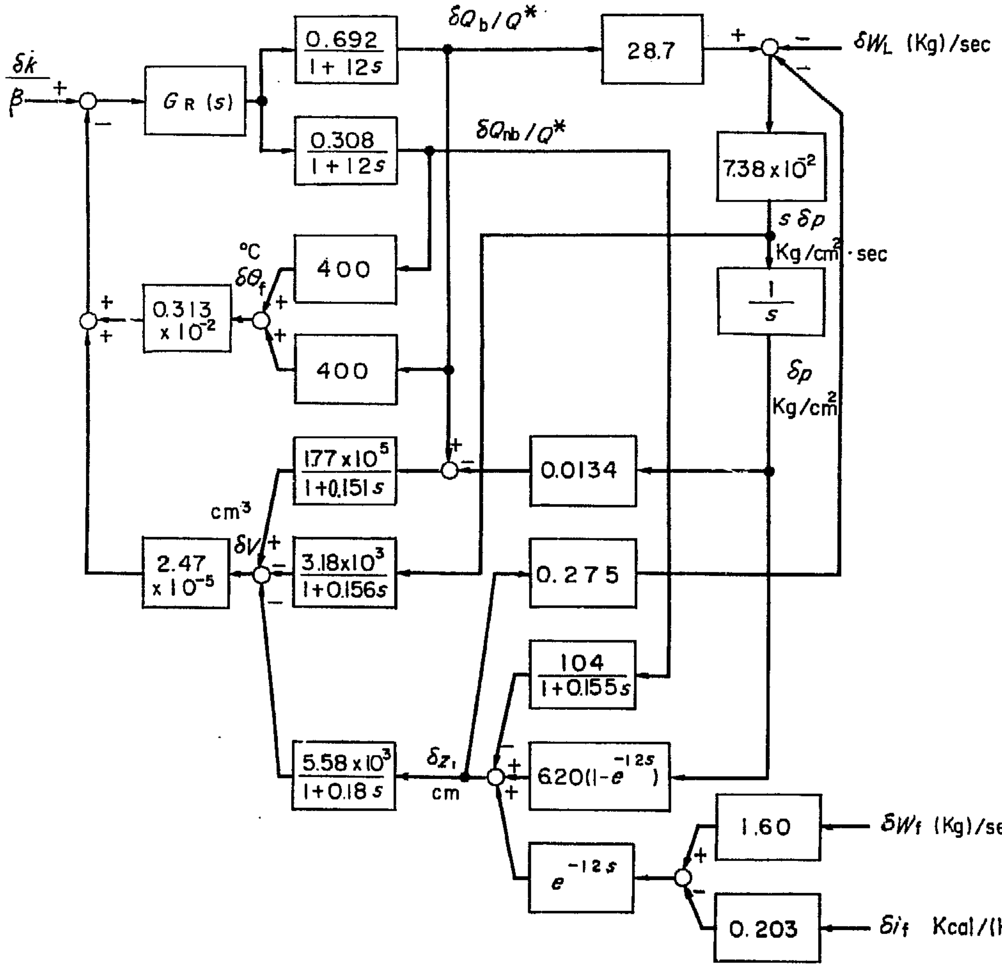

Fig. 31 Block diagram for JPDR by Akcasu's model

The grouping of the transfer functions derived in this report is developed so that these groups may be more readily associated with measurements of dynamic characteristics rather than the transfer functions of this report. In Appendix 6 are shown the groups of transfer functions developed. The frequency responses of the power effect group, the pressure effect group and the vessel dynamics group are derived for both models and are compared in Figs. 32 through 34.

The overall feedback transfer function are compared in Fig. 35.

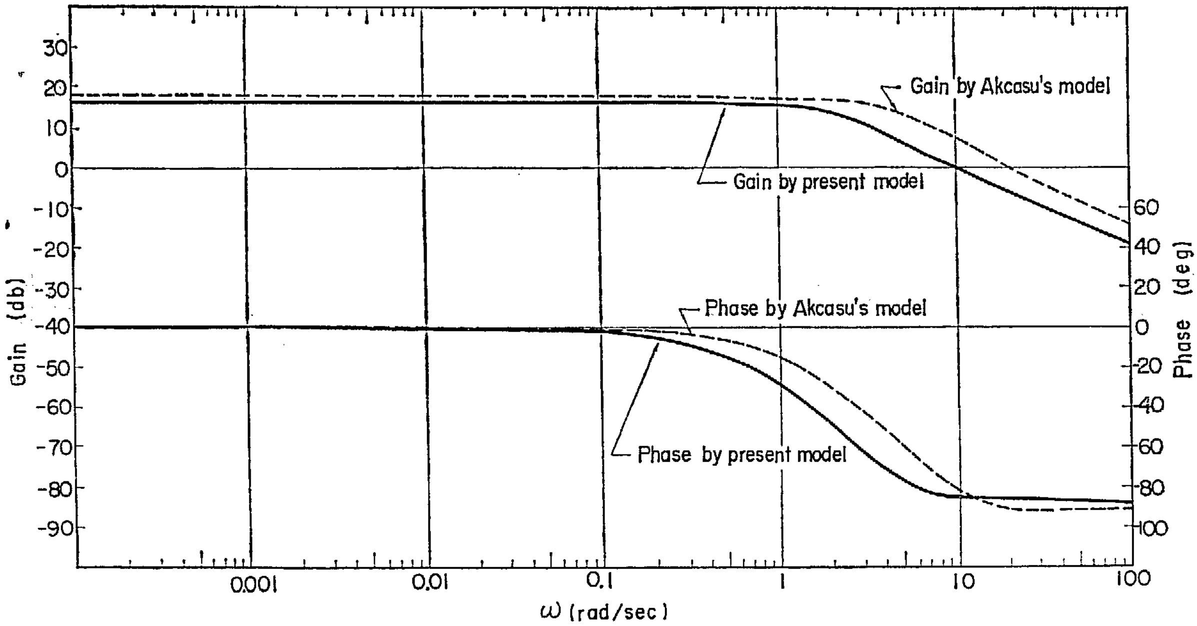

Fig. 32 Comparisons of two models——power effect group, $H_3(j\omega)$

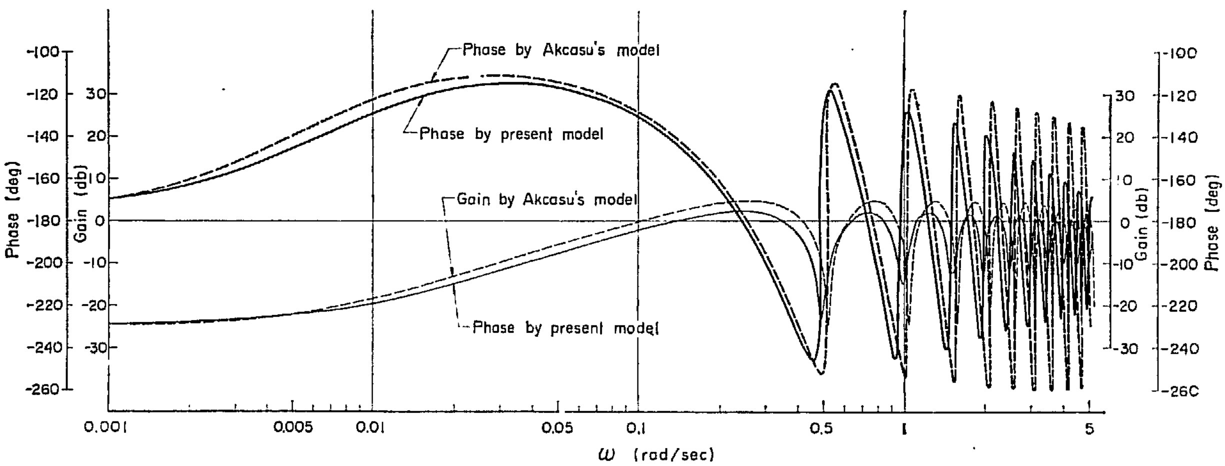

Fig. 33 Comparisons of two models——pressure effect group, $H_4(j\omega)$

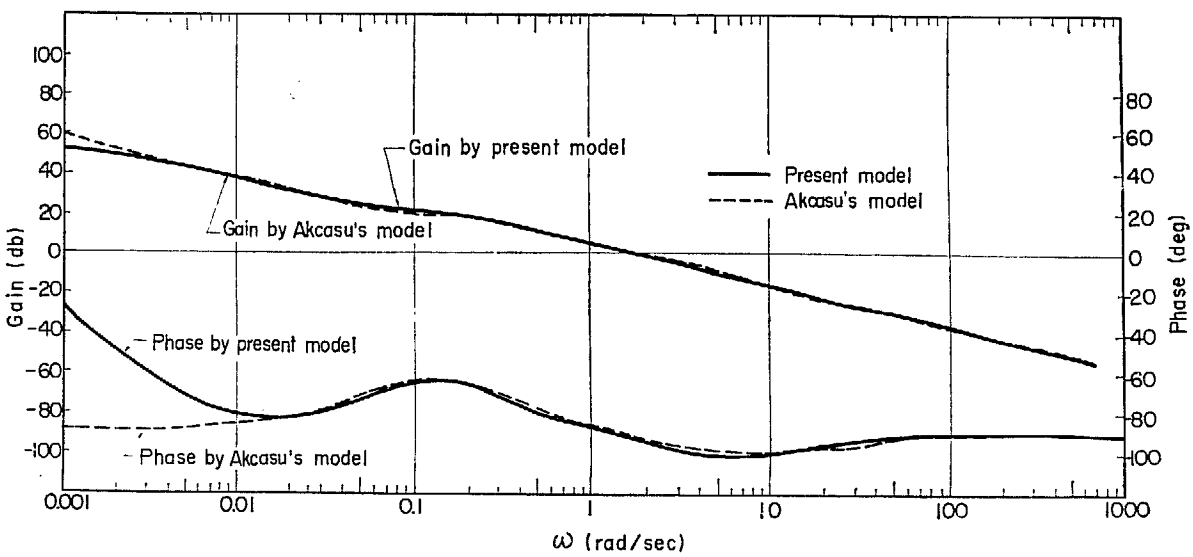

Fig. 34 Comparisons of two models——vessel pressure dynamics group, $H_2(j\omega)$

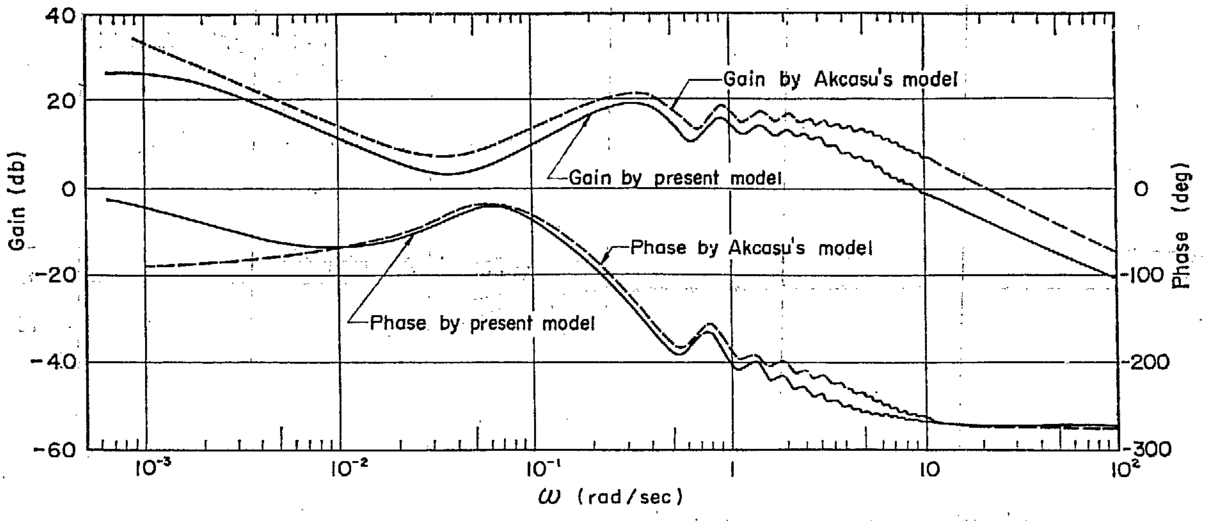

Fig. 35 Comparisons of two models——frequency characteristics of feedback transfer function

7. CONCLUSION

The simplified transfer functions are obtained, based on the transfer functions derived in the previous report, JAERI-1044; they are quite general for the dynamic analysis of natural circulation boiling water reactors. It is evident that the results obtained here are also applicable to the dynamic analysis of forced circulation boiling water reactors when the inlet velocity is assumed to be constant.

Most of the simplified transfer functions derived are in the form of combinations of single time constant terms which can be evaluated from design parameters. They are all summarized in Chapter 2.9 and TABLE 1. Analog simulation is simple except for those including pure delay terms.

The important conclusion obtained for simplifying the model is that the effects of inlet velocity and recirculation flow on the dynamic characteristics may be ignored. That is ascertained by analog computer studies. The simplified block diagram (Type-1) thus obtained is shown in Fig. 22.

The further simplified block diagram (Type-2) is shown in Fig. 23, where smaller time constants are ignored. The model derived above is of great use for investigating the dynamic characteristics of boiling water reactors from the viewpoint of the control. It also makes it possible to readily investigate the control of dual cycle boiling water reactors.

The feedback transfer function which relates void reactivity to power is investigated in Chapter 5 both on frequency and transient characteristics. This is the most important of the transfer functions, being characteristic of boiling water reactors.

The system stability is investigated in Chapter 5.3 by means of the Nyquist stability criterion and roots of the characteristic equation. A high frequency oscillating instability will be predicted when a more accurate model of fuel heat transfer will be adopted. A further study by the more accurate model is required. However, it is considered at the present time that the instability will not appear for a considerablely higher power level encountered in usual high power density boiling water reactors, so far as a fuel element of long time constant such as oxide fuel is used.

Comparison with other studies is made in Chapter 6 in order to make clear the significance of this study. In particular, comparison with the model developed by AKCASU[11] is given. The grouping of transfer functions derived in the preceding chapter is also developed in Chapter 6, so that these groups may be more readily associated with measurements of dynamic characteristics.

Analog computer studies and control system studies based on the model developed here will be given in the following report.

Acknowledgement

The authors wish to thank Mr. K. MOCHIZUKI, Mr. Y. TOGO and Mr. M. ISHIZUKA of JPDR Project for their inspiring discussion in the course of this study and for their continuous contribution to the evaluation of various important parameters. They are grateful to Mr. Y. KAMBAYASHI of Instrumentation and Controls Laboratory who has contributed in digital computer program and analog computer studies, and wish to acknowledge the assistance they have received from many of the students of the Nuclear Engineering School. Thanks are also due to Mrs. A. MATSUURA whose typing and assistence have aided greatly in the preparation of this report.

NOMENCLATURE

Symbol		Unit
A_{co}	flow area of core	cm^2
A_r	flow area of riser	〃
A_d	flow area of downcomer	〃
$A_v = A_r + A_d$	total sectional area of vessel	〃
A_{pr}	defined in Eq. (62e)*	cm^3/kg
A	$=\partial \Delta i/\partial p$	$\frac{kcal}{(kg)}\Big/\frac{kg}{cm^2}$
A'	$=A/\Delta i$	cm^2/kg
a	defined in Eq. (24)	cm^5/kg
$a_{01}, a_{12}, a_{23}, a_{34}, a_{45}$	defined in Eq. (71)	cm^2/kg
B	$=\partial i_w/\partial p$	$\frac{kcal}{(kg)}\Big/\frac{kg}{cm^2}$
B'	$=\frac{\Delta v}{\Delta i}\frac{B}{v_w}$	cm^2/kg
B_{pr}	defined in Eq. (62e)*	$cm^3/(kg \cdot sec)$
b	defined in Eq. (24)	cm^5/kg
C	$=\partial \Delta v/\partial p$	$\frac{cm}{(kg)}\Big/\frac{kg}{cm^2}$
C'	$=C/\Delta v$	cm^2/kg
c	defined in Eq. (24)	cm^5/kg
D	$=\partial v_w/\partial p$	$\frac{cm}{(kg)}\Big/\frac{kg}{cm^2}$
D'	$=D/v_w$	cm^2/kg
E	$=A'-B'-C'+D'$	〃
F	$=-A'-B'+C'+D'$	〃
f	void fraction	——
f_2	void fraction at core exit	——
$G(s)$	transfer function	
$G_{pr}(s)$	defined in Eq. (62e)*	$\frac{kg \cdot sec}{cm^3}$
$G_1(s), G_2(s), G_3(s), G_4(s)$	void transfer function	
$G_5(s), G_6(s), G_7(s), G_8(s)$	boiling boundary transfer function	
$G_{16}(s), G_{17}(s)$	vessel pressure transfer function	
$G_{18}(s), G_{19}(s)$	〃	
G_{16}'	$=-\Delta i$	kcal/(kg)
G_{17}'	$=\frac{v_w}{\Delta v}\Delta i$	〃
G_{18}'	$=(z_2-z_1)Q^*$	kcal/sec
G_{19}'	$=-Q^*$	kcal/sec·cm
$G_{21}(s), G_{22}(s)$	inlet water enthalpy transfer function	
$G_{23}(s), G_{24}(s)$	〃	

(kg) denotes the unit of mass.
kg denotes the unit of force.

Symbol		Unit
$G_{25}(s), G_{26}(s), G_{27}(s)$	recirculation flow transfer function	
$G_{t1}(s)$	fuel heat transfer function	
$G_{t2}(s)$	fuel heat transfer function	
$G_R(s)$	zero power transfer function	
g	acceleration of gravity	cm/sec^2
H_{pr}	defined in Eq. (38)	kcal $\Big/ \frac{kg}{cm^2}$
$(H_{pr})_{ves}$	〃	〃
$(H_{pr})_{co}$	〃	〃
h	reflecter height above the riser	cm
i	specific enthalpy	kcal/(kg)
i_s	specific enthalpy of saturated steam	〃
i_w	specific enthalpy of saturated water	〃
Δi	$=i_s-i_w$	〃
i_{sub}	average enthalpy of water in subcooled region	〃
i_f	specific enthalpy of feedwater	〃
i_w-i_{sub}	subcooling	〃
J	mechanical equivalent of heat	kg·cm/kcal
K	gain constant of transfer function	
k	gain constant of transfer function	
δk_{ex}	reactivity change	
δk_{void}	void reactivity change	
δk_T	reactivity change caused by temperature	
l	average neutron life time	sec
$M_{s\cdot co}$	saturated steam mass in core	(kg)
$M_{w\cdot co}$	saturated water mass in core	〃
$M_{sub\cdot co}$	subcooled water mass in core	〃
M_s	saturated steam mass in vessel (excluding core and riser)	〃
M_w	saturated water mass in vessel (excluding core and riser)	〃
M_{sub}	subcooled water mass in vessel (excluding core and riser)	〃
M_{Lp}	equivalent mass along flow in lower plenum	(kg)/cm^2
n	neutron density	cm^{-3}
p	pressure	kg/cm^2
Q	heat flux per unit length	kcal/sec·cm
r	slip ratio	——
T_f	fuel time constant, defined in Eq. (2)*	sec
T_l	time constant, defined in Eq. (80)	〃
T_r	$=\tau_{01}+\tau_d$	〃
T	time constant	〃
t	time	〃
U	steam void transmission velocity	cm/sec
u	condensation rate of steam	(kg)/sec
V	flow velocity	cm/sec
$\bar{V}$	void volume in core	cm^3
$\bar{V}_{sat\cdot co}$	saturated steam and water volume in core	cm^3
$\bar{V}_{sub\cdot co}$	subcooled water volume in core	〃

Symbol		Unit
$\overline{V}_{sat}$	saturated steam and water volume in vessel (excluding core and riser)	cm^3
$\overline{V}_{sub}$	subcooled water volume in vessel (excluding core and riser)	〃
$V_0{}^*$	inlet water velocity	cm/sec
v	$=1/\rho$	cm/(kg)
v'	$=1/\rho'$, specific volume	$cm^3/(kg)$
v_s	$=1/\rho_s$	cm/(kg)
v_w	$=1/\rho_w$	〃
$v_s{}'$	$=1/\rho_s{}'$	$cm^3/(kg)$
$v_w{}'$	$=1/\rho_w{}'$	〃
$\varDelta v$	$=v_s-v_w$	cm/(kg)
$\varDelta v'$	$=v_s{}'-v_w{}'$	$cm^3/(kg)$
v_{sub}	$=1/\rho_{sub}$	cm/(kg)
v'_{sub}	$=1/\rho'_{sub}$, average specific volume of water in subcooled region	$cm^3/(kg)$
W_L	steam flow to load	(kg)/sec
W_s	steam flow from riser	〃
W_w	water flow from riser	〃
W_0	water flow at core inlet	〃
W_R	recirculation flow	〃
W_f	feed water flow	〃
x_d	equivalent flow length from feedwater inlet to core inlet	cm
$y(z)$	defined as $\left(V_0{}^*+\frac{z-z_1}{\tau_e}\right)\Big/V_0{}^*=\frac{\rho_w}{\rho_w(1-f)+\rho_s f}$	——
y_2	$=y(z_2)$	——
y_3	$=y(z_3)$	——
z	position in axial direction (the origin at the inlet of core)	cm
$z_{L.p}$	equivalent flow length in lower plenum (from z_5 to z_0)	〃
$[FPD]$	frictional pressure drop	$(kg)\frac{cm}{sec^2}\cdot\frac{1}{cm^2}$
$[FPD]'$	$=\frac{\partial[FPD]}{\partial V_0}$	$(kg)/cm^2\cdot sec$
α	defined as $-\frac{v_s}{\varDelta v}\cdot\frac{1}{y_2{}^2}\Big\{A'(y_2-1)+B'+(C'-D')\times(y_2-1)\cdot\left(\frac{v_w}{v_s}y_2-1\right)\Big\}$	cm^2/kg
α_T	temperature coefficient of reactivity	1/C°
α_v	void coefficient of reactivity	cm^{-3}
α_r	$=H_{pr}\cdot k_2$	——
β_r	$=\left(1-\frac{W_R{}^*}{W_0{}^*}\right)^{-1}$	——
β	delayed neutron fraction	——
θ	temperature	℃
θ_f	fuel average temperature	〃
θ_w	water temperature	〃

Symbol		Unit
κ	defined as $\frac{1}{\mu}\left\{-\frac{1}{y_2}\frac{D'}{v_w}+\frac{y_2-1}{y_2}\frac{D'-C'}{v_s}\right\}$	$\frac{\text{cm(kg)}}{\text{kg}}$
μ	$=A_{co}/A_r$	—
μ_d	$=A_{co}/A_d$	—
ξ	defined in Eq. (70)	sec^2
$\rho=\rho' A_{co}$	density per unit length	(kg)/cm
ρ'	density	(kg)/cm^3
ρ_s	density per unit length of saturated steam	(kg)/cm
ρ_w	density per unit length of saturated water	〃
ρ_s'	density of saturated steam	(kg)/cm^3
ρ_w'	density of saturated water	〃
$\Delta\rho$	$=\rho_s-\rho_w$	(kg)/cm
$\Delta\rho'$	$=\rho_s'-\rho_w'$	(kg)/cm^3
ρ_{sub}	average water density per unit length in subcooled region	(kg)/cm
ρ'_{sub}	average water density in subcooled region	(kg)/cm^3
τ_e	$=\frac{\Delta i}{Q^*\Delta v}$: steam raising time, i. e., time during which the unit volume of steam is raised per unit volume of water	sec
τ_{01}	$=(z_1-z_0)/V_0^*$	〃
τ_{12}	$=\tau_e \ln y_2$: void transit time in boiling region	〃
τ_{23}	$=(z_3-z_2)/(\mu V_2^*)$	〃
τ_{34}	$=h/(\mu V_2^*)$	〃
τ_{45}	$=(z_3-z_0+h)/(\mu_d V_0^*)$	〃
τ_{50}	$=z_{Lp}/V_0^*$	〃
τ_d	time taken by flow from f. w. inlet to core inlet	〃
τ_r	time constant associated with the natural frequency of reflector free surface	〃
Ω	$=\tau_e^{-1}=Q^*\frac{\Delta v}{\Delta i}$, rate of steam raising	sec^{-1}
ω_1	defined in Eq. (9)	〃
ω_3	defined in Eq. (18)	〃

Subscript

w	water
s	steam
d	downcomer
r	riser
0	core inlet
1	boiling boundary
2	top of core
3	top of riser
4	top of reflector above the riser
5	the same level in downcomer as core inlet
sub	subcooled
sat	saturated
avg	average

Superscript

*	steady state value
$\sim$	variable associated with riser necessary to distinguish from those with core due to the different flow area in riser and core

Numerical Values of Parameters Used for JPDR at 46.7 MW and 62.5 kg/cm²

Symbol		Unit
A_{co}	$=5,900$	cm^2
A_r	$=13,100$	cm^2
A_d	$=21,000$	cm^2
$A_v=A_r+A_d$	$=34,100$	cm^2
A	$=-1.551$	$\frac{kcal}{(kg)}/\frac{kg}{cm^2}$
A'	$=-0.004154$	cm^2/kg
B	$=1.280$	$\frac{kcal}{(kg)}/\frac{kg}{cm^2}$
B'	$=0.07902$	cm^2/kg
C	$=-0.09457$	$\frac{cm}{(kg)}/\frac{kg}{cm^2}$
C'	$=-0.01831$	cm^2/kg
D	$=0.000542$	$\frac{cm}{(kg)}/\frac{kg}{cm^2}$
D'	$=0.00242$	cm^2/kg
E	$=-0.06244$	cm^2/kg
F	$=-0.09076$	cm^2/kg
f_2	$=0.5$	
g	$=980$	cm/sec^2
h	$=75$	cm
i_s	$=664.6$	kcal/(kg)
i_w	$=291.2$	kcal/(kg)
Δi	$=373.4$	kcal/(kg)
i_{sub}	$=284.59$	kcal/(kg)
i_f	$=127$	kcal/(kg)
i_w-i_{sub}	$=6.61$	kcal/(kg)
J	$=4.27\times10^4$	kg·cm/kcal
l	$=5\times10^{-5}$	sec
$M_{s\cdot co}$	$=5.975$	(kg)
$M_{w\cdot co}$	$=322.69$	(kg)
$M_{sub\cdot co}$	$=211.0$	(kg)
M_s	$=202.5$	(kg)
M_w	$=3015.7$	(kg)
M_{sub}	$=8.6\times10^3$	(kg)
M_{Lp}	$=0.06051$	$(kg)/cm^2$
p	$=62.4$	$(abs.)\,kg/cm^2$
Q^*	$=70.80$	kcal/sec·cm
r	$=1$	
T_f	$=12$	sec
$\bar{V}_{sat\cdot co}$	$=0.4266\times10^6$	cm^3
$\bar{V}_{sub\cdot co}$	$=0.2744\times10^6$	cm^3
$\bar{V}_{sat}$	$=3.995\times10^6$	cm^3
$\bar{V}_{sub}$	$=11.2\times10^6$	cm^3
V_0^*	$=112$	cm/sec
v_s	$=5.390$	cm/(kg)
v_w	$=0.2241$	cm/(kg)

Symbol		Unit
v_s'	$=31.8\times10^3$	cm³/(kg)
v_w'	$=1.322\times10^3$	cm³/(kg)
Δv	$=5.166$	cm/(kg)
$\Delta v'$	$=30.5\times10^3$	cm³/(kg)
v_{sub}	$=0.2204$	cm/(kg)
v'_{sub}	$=1300.4$	cm³/(kg)
W_L	$=19.88$	(kg)/sec
W_s	$=19.88$	(kg)/sec
W_w	$=477.12$	(kg)/sec
W_0	$=497.00$	(kg)/sec
W_R	$=477.12$	(kg)/sec
W_f	$=20.83$	(kg)/sec
x_d	$=296$	cm
y_2	$=1.915$	
z_{Lp}	$=80$	cm
z_0	$=0$	cm
z_1	$=46.5$	cm
z_2	$=151$	cm
z_3	$=285$	cm
z_2-z_1	$=104.5$	cm
z_3-z_2	$=134$	cm
$\dfrac{\partial[FPD]}{\partial V_0}$	$=0.604$	(kg)/cm²·sec
α_T	$=-2\times10^{-5}$	1/°C
α_v	$=-1.58\times10^{-7}$	1/cm³
β	$=0.0064$	
θ_w	$=277$	°C
λ	$=0.077$	sec⁻¹
μ	$=0.45$	
μ_d	$=0.281$	
ρ_s	$=0.1855$	(kg)/cm
ρ_w	$=4.462$	(kg)/cm
ρ_s'	$=3.145\times10^{-5}$	(kg)/cm³
ρ_w'	$=7.564\times10^{-4}$	(kg)/cm³
$\Delta\rho$	$=4.276$	(kg)/cm
$\Delta\rho'$	$=-7.249\times10^{-4}$	(kg)/cm³
ρ_{sub}	$=4.537$	(kg)/cm
ρ'_{sub}	$=0.00076$	(kg)/cm³
τ_e	$=1.02$	sec
τ_{01}	$=0.415$	sec
τ_{12}	$=0.663$	sec
τ_{23}	$=1.389$	sec
τ_{34}	$=0.777$	sec
τ_{45}	$=11.4$	sec
τ_{50}	$=0.715$	sec
τ_d	$=12$	sec
τ_r	$=0.18$	sec
Ω	$=0.980$	sec⁻¹

Numerical Values of Derived Parameters Used for JPDR at 46.7 MW and 62.5 kg/cm²

Symbol		Unit
A_{pr}	$=67.25$	cm^3/kg
a	$=-0.2076\times10^5$	cm^5/kg
a_{01}	$=0.00877$	cm^2/kg
a_{12}	$=0.0272$	〃
a_{23}	$=-0.024$	〃
a_{34}	$=0.00123$	〃
a_{45}	$=-0.0677$	〃
B_{pr}	$=-0.426$	$cm^3/(kg\cdot sec)$
b	$=-0.0171\times10^5$	cm^5/kg
c	$=0.1905\times10^5$	〃
G_{16}'	$=-373.4$	kcal/(kg)
G_{17}'	$=16.19$	kcal/(kg)
G_{18}'	$=7.4\times10^3$	kcal/sec
G_{19}'	$=-70.80$	kcal/sec·cm
H_{pr}	$=4.86\times10^3$	$kcal\Big/\dfrac{kg}{cm^2}$
$(H_{pr})_{ves}$	$=4.814\times10^3$	〃
$(H_{pr})_{co}$	$=4.4\times10$	〃
K_1	$=1.21\times10^5$	cm^3
K_3	$=-2.94\times10^3$	cm^3/cm
K_5	$=-46.5$	cm
K_7	$=-7.07$	$cm\Big/\dfrac{kcal}{(kg)}$
K_8	$=9.03$	$cm\Big/\dfrac{kg}{cm^2}$
K_{21}	$=0.01385$	$\dfrac{kcal/(kg)}{(kg)/sec}$
K_{22}	$=-0.315$	〃
K_{23}	$=1.23$	$\dfrac{kcal/(kg)}{kg/cm^2}$
K_{23}'	$=0.489$	$\dfrac{kcal/(kg)}{kg/cm^2}\cdot sec$
K_{24}	$=0.042$	——
K_q	$=14.5$	$(kg)/cm\cdot sec^2$
K_q'	$=1.53$	——
K_v	$=0.902$	$(kg)/cm^2\cdot sec$
K_v'	$=10.66$	——
K_{z1}	$=-0.140$	$(kg)/cm^2\cdot sec^2$
K_{z1}'	$=-1.68$	——
K_p	$=-0.515$	$\dfrac{(kg)cm}{cm^2\cdot sec^2}\Big/\dfrac{kg}{cm^2}$
K_p'	$=-0.0542$	cm^2/kg
k_1	$=2.47\times10^5$	cm^3
k_2	$=8\times10^{-5}$	$kg/cm^2\cdot kcal$
k_3	$=-3.05\times10^5$	$cm^5\cdot sec/kg$
k_4	$=-1.64\times10^3$	cm^5/kg

Symbol		Unit
k_5	$=39.9$	$cm^3 \cdot sec/kcal$
T_l	$=490$	sec
T_r	$=12$	〃
T_{z1}	$=0.049$	〃
T_{z1}'	$=-0.0823$	〃
T_v	$=0.24$	〃
T_v'	$=2.535$	〃
T_q	$=-0.45$	〃
T_q'	$=-0.689$	〃
T_1	$=0.2667$	〃
T_3	$=0.4664$	〃
T_4	$=0.4215$	〃
T_5	$=0.27$	〃
α	$=-0.02638$	cm^2/kg
α_r	$=0.389$	——
β_r	$=25$	——
κ	$=-0.00845$	cm・(kg)/kg
ξ	$=-1.45$	sec^2
ξ'	$=0.0786$	$cm^2 \cdot sec^2/kg$
ξ_{12}'	$=0.0176$	〃
ξ_{23}'	$=0.033$	〃
ξ_{34}'	$=0.028$	〃

Appendix 1. Several Methods for Obtaining a Single Time Constant Approximation of $G_1(s)$

1) $G_1(s)$ is approximated by a single time constant lag, i. e.,

$$G_1(s) \simeq \frac{K_1}{1+T_1 s} \tag{A1}$$

2) Static gain is obtained as

$$K_1 = \lim_{s \to 0} G_1(s) \tag{A2}$$

3) 45°-phase-lag method for obtaining T_1.

$$T_1 = \frac{1}{\omega_1} \tag{A3}$$

where ω_1 is a solution of the equation,

$$\mathrm{Arg}\, G_1(j\omega_1) = -\frac{\pi}{4} \tag{A4}$$

Phase shift of two factors of $G_1(j\omega)$ is obtained as follows.

$$\mathrm{Arg}\left(\frac{1}{\tau_e j\omega - 1}\right) = \mathrm{Arg}\left(-j \cdot \frac{1}{\tau_e \omega + j}\right) = -\frac{\pi}{2} - \tan^{-1}\frac{\ln y_2}{2x_1} \tag{A5}$$

where $x_1 = \frac{\tau_{12}\omega}{2}$, and

$$\mathrm{Arg}\left(\frac{y_2-1}{y_2 \ln y_2} - \frac{1-e^{-\tau_{12} j\omega}}{\tau_{12} j\omega}\right) = \mathrm{Arg}\left(a - \frac{\sin x_1}{x_1} e^{-jx_1}\right) \tag{A6}$$

where $a = \frac{y_2 - 1}{y_2 \ln y_2}$.

Assuming that x_1 is almost close to $\pi/2$, one obtains

$$e^{-jx_1} \simeq (-j)\left\{1 + j\left(\frac{\pi}{2} - x_1\right)\right\}$$

and $\frac{\sin x_1}{x_1} \simeq \frac{1}{x_1}$

Thus,

$$\mathrm{Arg}\left(a - \frac{\sin x_1}{x_1} e^{-jx_1}\right) = \mathrm{Arg}\left\{\left(a + 1 - \frac{\pi}{2x_1}\right) + j\frac{1}{x_1}\right\}$$

$$= \tan^{-1}\frac{1}{(a+1)x_1 - \frac{\pi}{2}} \tag{A7}$$

Combining Eqs. (A4), (A5) and (A7), one obtains

$$-\frac{\pi}{2} - \tan^{-1}\frac{\ln y_2}{2x_1} + \tan^{-1}\frac{1}{(a+1)x_1 - \frac{\pi}{2}} = -\frac{\pi}{4}$$

From the above equation, a quadratic equation of x_1 is obtained

$$2(a+1)x_1^2 - \{\pi + 2 - (a+1)\ln y_2\}x_1 - \left(\frac{\pi}{2} - 1\right)\ln y_2 = 0 \tag{A8}$$

The solution of the above equation is

$$x_1 = \frac{C + \sqrt{C^2 + 8\left(\frac{\pi}{2} - 1\right)(a+1)\ln y_2}}{4(a+1)} \tag{A9}$$

where

$$C=\pi+2-\ln y_2-\frac{y_2-1}{y_2}$$

4) Approximate method by step response of $G_1(s)$ for obtaining T_1.

The step response of $G_1(s)$ is given in Eq. (5). T_1 is obtained such that the step response at T_1 is equal to $(1-e^{-1})$ times the final value of the step response.

From Eq. (5) T_1 is obtained as

$$T_1=\tau_e(y_2-1)\left\{1-\sqrt{1-1.264\left(\frac{1}{y_2-1}\right)\left(\frac{y_2\ln y_2}{y_2-1}-1\right)}\right\} \tag{A10}$$

The calculated value of T_1 for JPDR is shown in **Fig. 3.2** as a function of power level. It should be noted that the value by this method is very close to the one by 45°-phase-lag method.

5) Approximate method by gain characteristics for obtaining T_1.

T_1 is obtained from the following equation.

$$T_1=\frac{G_1(0)}{\lim_{s\to 0} sG_1(s)} \tag{A11}$$

This gives

$$T_1=\tau_{12}\left(\frac{y_2}{y_2-1}-\frac{1}{\ln y_2}\right) \tag{A12}$$

The numerical value of T_1 for JPDR is also shown in **Fig. 3.2** as a function of power level. T_1 obtained by this method gives a larger value than those obtained by the former methods. This tendency is evident from **Fig. 1**.

Appendix 2. Power Dependence of Parameters

The power dependences of some of the important parameters in the simplified transfer functions are investigated in order to obtain the transfer functions of different power levels.

These parameters are y_2 and τ_e. They are determined as a function of power level Q^* which is proportional to n^*. The definitions of the parameters are repeated here.

$$y_2=1+\frac{z_2-z_1}{V_0^*\tau_e} \tag{A13}$$

$$\tau_e=\frac{1}{Q^*}\left(\frac{\Delta i}{\Delta v}\right) \tag{A14}$$

Assuming that the boiling boundary z_1 and the inlet velocity V_0^* are independent of power level Q^*, one obtains

$$y_2=1+\left(\frac{z_2-z_1}{V_0^*}\frac{\Delta v}{\Delta i}Q^*_{\text{full power}}\right)m \tag{A15}$$

$$\tau_e=\left(\frac{\Delta i}{\Delta v}\cdot\frac{1}{Q^*_{\text{full power}}}\right)\cdot\frac{1}{m} \tag{A16}$$

where m is defined as a normalized power level, i. e., the ratio of operating power to full power.

Substituting numerical values of parameters of JPDR into the above equations, one obtains

$$y_2=1+0.915m \tag{A17}$$

$$\tau_e=1.02/m \tag{A18}$$

For convenience y_2 and τ_e are plotted in **Fig. A 2.1** and **A 2.2** as a function of normalized power level, where $\ln y_2$ and $\tau_{12}=\tau_e \ln y_2$ are also plotted.

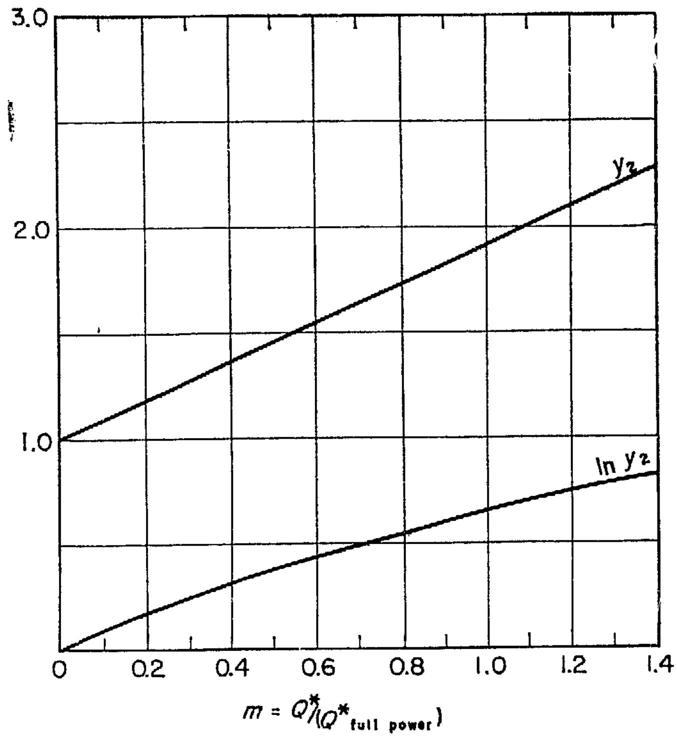

Fig. A 2.1 Power dependence of τ_e and τ_{12}

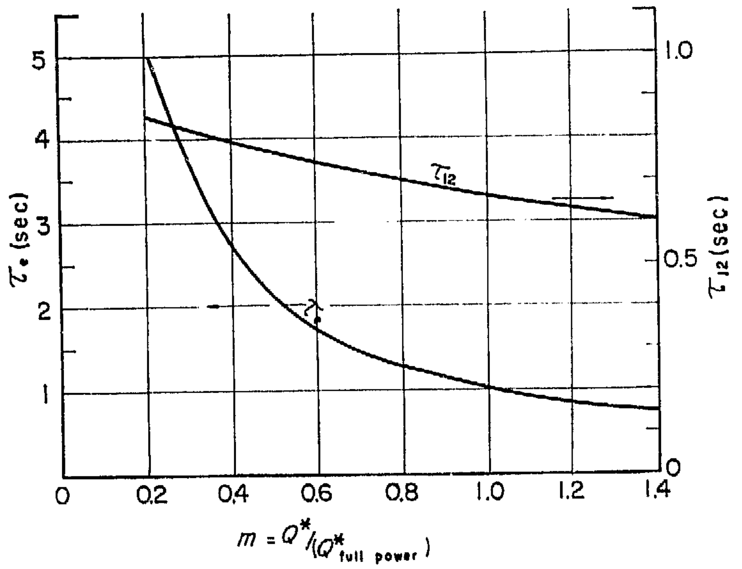

Fig. A 2.2 Power dependence of y_2 and ln y_2

Appendix 3. Parameters in K_p' and ξ' of Eq. (71)

$$\left.\begin{array}{l} K_p' = a_{01} + a_{12} + a_{23} + a_{34} + a_{45} \\ \xi' = \xi_{12}' + \xi_{23}' + \xi_{34}' \end{array}\right\} \quad (71)$$

where

$$a_{01} = D'\tau_{01}\frac{g}{V_0{}^*}$$

$$a_{12}=(y_2-1)(A'-C'+D')-\frac{\tau_e g}{V_0^*}\frac{v_w}{v_s}\Big\{(D'-C')(y_2-1)$$

$$-\left(\frac{v_s+v_w}{v_w}D'-C'\right)\frac{\tau_{12}}{\tau_e}\Big\}$$

$$a_{23}=\mu\frac{\tau_{23}g}{y_2 V_0^*}\{(A'-C')-y_2(A'-C'-D')\}$$

$$a_{34}=\mu\Big[\left(\frac{g\tau_r}{y_2 V_0^*}-2\mu\right)(A'-C')(y_2-1)+\mu^2\kappa v_w y_2^2$$

$$+\mu(y_2-1)\left\{\frac{v_w}{v_s}y_2(C'-D')+A'-C'\right\}\Big]$$

$$a_{45}=-\mu_d D'\frac{\tau_{45}g}{V_0^*} \qquad (\mu_d^2 D' \text{ is neglected})$$

$$b_{12}=(A'-C')(y_2-1-\ln y_2)\tau_e^2-\frac{E}{2}\tau_{12}^2$$

$$b_{23}=\mu^2\tau_{23}\Big[(A'-C')(y_2-1)\tau_e-E\tau_{12}+\frac{\tau_{23}}{2}\{(A'-C')(y_2-1)+B'-D'\}\Big]$$

$$b_{34}=\mu^2\tau_{34}[(A'-C')\{(y_2-1)\tau_e+y_2\tau_{23}\}-(\tau_{12}+\tau_{23})E]$$

Appendix 4. Computer Results for the Simplification of the Model

Several assumptions have been introduced in Chapter 3 for simplifying the model, so that the simplified block diagram, Type-1, of Fig. 22.1 may be obtained. These assumptions are demonstrated by an analog computer to be appropriate for the present purpose.

It is evident from Fig. 21 that important variables, such as $d\bar{V}$, δp, δz_1 and others, each consist of effects of four variables. Transient responses of these four effects are recorded and compared with each other. Computer results show that the following effects may be ignored compared with other effects.

(1) the effect of δV_0 on $\delta\bar{V}$,
(2) the effect of δV_0 on δz_1,
(3) the effect of δW_R on δi_0,
(4) the effect of $s\delta p$ on δi_0.

From the above conclusions may be reduced the assumptions given in Chapter 3.

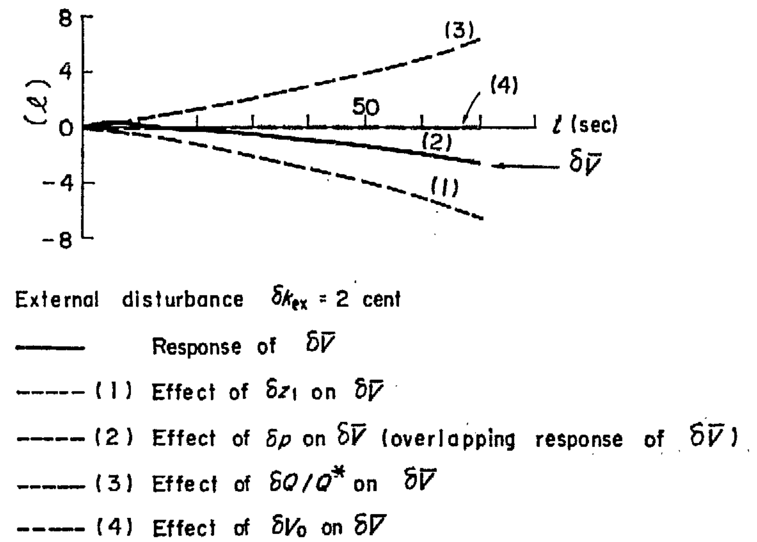

Fig. A 4.1 Various effect of responses on $\delta\bar{V}$

The same analysis as mentioned above also show the important conclusion; the effect of δz_1 on δp may not be ignored compared with the effect of $\delta Q/Q^*$ on δp. This conclusion indicates that the boiling boundary effect on the vessel pressure dynamics is quite important.

Some recordings of the effects of $\delta Q/Q^*$, δV_0, δz_1 and δp on $\delta\overline{V}$ are shown in **Fig. A 4.1** as one of the examples. The effect of δV_0 is very small.

In **Fig. A 4.2** are shown the transient responses of $\delta n/n^*$ and $\delta\overline{V}$, where the result of complete simulation without the simplification is shown by the dotted line and that of the simplified simulation by the solid line. It is concluded that the difference is quite small.

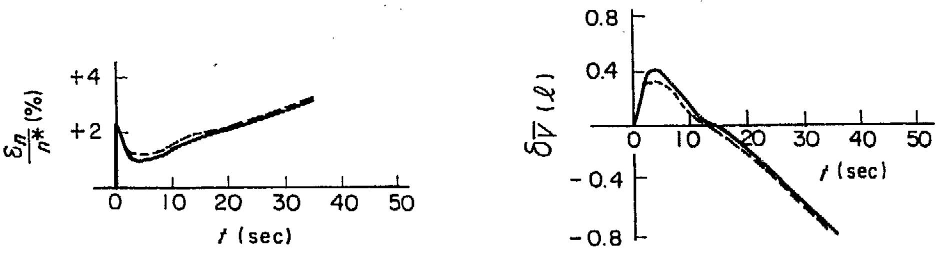

External disturbance δk_{ex} = 2 cent

—— Response of simplified model of chapter 3

---- Response of original model

Fig. A 4.2 Comparison of transient responses between original model and simplified model

Appendix 5. Calculations of Transfer Functions in the Block Diagram of Fig. 23

Based on the assumptions described in Chapter **4**, calculations of transfer functions in **Fig. 23** are given below. By the use of these results, the simplified block diagram, Type-2, given in **Fig. 24** is obtained.

$$G_1+G_3\cdot G_5\simeq K_1+K_3\cdot K_5\simeq V_0^*A_{co}\tau_{12}\left(1-\frac{y_2-1}{y_2\ln y_2}\right)+(z_1-z_0)A_{co}\frac{y_2-1}{y_2}\equiv k_1 \qquad \text{(A19)}$$

$$G_{18}+G_5\cdot G_{19}\simeq(z_2-z_1)Q^*\frac{1}{H_{pr}}\cdot\frac{1}{s}+K_5(-Q^*)\frac{1}{H_{pr}}\cdot\frac{1}{s}$$

$$=(z_2-z_0)Q^*\frac{1}{H_{pr}}\cdot\frac{1}{s} \qquad \text{(A20)}$$

$$H=\frac{1}{1-G_{19}(G_8+G_7\cdot G_{23})}\simeq\frac{1}{1+Q^*\frac{1}{H_{pr}}\cdot\frac{1}{s}(K_8+K_7e^{-\tau_{01}s}\cdot K_{23}e^{-\tau_d s})}$$

$$\simeq\frac{H_{pr}}{H_{pr}+\frac{Q^*}{s}\left(\frac{V_0^*}{Q^*}\rho_w B-\frac{V_0^*}{Q^*}\rho_w B\frac{W_R^*}{W_0^*}e^{-T_r s}\right)}=\frac{H_{pr}}{H_{pr}+\rho_w V_0^* B\left(1-\frac{W_R^*}{W_0^*}e^{-T_r s}\right)\frac{1}{s}}$$

$$\simeq\frac{H_{pr}}{H_{pr}+W_0^*B\left(1-\frac{W_R^*}{W_0^*}\frac{1}{1+T_r s}\right)\frac{1}{s}}=\alpha_r T_l\frac{s(1+T_r s)}{1+T_l s(1+\alpha_r T_r s)} \qquad \text{(A21)}$$

where $\alpha_r\equiv\frac{H_{pr}}{H_{pr}+W_0^*T_rB}$ and $T_l\equiv\frac{H_{pr}}{\alpha_r W_0^* B}\left(1-\frac{W_R^*}{W_0^*}\right)^{-1}$

$$G_3(G_8+G_7\cdot G_{23})\simeq K_3\frac{W_0^*B}{Q^*}\left(1-\frac{W_R^*}{W_0^*}e^{-T_r s}\right)$$

$$\simeq -A_{co}\frac{y_2-1}{y_2}\frac{W_0{}^*B}{Q^*}\left(1-\frac{W_R{}^*}{W_0{}^*}\frac{1}{1+T_rs}\right)$$

$$=\frac{k_3}{\beta_r T_r}\frac{1+\beta_r T_r s}{1+T_r s} \tag{A22}$$

where $k_3\equiv -A_{co}\dfrac{y_2-1}{y_2}\dfrac{W_0{}^*T_rB}{Q^*}$, and $\beta_r=1-\left(\dfrac{W_R{}^*}{W_0{}^*}\right)^{-1}$

$$G_4\simeq K_4\simeq -V_0{}^*A_{co}\tau_{12}(A'-C')\left(1-\frac{y_2-1}{y_2\ln y_2}\right)\equiv k_4 \tag{A23}$$

$$G_{17}+G_7G_{19}G_{22}\simeq\frac{1}{H_{pr}s}\left\{\frac{v_w}{\Delta v}\Delta i-(i_w-i_f)e^{-T_rs}\right\}$$

$$\simeq -\frac{i_w-i_f}{H_{pr}}\frac{1}{1+T_rs}\frac{1}{s} \tag{A24}$$

$$G_3G_7G_{22}\simeq K_3K_7K_{22}e^{-T_rs}$$

$$\simeq -(i_w-i_f)\frac{A_{co}}{Q^*}\frac{y_2-1}{y_2}\frac{1}{1+T_rs}=-(i_w-i_f)\frac{k_5}{1+T_rs} \tag{A25}$$

where $k_5\equiv\dfrac{A_{co}}{Q^*}\dfrac{y_2-1}{y_2}$

$$G_7G_{19}G_{24}\simeq K_7\left(-\frac{Q^*}{H_{pr}}\frac{1}{s}\right)\frac{W_f{}^*}{W_0{}^*}e^{-T_rs}\simeq\frac{W_f{}^*}{H_{pr}}\frac{1}{1+T_rs}\frac{1}{s} \tag{A26}$$

$$G_3G_7G_{24}\simeq K_3K_7K_{24}e^{-T_rs}\simeq W_f{}^*\frac{A_{co}}{Q^*}\frac{y_2-1}{y_2}\frac{1}{1+T_rs}$$

$$=W_f{}^*\frac{k_5}{1+T_rs} \tag{A27}$$

Appendix 6. Experimental Determination of Feedback Transfer Function

Many different mathematical models of boiling water reactor dynamics have been developed. Experiments are also made to determine the transfer function. However, if only the reactor power response to the sinusoidal variation in reactivity is observed, only the overall closed loop transfer function is determined experimentally. Thus, the comparison between the mathematical model and the results of experiments is restricted to the overall dynamic behavior. In this article is discussed the possibility of experimental determination of the details of the feedback transfer function, which makes possible more detailed comparisons between the analytical and

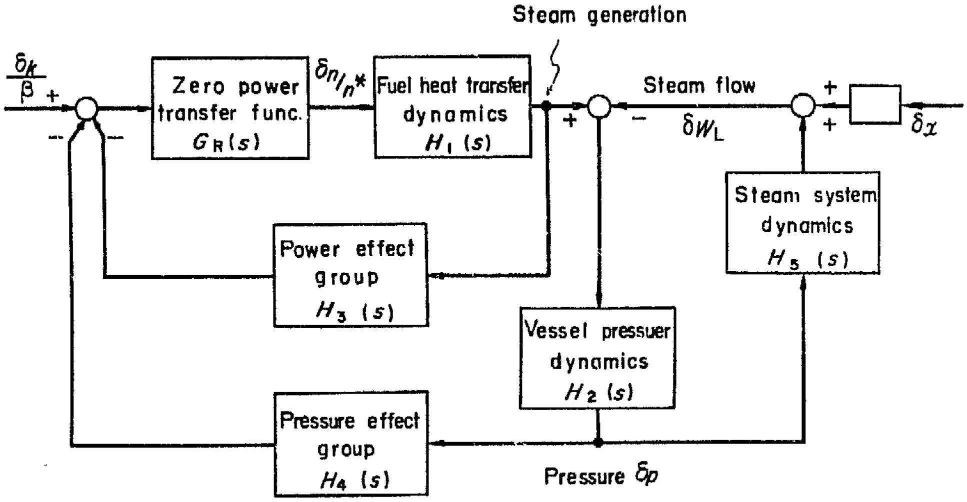

Fig. A 6. 1 System diagram for boiling water reactors experimental results.

It is assumed that the system is represented by the block diagram in Fig. A 6.1. This diagram is derived from the more complete one in Fig. 22.1 by lumping some transfer functions to form the transfer function groups. For example, the power effect group in Fig. A 6.1 is equivalent to

$$H_3(s) = -\frac{\alpha_v}{\beta}[G_1(s) + G_3(s) \cdot G_5(s)]$$

in Fig. 22.1. The transfer function groups are formed since not every transfer function in Fig. 22.1 could be determined experimentally. For example, it is not possible to measure the boiling boundary to void transfer function.

Now it is assumed that two kinds of experiment are performed, namely, introducing sinusoidal variation in reactivity, δk, and in steam valve position δx, and the responses of the reactor power, the reactor pressure and the net steam flow, δW_L, are observed. Thus, the following transfer functions are assumed to be available.

$$F_1(s) = \frac{\delta n(s)/n^*}{\delta k(s)/\beta}, \quad F_2(s) = \frac{\delta p(s)}{\delta k(s)/\beta}, \quad F_3(s) = \frac{\delta W_L(s)}{\delta k(s)/\beta},$$

$$F_4(s) = \frac{\delta p(s)}{\delta x(s)}, \quad F_5(s) = \frac{\delta n(s)/n^*}{\delta x(s)}$$

The transfer function groups $H_2(s)$ through $H_5(s)$ are obtained from the data of $F_1(s)$ through $F_5(s)$, as follows,

$$H_2(s) = \left[\frac{F_1(s) H_1(s)}{F_2(s)} - H_5(s)\right]^{-1}$$

$$H_3(s) = \left[-\frac{F_4(s)}{F_5(s)}\left(\frac{1}{F_1(s)} - \frac{1}{G_R(s)}\right) - \frac{1}{G_R(s)} \cdot \frac{F_2(s)}{F_1(s)}\right] \Big/ \left[H_1(s)\left(\frac{F_2(s)}{F_1(s)} - \frac{F_4(s)}{F_5(s)}\right)\right]$$

$$H_4(s) = \frac{1}{F_1(s)} \Big/ \left[H_1(s)\left(\frac{F_2(s)}{F_1(s)} - \frac{F_4(s)}{F_5(s)}\right)\right]$$

$$H_5(s) = \frac{F_3(s)}{F_2(s)}$$

Since the zero power transfer function $G_R(s)$ is readily obtained experimentally and the heat transfer dynamics $H_1(s)$ may be obtained from out-of-pile experiments, all the transfer function groups $H_1(s)$ through $H_5(s)$ are determined from the experimental data.

References

1) J. Miida and N. Suda: JAERI-1044 (1963)
2) J. A. DeShong, Jr., and W. C. Lipinski: ANL-5850 (1958)
3) J. MacPhee: *IRE Trans. on Nucl. Sci.*, 25-29 (1957)
4) J. J. Hogle: GEAP 0971 (1957)
5) M. A. Head and E. R. Owen: GER-1468 (1958)
6) D. W. Leiby: *Trans. AIEE, Part 1*, 17 (1958)
7) M. A. Head: GEAP-3166 (1959)
8) J. M. Case and L. K. Holland: GEAP-3795 (1962)
9) E. S. Beckjord: ANL-5799 (1957)
10) J. A. Thie: ANL-5849 (1959)
11) A. Z. Akcasu: ANL-6221 (1960)
12) N. Suda and F. Rehbach: ANL-6478 (1962)
13) J. A. Fleck, Jr.: *J. of Nucl. Energy, Part A*, **11**, 114-130 (1960)
14) J. A. Fleck, Jr.: *Nucl. Sci. Engg.* 9, (2), 271 (1961)
15) H. Schmidl, G. Ambresini, N. Rydell and O. Vapaavuori: HPR-5 (1960)
16) P. la Cour Christensen and K. Solberg: KR-45 (1963)
17) K. O. Solberg: KR-51 (1963)
18) A. Kirchenmayer: *J. of Nucl. Energy, part A*, 11 (1960)
19) A. Kirchenmayer: *Nucleonik*, **4**, (3) 122-137 (1962)
20) A. Kirchenmayer: KR-35 Vol. II (1962)
21) M. Iriarte, Jr.: PhD. Thesis submitted to Univ. of Michigan (1958)
22) T. Kanai, T. Kawai and R. Aoki: *Journal of Atomic Energy Society of Japan*, **3**, 168 (1961)